Electronic Thesis and Dissertation Repository

8-14-2014 12:00 AM

Uncertainty Quantification for a Class of MEMS-based Vibratory Angular Rate Sensors

Nujhat Abedin
The University of Western Ontario

Supervisor
Dr. S. F. Asokanthan
The University of Western Ontario

Graduate Program in Mechanical and Materials Engineering
A thesis submitted in partial fulfillment of the requirements for the degree in Master of Engineering Science
© Nujhat Abedin 2014

Follow this and additional works at: https://ir.lib.uwo.ca/etd

Part of the Acoustics, Dynamics, and Controls Commons, and the Electro-Mechanical Systems Commons

Recommended Citation

Uncertainty Quantification for a Class of MEMS-based Vibratory Angular Rate Sensors

By

Nujhat <u>Abedin</u>

Graduate Program in Engineering Science

Department of Mechanical and Material Engineering

Submitted in partial fulfilment

of the requirements for the degree of

Master of Engineering Science

School of Graduate and Postdoctoral Studies

The University of Western of Ontario

London, Ontario, Canada

August 2014

© Nujhat Abedin 2014

ABSTRACT

Numerical schemes that are suitable for predicting response statistics of mass-spring and ring gyroscopes are developed when this class of vibratory gyroscopes are subjected to certain system parameters as well as environment uncertainties. The emphasis is placed on the steady-state part of the response since it is more critical to the operation of a gyroscope. A peak-picking approach which simulates the demodulation process which is used in practice is employed first before applying the Monte Carlo simulation method to predict the response statistics. A number of simulation trials to predict response statistics have been performed for mass-spring and ring-type gyroscopes in an effort to ascertain the optimal temporal points as well as sample paths for the impending uncertainty quantification study. Based on the optimal temporal and sample paths, uncertainties in input angular rate, mass/frequency mismatch and damping have been quantified.

Keywords: MEMS based gyroscope, General coordinate, Uncertainty quantification, Monte Carlo method, Numerical prediction, Ensemble mean, Mass mismatch, Frequency mismatch, Quality factor, Dynamic response.

ACKNOWLEDGEMENTS

The work is dedicated to my beloved mother Zinnat Zahanara

I am who I am because of my mom

Whatever I have achieved, I owe to my mom

Table of Contents

List of Tables

List of Figures

Nomenclature

Ω	Input angular rate (rad/sec)
v	Radial velocity (m/s)
F_r	Force in radial direction (N)
F_θ	Force in tangential direction (N)
r	Radial displacement mass-spring gyroscope (m)
m_p	Proof mass (non-dimensional)
C_x	Viscous damping constant along x-axis (Ns/m)
C_y	Viscous damping constant along y-axis (Ns/m)
k_x	Linear spring constant along x-axis (N/m)
k_y	Linear spring constant along y-axis (N/m)
F	Harmonic driving force (N)
ω_x	x-axis natural frequency (rad/sec)
ω_y	y-axis natural frequency (rad/sec)
Q	Quality factor (non-dimensional)
Q_x	x-axis quality factor (non-dimensional)
Q_y	y-axis quality factor (non-dimensional)
M	Mass matrix
G	Gyroscopic matrix
D	Damping matrix
K	Stiffness matrix

$\boldsymbol{q}$	Generalized coordinate vector
q_1	Generalized coordinate vector along x-axis (m) for mass-spring gyroscope
q_2	Generalized coordinate vector along y-axis (m) for mass-spring gyroscope
q_1, q_2	Generalized coordinates corresponding to the flexural mode for ring gyroscope
q_3, q_4	Generalized coordinates corresponding to the circumferential mode for ring gyroscope
$\overline{\Omega}$	Steady-state angular speed (rad/sec)
σ_1	Drift coefficient
σ_2	Uncertainty coefficient
a_d	Drift exponential coefficient
ξ	Damping ratio (non-dimensional)
ϑ	Frequency mismatch parameter (non-dimensional)
$\sigma_{response}$	Standard deviation of output response (m)
$\sigma_{f.mismatc\ h}$	Standard deviation of frequency mismatch (rad/s)
$\sigma_{q.mismatc\ h}$	Standard deviation of quality factor mismatch (non-dimensional)
$F_1(s)$	Laplace transform of $f_1(t)$
$Q_1(s)$	Laplace transform of $q_1(t)$
$Q_2(s)$	Laplace transform of $q_2(t)$
n	Number of modes (non-dimensional)

θ	Angle of separation between a set of degenerate modes (rad)
γ and κ_2	Constant (non-dimensional)
κ_1	Angular rate (rad/sec)
$\zeta(t)$	Random component (dependent on uncertain variable)
ω_{01}	Non-rotating ring natural frequency associated with the flexural generalized coordinates q_1 (rad/sec)
ω_{02}	Non-rotating ring natural frequency associated with the flexural generalized coordinates q_2 (rad/sec)
ρ	Density (Nickel) (kg/m^3)
E	Young's Modulus (Nickel) (N/m^2)
r	Mean Radius of ring (μm)
h	Radial Thickness of ring (μm)
b	Axial Thickness of ring (μm)
δ_m	Mass mismatch (non-dimensional)
$\sigma_{m.mismatc\ h}$	Standard deviation of mass mismatch (non-dimensional)
$\sigma_{d.mismatc\ h}$	Standard deviation of damping ratio mismatch (non-dimensional)

Chapter 1

1. Introduction and literature review

1.1. Introduction

MEMS (Micro-Electro-Mechanical Systems) based inertial sensors, namely the accelerometer and the gyroscope, have gained much attention in the past few years. These devices have found several useful engineering applications that include spacecraft orientation, vehicle stability control, navigation assist, vehicle roll over detection, image stabilization and cellular phones. Current MEMS gyroscopes are lighter and compact. They utilize less power and therefore, are considered to provide a cost-effective solution when compared to the moderately priced spinning-disk mechanical gyroscopes and the expensive Fiber-optic as well as Ring Laser gyroscopes.

The design methodologies for MEMS devices are based on deterministic approaches, where the input parameters, for example geometrical and physical properties are assumed to be known precisely. However, in practice, due to the batch-production processes used in MEMS fabrication as well as the micron-scale dimensions of the structural elements, consideration of uncertainties in system parameters and an understanding of their effects are warranted. Hence, the primary purpose of the present thesis is to develop a systematic process for uncertainty quantification based on the dynamic response.

All MEMS based gyroscopes that have been developed thus far are based on internal vibratory motion of structural elements housed within a gyroscope. In order to characterize uncertainties,

two types vibratory MEMS gyroscopes are considered in the present thesis, namely the mass-spring type vibratory gyroscope and the ring-type gyroscope. In order to predict response statistics, for both MEMS gyroscopes, in time as well as in the frequency domain, numerical schemes are developed from suitable mathematical models. In the interest of examining the effect of randomness on output responses, random inputs are introduced in the numerical schemes in the form of noise and drift terms. Monte Carlo method is employed in the simulations for predicting the response statistics. Based on these numerical schemes uncertainty quantification is performed via quantifying standard deviations of output responses, when both mass-spring and ring gyroscopes are subjected to parameter uncertainties. It is envisaged that this quantitative understanding will lead to improved performance of this class of gyroscopes.

1.2. Literature review

MEMS gyroscopes include the micromechanical and electronic parts which have been fabricated on a single chip (see, e.g., Geen at el., 2002 and Lai at el., 2009). For this class of gyroscopes, the batch production with low cost and high precision is a target in the future. The implementation used thus far for the MEMS gyroscopes utilize a vibratory configuration where the Coriolis effect is exploited for the precise sensing of angular rotation rates. Different types of micromachined structures can be used as the vibratory elements in the design of angular rate sensors, including prismatic beams, tuning forks, single or dual masses, disks, and rings (see e.g., Maluf, 2000).

Mechanical coupling between the drive and detection modes of a single mass-spring micro-machined-vibrating gyroscope was studied by Mochida, Tamura and Ohwada (2000) giving importance to the mechanical coupling. A suitable mathematical model for a dual axis gyroscope was proposed by Davis (2001). Davis represented an accurate model for the single mass-spring gyroscope by considering the coupling effect for both the driving and sensing axes.

Figure 1-1 shows a typical configuration for mass-spring gyroscope where the effective spring supports have been represented by the thin beams, and the mass situated in the middle is referred to as the proof mass which is capable of vibrating in the plane of the structure. This proof mass is subjected to oscillation in a plane along one axis (driving axis), and if the device is subjected to a rotational motion about an axis orthogonal to this plane, as a result of the Coriolis effect, the proof mass will tend to oscillate in the same plane along an axis referred to as the sensing axis which is orthogonal to the driving axis. The input angular rate can be determined by measuring the motion along the sensing axis.
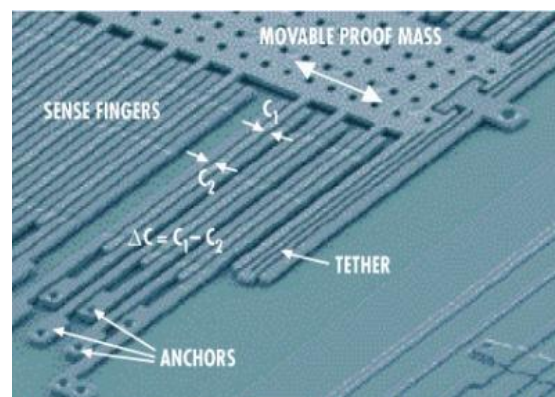
Figure 1- 1. Analog MEMS Vibratory Gyroscope (reproduced from Giunta at el., 2006)

Bifurcation behaviour of a single-axis mass-spring MEMS gyroscope has been studied by Wang (2009) considering nonlinear stiffness elements when the input angular rate of this system is subjected to a periodic angular speed fluctuation. Closed-form predictions of the bifurcation

paths for both sub-harmonic and combination resonance cases have been formulated and examined by employing the method of averaging as well as a numerical approach.

In the case of ring-type gyroscopes, models to study in-plane vibrations of a rotating ring has been developed and represented by Bickford and Reddy (1985). The effects due to shear deformation and rotary inertia for higher rotational speeds and for higher bending modes were demonstrated. Huang and Soedel (1987) also investigated the in-plane vibrations of rotating rings. In particular, variations of natural frequencies and mode shapes influenced by rotational speed and elastic supports were examined. The research presented by Putty and Najafi (1994) provided information of a vibrating ring gyroscope in which the ring structure is driven into resonance in the plane of the chip and provided suitable design details. Delphi reported about a vibratory ring gyroscope using electroplated metal to form a ring structure on top of complementary metal-oxide semiconductor (CMOS) chips (see, Sparks et al. 1999). A scanning electro-micrograph (SEM) of the device is shown in Figure 1-2. Semicircular springs support the ring and stored the vibration energy. The spring design has greater effect of packaging stresses on the sensor.
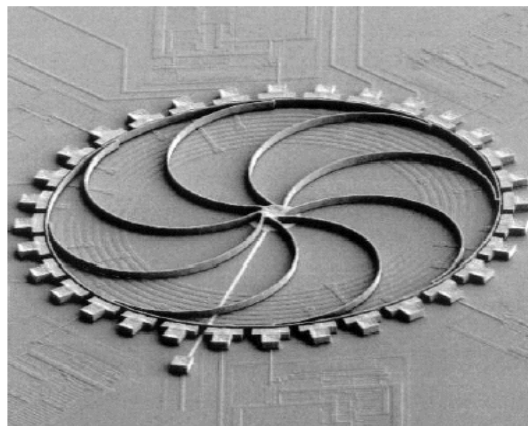
Figure 1-2. Delphi's metal ring gyroscope (reproduced from the website of Silicon Sensing Systems Japan Ltd.)

Ring gyroscope has balanced symmetrical structure which is less sensitive to environmental vibrations. Since two identical flexural modes of the structure are used to sense rotation, the sensitivity of the sensor is amplified by the quality factor of the structure. Ring gyroscope is less temperature sensitive while two flexural vibration modes are equally affected by temperature (see, e.g., Putty, 1995). However, the ring structure is known to be more resistive to ambient vibrations (see, e.g., Lee, et al, 2011).

A suitable mathematical model for examining the stability and response of a rotating ring perturbed by periodic fluctuations were developed by Cho (2004). For the purpose of investigating the dynamic behaviour of a ring gyroscope, the reduction of the equations of motion to a suitable discrete linear form is performed first. Under external excitation and body rotation, time and frequency responses for varying parameter values of damping and input angular rate with the effects due to ring asymmetry were quantified. The ring gyroscope model used in the present thesis is based on the above research.

The practical application of the Monte Carlo Simulation (MCS) method is based on the fact the next best situation to having the probability distribution of a certain random quantity is to have a corresponding large population. The execution process of the method consists of numerically simulating a population corresponding to the random quantities in the physical problem, solving the deterministic problem associated with each member of that population, and obtaining a population corresponding to the random response quantities. This population can then be used to get statistics of the response variables (see e.g., Ghanem and Spanos, 2012).

The Monte Carlo method is a quite versatile mathematical tool having the ability of handling situations where all other methods fail. The method has been known and used extensively in

various fields such as health care, agriculture, and econometrics. However, in engineering mechanics it has attracted intense attention only recently following the universal availability of low-cost computational systems. The computational availability has caused an interest in developing sophisticated and efficient simulation algorithms. Shinozuka and Jan (1972) have had a pioneering role in introducing the method to the field of engineering mechanics. Most of the applications of the MCS have been in the study of random variation of deterministic media (see e.g., Ghanem and Spanos, 2012). Generating samples to create the response surface is a very important part of the uncertainty quantification process and there are a number of ways to do it. Though one can again use the Monte Carlo approach, significant gains are to be had by sampling more intelligently (see e.g., Snow and Bajaj, 2010). In their study, MCS has also been successfully employed in understanding the uncertainty quantification in a MEMS switch. An efficient stochastic framework for quantifying the effect of stochastic variations in various design parameters on the performance of MEMS devices has been performed by Agarwal and Aluru (2009). The above two studies limit their analysis to static behavior as well as spatial co-ordinates.

Following the above research on the use of Monte Carlo Simulation to MEMS devices for uncertainty quantification, the research performed in the present thesis, unlike the previous studies focuses on the prediction of response statistics of MEMS gyroscopes based on the dynamic behavior.

1.3. Motivation

The application of MEMS vibratory gyroscopes are expanding from consumer electronics to aerospace and are now one of the most common MEMS products. In many applications, consumers demand MEMS gyroscopes that are reliable even in rough environments. Some of these harsh environments include high temperature, high humidity, high-G mechanical shock/drop, high mechanical vibration, high frequency acoustic noise, high radiation, high magnetic and electric field. In many applications like navigation and tracking, deep water energy exploration, down-hole drilling and high-temperature industrial applications, the MEMS gyroscope sensor experiences temperatures that are beyond the manufacturer's recommended temperature range. In this type of environment, the device is likely to be subjected to environmental uncertainties that may adversely affect the performance, reliability as well as durability. To investigate the performance characteristics of MEMS gyroscopes by using laboratory experiments to simulate the above environmental conditions usually expensive and time-consuming. Thus, a simulation approach is preferred.

A sensor such as a rate gyroscope can directly measure the angular velocity of a rotating body without a need for processes such as integration (of angular acceleration) or differentiation (of angular displacement). In general, the performance level of gyroscopes can be classified into three different categories: rate-grade, tactical-grade and inertial-grade. The inertial grade can be considered as the most accurate and sensitive while the other two classes are listed in the order of lower accuracy and sensitivity. Until now, although many types of micro-machined vibratory gyroscope have been proposed and developed as inertial sensors, to date the performance level of these sensors barely achieved the rate-grade. MEMS gyros are generally not considered

appropriate for long-term operations or for a signal integration process since they possess significantly high drift error as well as noise. Thus, it is clear that many challenges are ahead for the design of MEMS gyros in order that their performance levels can be increased to those offered by conventional rate-grade gyros, and to achieve tactical and inertial-grade performance level (see e.g., Cho, 2004). Drift and noise are random in nature and to predict the effects of drift on MEMS gyroscope one of the appropriate ways is to employ the Monte Carlo method to numerically simulate the response of MEMS gyroscopes using suitable mathematical models.

The manufacturing tolerances in MEMS are notoriously poor and additionally the effects that parameters variations have on device behaviour are poorly understand. The result is that gyroscope performance and life time are difficult to control or predict. Understanding the effects of these deviations is important for predicting the ranges of performance exhibited by a manufactured product can vary significantly from that of the nominal design. Uncertainty Quantification also permits prediction of device yield and is a first step towards predicting gyroscope lifetime.

In order to address some of the limitations proposed above, an uncertainty quantification study is proposed. Extensive studies on the dynamics and uncertainty quantification of different system as well as environmental parameters associated with MEMS inertial sensors, it is envisaged that the design process and performance of these devices can be improved further.

1.4. Aims of the thesis

The primary intent of the present thesis is to predict dynamic response behaviour of mass-spring as well as ring gyroscopes when subjected to an angular motion and perform an uncertainty quantification study for quantifying the effect of parameter uncertainties. To this end, Monte Carlo simulation is used to compute the response statistics as well as for determining a suitable measure. To date, a systematic procedure for performing this analysis is not available, hence the results and the procedures to be developed is envisaged to pave the way towards future research in this area. To achieve this objective, the following steps are considered:

- Develop a numerical scheme based on a suitable mathematical model for systematic characterization of mass-spring gyroscopes giving emphasis to uncertainty quantification.

- Develop a numerical scheme based on a suitable mathematical model for systematic characterization of ring gyroscopes giving emphasis to uncertainty quantification.

- Develop a systematic process to illustrate the optimal temporal as well as sample paths for predicting output statistics in time domain as well as frequency domain via Monte Carlo method for both types of gyroscopes.

- Perform uncertainty quantification analysis for mass-spring gyroscope based on output response statistics in time domain as well as in the frequency domain when the system is subjected to uncertainties in angular rate, quality factor and frequency mismatch. A suitable measure for characterizing this uncertainty is also expected.

- Perform uncertainty quantification analysis for ring gyroscope based on output response statistics in time domain as well as in the frequency domain for varying parameter values

of input angular rate, damping ratio and mass mismatch. A suitable measure for characterizing this uncertainty is also proposed.

1.5. Thesis Outline

This thesis mainly focuses on two types of gyroscopes namely, the mass-spring gyroscope and the ring-type gyroscope. It may be noted that the methodology applied for both types of gyroscopes are the same and for this reason readers will find similarities in paragraphs, sentences and phrases in *Chapters 2* and *4*, and also in *Chapters 3* and *5*.

In *Chapter 2*, a mathematical model for the mass-spring gyroscope for the purposes of dynamic response predictions are introduced and discussed. When the gyroscope is subjected input angular rotation, dynamic response analysis is performed to characterize the dynamic behavior of mass-spring system in time domain via suitable numerical schemes. Time response analyses are preformed, and are examined for cases without and with drift. Monte Carlo simulation method is applied to achieve optimal characteristics for the output response statistics which are suitable for further analyses.

Chapter 3 discusses briefly the results obtained via the numerical simulations performed in the previous chapter for the mass-spring gyroscope. The effect of varying input angular rate, frequency/stiffness mismatch and quality factor for the mass-spring gyroscope due to presence of noise and drift in the system are obtained and discussed. This analysis forms the basis for the uncertainty quantification study based on the response statistics and are expressed in terms of the input and the output standard deviation. Uncertainty quantification in the frequency domain is

examined next and the results are discussed in terms of the peak magnitude statistics associated with amplitude ratio as well as the forced response.

In *Chapter 4*, a mathematical model for the ring-type gyroscope for the purposes of dynamic response predictions are introduced and discussed. When the gyroscope is subjected input angular rotation, dynamic response analysis is performed to characterize the dynamic behavior of mass-spring system in time domain via suitable numerical schemes. Time response analyses are preformed, and are examined for cases without and with drift. Monte Carlo simulation method is applied to achieve optimal characteristics for the output response statistics which are suitable for further analyses.

Chapter 5 discusses briefly the results obtained via the numerical simulations performed in the previous chapter for the mass-spring gyroscope. The effect of varying input angular rate, mass mismatch and quality factor for the ring gyroscope due to presence of noise and drift in the system are obtained and discussed. This analysis forms the basis for the uncertainty quantification study based on the response statistics and are expressed in terms of the input and the output standard deviation. Uncertainty quantification in the frequency domain is examined next and the results are discussed in terms of the peak magnitude statistics associated with amplitude ratio as well as the forced response.

Chapter 6 presents the conclusions based on the response and uncertainty quantification results for the mass-spring and ring-based vibratory angular rate sensors, along with contributions, and recommendations for further research.

Chapter 2

2. Dynamic Response Analysis for Mass-Spring Gyroscopes

2.1.   Introduction

In this chapter, numerical schemes that are suitable for simulating the time-domain dynamic behavior of mass-spring type vibratory gyroscopes are developed. These schemes are intended for the purpose of uncertainty quantification and, in particular, for the purpose of predicting the dynamic behavior of this class of devices under uncertain environment as well as system parameters. To this end, a mathematical model is used to represent the dynamic behavior of a translation-based single-axis mass-spring gyroscope and in particular a model presented by Davis (2001) is adopted. For the purposes of characterizing the behavior due to uncertain system as well as environmental parameters of mass-spring type gyroscopes, steady state portion of transient responses are employed. In order to examine the effects of randomness on the MEMS gyroscope response, Monte Carlo simulation method is used for estimating the ensemble mean as well as the standard deviation (measure of variance) of response samples. The propagation of mean and standard deviation are investigated so that optimal as well as robust sampling strategies can be developed based on the simulated dynamic responses. These strategies as well as suitable sample selections form the basis of further uncertainty quantification to be performed in chapter 3 for the mass-spring type gyroscopes.

2.2. Model description

Mass-spring gyroscope model used in the present thesis is based on the equations developed by Davis (2001) and later presented in the work by Tianfu Wang (2004) and Ye Tian (2005). The gyroscope configuration consists of a lumped point mass (proof mass) at the center and four springs that support the mass as shown in Figure 2-1. It may be noted that the proof mass type general configuration can represent several practical vibrating gyroscope designs that have been used in MEMS fabrications. In order to achieve maximum sensitivity, this gyroscope is excited at a resonant drive frequency, along the x-axis in steady-state (driving direction), while the input angular rate Ω is introduced along the z-axis (input axis) which is orthogonal to the driving axis. Owing to the Coriolis effect that result from velocity along the x-axis and frame rotation rate Ω along the z-axis, the lumped proof mass oscillates along the direction of y-axis which is referred to as the sensing axis. It may be noted that the mass is confined to oscillate in the x-y plane at all times and the steady oscillatory motion along the sensing axis is used as a basis for the measurement of the angular rate ' Ω '.
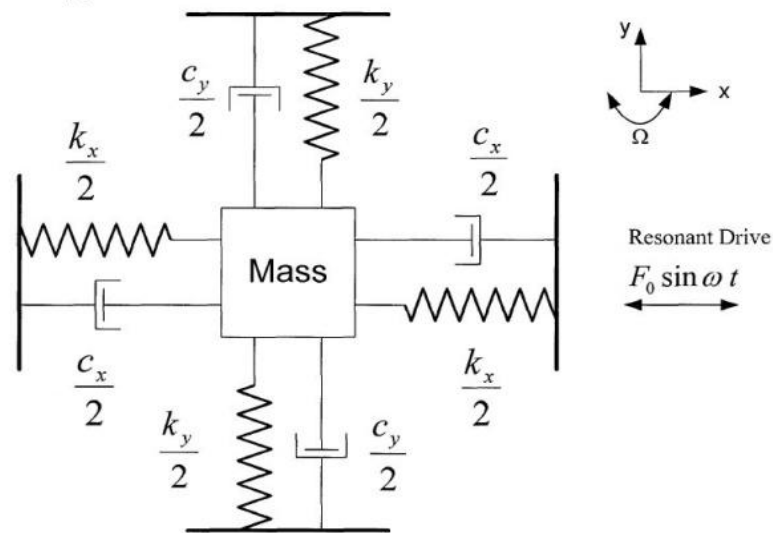
Figure 2-1. Translation-based single-axis vibratory gyroscope

13

2.3. Equations of Motion

It is known that Coriolis acceleration plays a significant role in governing the dynamics of this class of gyroscopes that are of interest to the present thesis. A rigid body is considered to be subjected to Coriolis acceleration when it moves with a velocity with respect to a rotating frame of reference. If a body of mass m is considered to move along the x-axis with a velocity v, this acceleration component is represented as $2\Omega \times v$, where the body fixed-frame x-y-z rotates at an angular velocity Ω about a fixed frame of reference (inertial frame) X-Y-Z as shown in Figure 2-2.
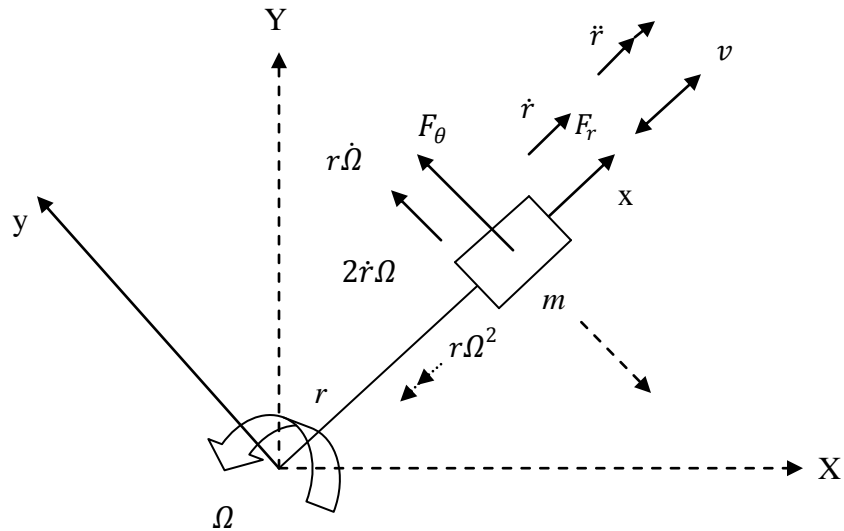
Figure 2-2. Motion of a particle in body-fixed frame that rotates relative to an inertial frame

Equations that govern the motion of this body when subjected to forces F_r and F_θ in the directions shown in Figure 2-2 can be derived as: $m(\ddot{r} - r\Omega^2) = F_r$, $m(r\dot{\Omega} + 2\dot{r}\Omega) = F_\theta$. The $r\Omega^2$ term represents the centripetal acceleration, while the $2\dot{r}\Omega$ term represents the Coriolis acceleration in accordance with the vector product $2\Omega \times v$ described earlier. The terms $\ddot{r}$ and $\dot{\Omega}$, respectively, are the radial and tangential acceleration.

Based on a linear model that represents a harmonically excited gyroscopic system by Wang and Asokanthan (2009), the homogenous system of equations that represent the free motion is formulated as follows

$$m\ddot{x} + C_x\dot{x} + k_x x - m\Omega^2 x - 2m\Omega\dot{y} - m\dot{\Omega}y = 0, \tag{2.1}$$

$$m\ddot{y} + C_y\dot{y} + k_y y - m\Omega^2 y + 2m\Omega\dot{x} + m\dot{\Omega}x = 0, \tag{2.2}$$

where x, y represent the system generalized coordinates, while m represents the proof mass. k_x and k_y denote the linear spring constants while C_x and C_y are the viscous damping constants. Here, the gyroscope is considered to be subjected to an input angular rate Ω about the Z-direction. It may be noted that the motion along the z-axis is decoupled from the motion along x and y axes and hence are not considered to be important for the present analysis.

When the gyroscope is subjected to a harmonic force $F = F_0 \sin \omega_x t$ along the driving direction (i.e., x-axis), the equations of motion for this gyroscopic configuration can be obtained as

$$\ddot{x} + \frac{\omega_x}{Q_x}\dot{x} - 2\Omega\dot{y} + (\omega_x^2 - \Omega^2)x - \dot{\Omega}y = \frac{F_0}{m_p}\sin \omega_x t, \tag{2.3}$$

$$\ddot{y} + 2\Omega\dot{x} + \frac{\omega_y}{Q_y}\dot{y} + \dot{\Omega}x + \left(\omega_y^2 - \Omega^2\right)y = 0, \tag{2.4}$$

where F_0 represents the excitation force magnitude, m_p the mass of the gyroscope proof-mass while ω_x and ω_y represent, respectively, the undamped natural frequencies associated with the x and y directions. The quality factors representing damping in the x and y directions are denoted

by Q_x and Q_y while Ω represents the angular rate of the rotating frame of reference, which is essentially the angular rate signal to be sensed by the gyroscope.

The governing equations (2.3) and (2.4) can then be written in matrix form as follows:

$$M\ddot{\boldsymbol{q}} + (G + D)\dot{\boldsymbol{q}} + K\boldsymbol{q} = F \tag{2.5}$$

where, $\boldsymbol{q} = [x\ y]^T = [q_1\ q_2]^T$ represents generalized coordinate vector, and the system matrices are defined as

$$M = \begin{bmatrix} 1 & 0 \\ 0 & 1 \end{bmatrix}, G = \begin{bmatrix} 0 & -2\Omega \\ 2\Omega & 0 \end{bmatrix}, K = \begin{bmatrix} \omega_x^2 - \Omega^2 & 0 \\ 0 & \omega_y^2 - \Omega^2 \end{bmatrix}, \tag{2.6}$$

$$D = \begin{bmatrix} \dfrac{\omega_x}{Q_x} & 0 \\ 0 & \dfrac{\omega_y}{Q_y} \end{bmatrix}, F = \begin{bmatrix} \dfrac{F_0}{m_p} \sin \omega_x t \\ 0 \end{bmatrix}, \tag{2.7}$$

with

$$\omega_x^2 = \frac{k_x}{m}, \ \omega_y^2 = \frac{k_y}{m}, Q_x = \frac{m\omega_x}{c_x}, \ Q_y = \frac{m\omega_y}{c_y}.$$

Equations (2.5) are employed for the purposes simulating the time response analysis for fixed system parameter values which is described in the following section. In addition these equations are also suitably modified to accommodate uncertainties via random variation of parameters to aid uncertainty quantification. The uncertainty results are presented partly in this chapter and in detail in Chapter 3.

2.4. Simulation of Deterministic Time Response

2.4.1. Introduction

In the present chapter, in order to investigate the dynamic characteristics of mass-spring gyroscope time response analysis is performed considering the mathematical model derived in the previous section. The time response analysis is then performed assuming that the mass is excited with a periodic external force in which the excitation frequency is set to be the same as the natural frequency associated with a non-rotating system so that the system gain can be maximized. It may be noted that the natural frequency variation with the input angular rate has been marginal and hence this choice for the excitation frequency is considered to have minimal influence on resonance. The dynamic effects due to variation of typical parameters of a MEMS mass-spring gyroscope are examined via numerical simulations and are depicted via suitable transient response plots. Results for the varying system parameters such as the input angular rate, damping and frequency/stiffness mismatch are then presented.

2.4.2. Numerical Simulations

In a mass-spring gyroscope, it is assumed that the mass-spring element is excited by a harmonic external force while the gyroscope as a whole is subjected to an angular rate that is measured. When the system is under the influence of typical input signals it is useful to perform a dynamic response analysis for the mass-spring system. For this purpose, a numerical simulation procedure is developed. This procedure forms the basis of Uncertainty Quantification to be

performed later in Chapter 3. The simulation is performed via the fourth-order Runge-Kutta scheme available within the MATLAB computing environment.

Typical parameters associated with a MEMS-based mass-spring type gyroscope are considered as shown in Table 2-1, for the purpose of numerical simulations.

Table 2-1. Parameters of Mass-spring Gyroscope for the Numerical Simulations

Proof mass	$m_p = 3.6 \times 10^{-10} \ (kg)$
x-axis natural frequency	$\omega_x = 164536 \ (rad/sec) \approx 26.2 \ (kHz)$
y-axis natural frequency	$\omega_y = 164536 \ (rad/sec) \approx 26.2 \ (kHz)$
x-axis quality factor	$Q_x = 1000$ (non-dimensional)
y-axis quality factor	$Q_y = 1000$ (non-dimensional)

The equations of motion (2.3) and (2.4) are written in the first order form that is suitable for numerical integration of the ODE's as follows:

$$\dot{q}_1 = q_3, \tag{2.8a}$$

$$\dot{q}_2 = q_4, \tag{2.8b}$$

$$\dot{q}_3 = -(\omega_x^2 - \Omega^2)q_1 + \dot{\Omega}q_2 - \frac{\omega_x}{Q_x}q_3 + 2\Omega q_4 + \frac{F_0}{m_p}\sin\omega_x t, \tag{2.8c}$$

$$\dot{q}_4 = -\dot{\Omega}q_1 - (\omega_y^2 - \Omega^2)q_2 - 2\Omega q_3 - \frac{\omega_y}{Q_y}q_4, \tag{2.8d}$$

Equations (2.8) are implemented in MATLAB and fourth order Runge-Kutta scheme is employed for integrating the set of ODE's. System parameter listed in Table 2-1 has been used in the simulations while the two natural frequencies ω_x and ω_y along the *x*-axis and *y*-axis respectively are considered to be identical first to examine the behavior in the absence of frequency/stiffness mismatch. The ODE45 integration routine has been found to be suitable for the numerical simulations, with initial conditions set to be zero and the value of time step is set to be 0.00001 seconds.

2.4.2.1. Time response without input angular motion

When the mass-spring system is subjected to harmonic excitation without any input angular motion (Ω=0 rad/sec), the response of the mass-spring gyroscope along the driving direction is achieved numerically and the results are illustrated in Figure 2-3 (a). It can be seen that the vibration amplitude of the proof mass reaches a steady-state after about 0.04 seconds from the commencement of the excitation. On the other hand, the response of the mass-spring gyroscope along the sensing direction is zero as shown in Figure 2-3 (b) as there is no input angular motion.
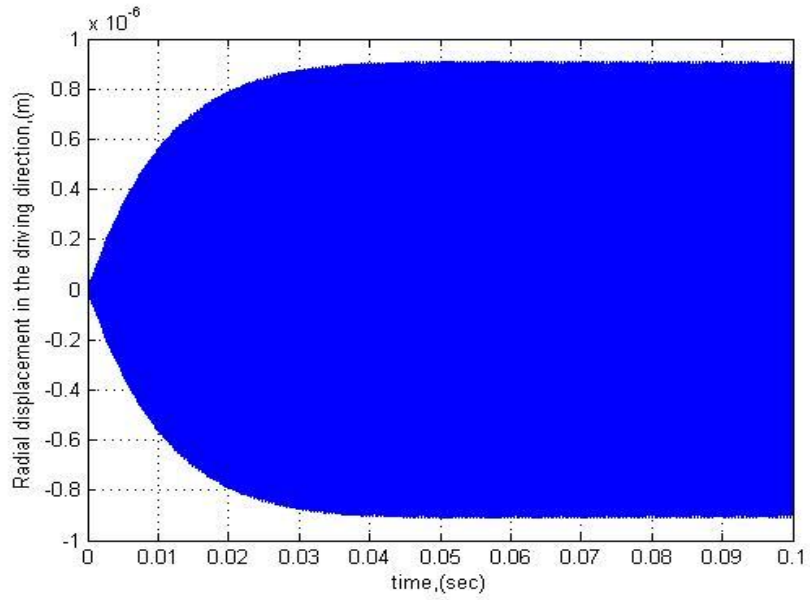
(a)
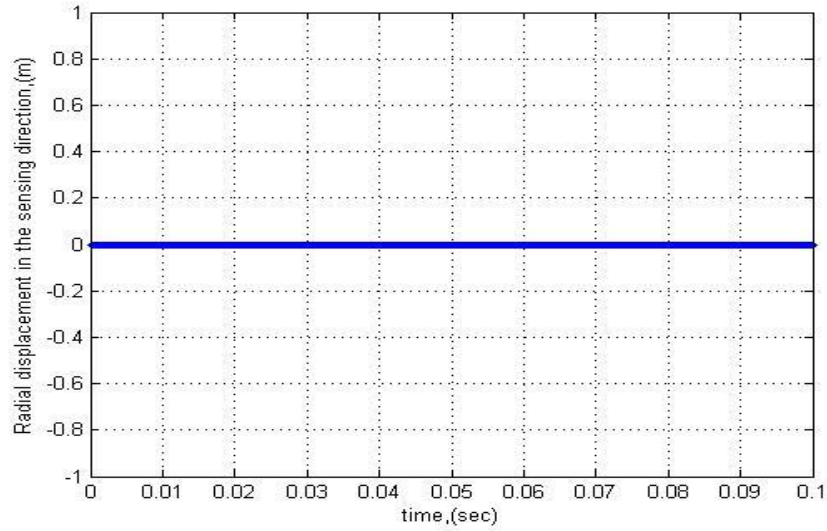
(b)

Figure 2-3. Radial displacement in the (a) driving direction and (b) sensing direction without input angular rate

2.4.2.2.   Time response with input angular motion

It has been shown that the variations of natural frequencies with the input angular rates are significantly small in the low speed range (i.e., less than 2π rad/sec) for which typical mass-spring gyroscopes are designed (Cho, 2004). Hence, the excitation frequency ω can be assumed to be constant and to coincide with one of the two non-rotating natural frequencies (say ω_x associated with the generalized coordinate x).

In order to examine the response of the mass-spring gyroscope associated with the generalized coordinate q_2 (sensing direction), a suitable profile for the input angular rate must be applied. In the present analysis, this profile is assumed to start from a zero value and reach a steady-state angular speed $\overline{\Omega}$ via a smooth increase in speed as depicted in Figure 2-4. The equation used to represent an input angular rate profile that represents a smooth increase in the angular rate has been chosen to be

$$\Omega = \frac{n\pi}{2}\sin\left(\frac{\pi t}{0.005} - \frac{\pi}{2}\right) + \frac{n\pi}{2} \qquad \text{for } t < 0.005 \tag{2.9}$$

At time $t = 0.005$ seconds the input angular rate time-profile is set to reach the steady-state. Different steady-state angular speeds can be used to investigate the dynamic response for mass-spring gyroscopes, such as $\overline{\Omega} = \pi, 2\pi, 5\pi, 8\pi, 10\pi$ etc.
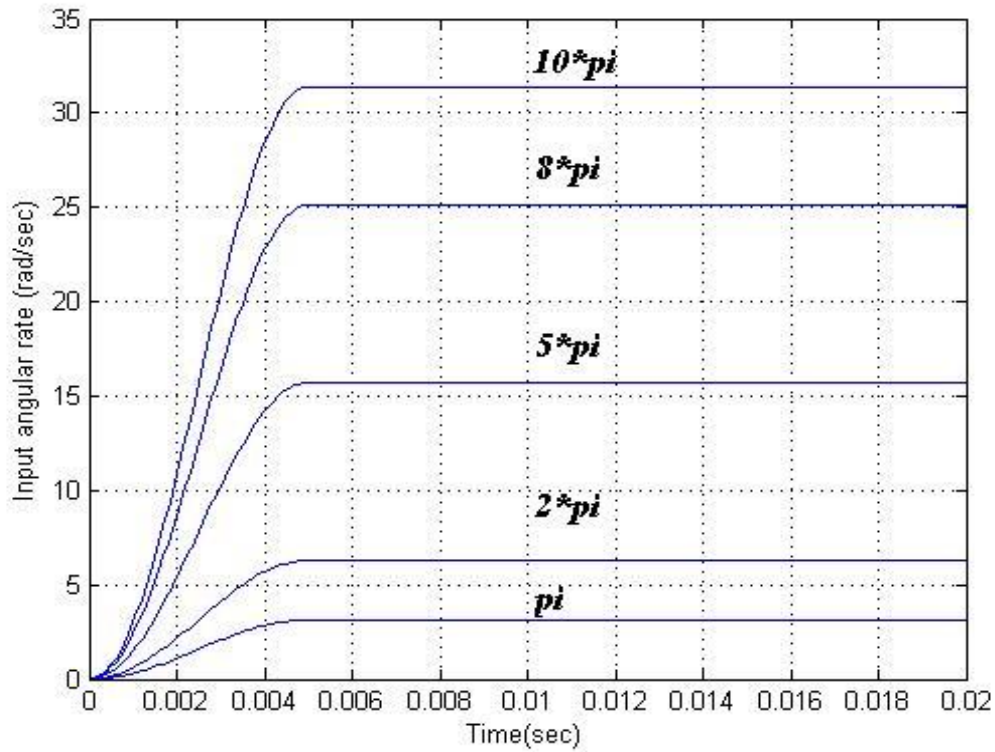
Figure 2- 4. Input angular rate time-profile

In this chapter, a steady-state angular speed of $\overline{\Omega} = 2\pi$ has been chosen for the purpose of illustrating typical dynamic responses. When both the input angular motion and the harmonic excitation are introduced simultaneously, the time responses of the system in the driving and the sensing directions, respectively, are shown in Figures 2-5 (a) and (b).
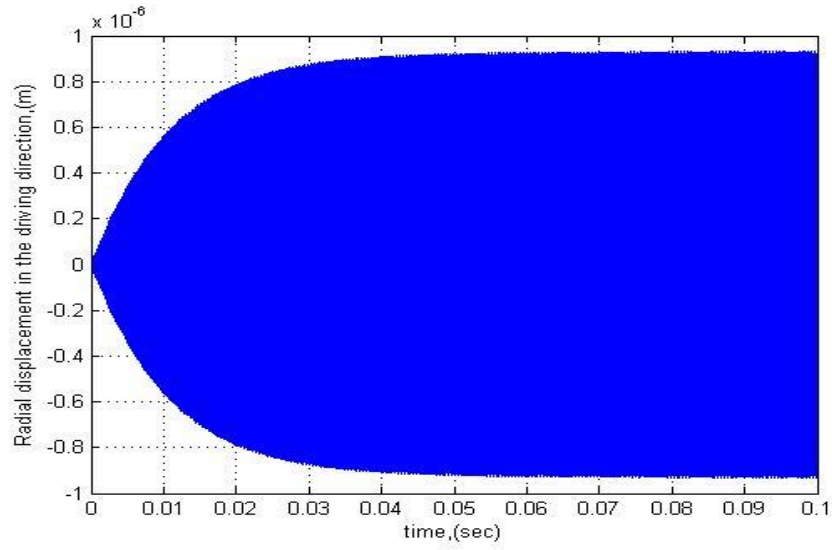
(a)
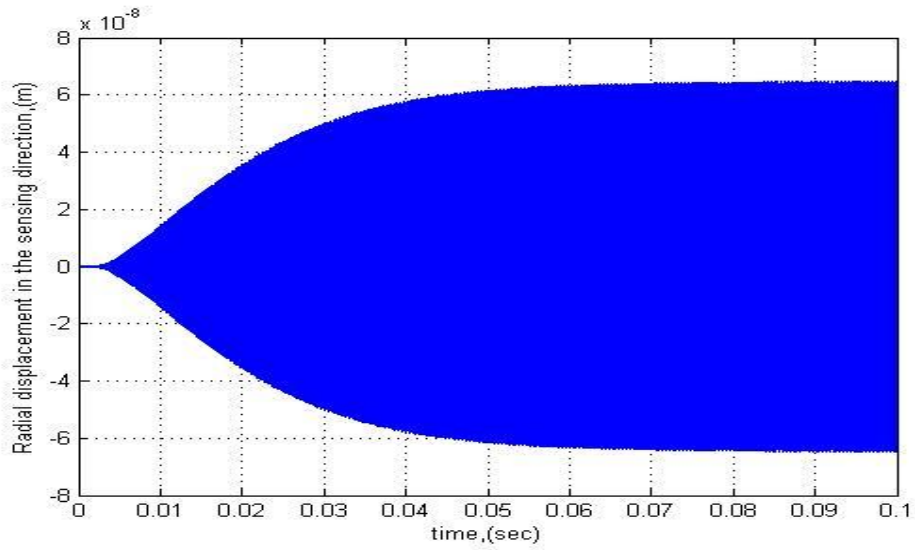
(b)

Figure 2-5. Radial displacement in the (a) driving direction and (b) sensing direction with $\overline{\Omega} = 2\pi$ rad/sec input angular rate

2.4.2.3. Frequency mismatch

Owing to the uncertainties present in the MEMS fabrication process, it is impossible to obtain equal stiffness for the suspension elements in the x-y direction. This will manifest in the system as a frequency mismatch for the driving and sensing motion. Hence, this form of frequency/mass mismatch is considered as one of the important parameters that affect the system dynamics significantly. Hence, the effects of frequency mismatch on the time response of the mass-spring gyroscope are examined in this section. Figures 2-6 (a) and (b) show the response amplitudes for the mass-spring system in the driving and sensing directions until t=0.1 seconds. It may be noted that although the simulation was performed for 0.2 seconds, for the purpose of clear demonstration of the transient part of the response, only the response until 0.1 seconds has depicted in the figures. As illustrated in Figure 2-6 (b), a reduction in the response in the sensing direction is evident when the frequency mismatch of the vibratory system is increased. It may be noted that this reduction can be detrimental to the achievable performance of this forms of gyroscopes, e.g., it can lead to lower sensitivity for the angular rate sensor. Comparison of the corresponding steady state responses in the driving and sensing directions indicate that this mismatch causes relatively larger reductions in the response in the sensing direction. Further, uncertainty propagation of the parameter can be considered to be important and forms a basis for one of the uncertainty quantification study which is presented in Chapter 3.
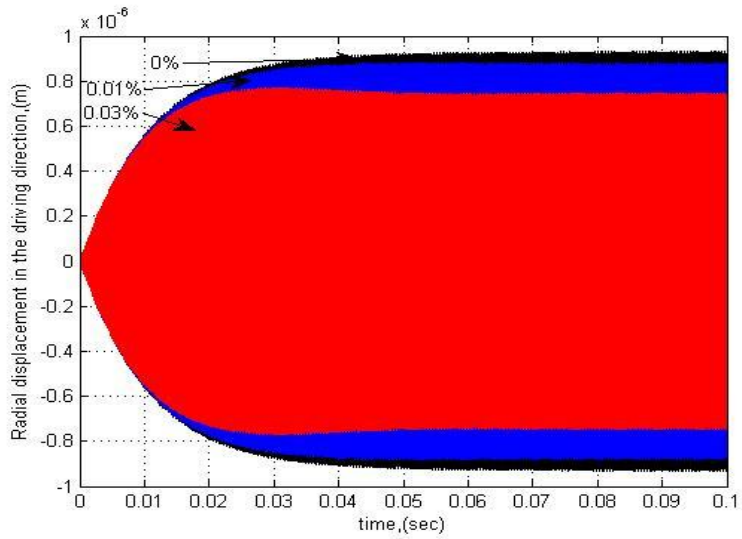
(a)
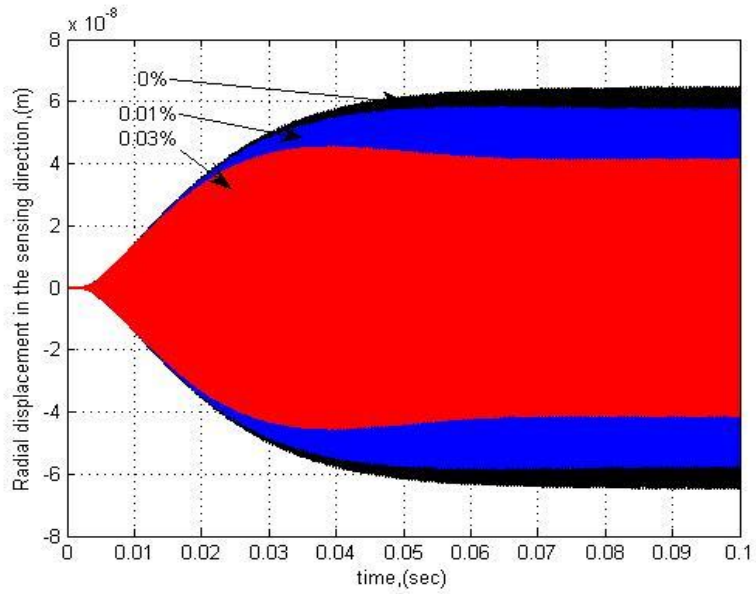
(b)

Figure 2-6. Variation of radial displacement in the (a) driving direction and (b) sensing direction when frequency mismatch values change from 0 to 0.03% while one frequency is fixed another is changing for $\overline{\Omega} = 2\pi$ rad/sec input angular rate

2.5. Simulation of Random Time Response

2.5.1. Introduction

In the present study, to see the effect of randomness and drift due to input angular rate and certain important parameters of MEMS mass-spring gyroscope model, a drift noise model is assumed in the form of an equation as

$$d_d = \sigma_1(e^{a_d t} - 1) + \sigma_2 \zeta(t) \tag{2.10}$$

This model consists of two parts. The first part represents the drift, which is an exponential term, while the second part denotes the uncertainty, which is a random component. In order to obtain the typical drift rate from equation (2.10), the drift exponential coefficient a_d is set at a value 1.0 and the drift coefficient σ_1 is set at a value 0.0245. Uncertainty coefficient σ_2 is chosen to be 0.001.

For the present study, the model presented via Equation (2.10) is to represent additive noise and drift to the nominal input angular rate Ω. Hence, the input angular rate takes the form:

$$\Omega = \Omega + d_d \tag{2.11}$$

The drift/noise model presented in equation (2.10) is also employed for representing uncertainties in other system parameters such as mass/frequency mismatch, and quality factor/damping ratio.

2.5.2. Monte Carlo Simulation

As MEMS gyroscopes are developed using micro manufacturing technologies, micro scale products usually have a relatively large manufacturing uncertainties compared to normal macro scale products. Reduction of the variance of material properties as well as the geometric properties of a micro scale product is quite expensive. The geometric and materials uncertainties caused by a micro manufacturing process inevitably lead to the uncertainty of the product performance. Therefore, to achieve a reliable design of a product, the performance uncertainty of the product, which is often expressed by the variance or standard deviation, needs to be estimated in a reliable way. Estimated standard deviation may prove to be useful in quantifying the quality of the manufacturing product prior to determining the quality via testing of product samples. Here, Monte Carlo simulation is used to aid prediction of the effects of uncertainties so that metrics for the response standard deviation can be quantified.

Monte Carlo methods may vary from system to system but it has obviously followed a particular pattern, such as, determination of a input domain, generation of random inputs with a probability distribution, calculation of the results for many samples of the inputs and prediction of a suitable measure of response statistics. Monte Carlo simulation relies on the process of precisely representing uncertainties by specifying inputs as probability distributions. If some of the inputs to a system are uncertain, the future performance must also be uncertain. That is, the result of any analysis based on inputs represented by probability distributions is itself a probability distribution.

Every Monte Carlo simulation starts off with developing a deterministic model which closely resembles the real scenario. In this deterministic model, performance is predicted when

nominal values (or the base case) of the input parameters are used. Mathematical relationships are applied using the nominal values of the input variables, and transformed into the desired output. After adequate performance from the deterministic models is predicted, the risk components are added to the model. As mentioned before, since the risks originate from the stochastic nature of the input variables, these variables are generated from suitable distributions. A set of random numbers (also called random variates or random samples) are generated from these distributions after identifying the underlying distributions. One set of random numbers, consisting of one value for each of the input variables, will be used in the deterministic model, to provide one set of output values. Then this process needs to be repeated to generate more sets of random numbers, one for each input distribution, different sets of possible output values must be collected. This part is the core of Monte Carlo simulation (see e.g., Raychaudhuri, 2008).

In this case input angular rate $\mathbf{\Omega}$ has been considered as a sample which contains the random component $\zeta(t)$ is presented in Figure 2-7. Monte Carlo method has been applied for many samples of input angular rate $\mathbf{\Omega}$. Owing to the presence of randomness, the simulations are run repeatedly for randomly generated values for $\mathbf{\Omega}$. As a result, many several samples of output responses are obtained for further analysis and the examination of useful measures of response statistics forms the basis of the uncertainty quantification.

When the mass-spring system is subjected to uncertainties in input angular rate (Ω), frequency (ω_y) and quality factor (Q_y), randomness is usually incorporated in those parameters and Monte Carlo simulation is used to generate many output samples that correspond to uncertain input parameters.

2.5.3. Robustness of simulation

2.5.3.1.　　Stochastic response simulation after peak-picking

As demonstrated in section 2.4.2.2, the output time response in the sensing direction contains two parts, namely transient and steady-state. The transient part of the time response changes with time until it reaches the steady state. Since the steady-state part of the response is more critical to the operation of a gyroscope, this part has been chosen for applying the Monte Carlo method. Further, the high frequency oscillatory motion has been removed via a suitable peak-picking method. Peak-picking method is employed to find peak values of an oscillating response. There are several processes to do peak-picking and in the present thesis, MATLAB command 'findpeaks' is used to get peak values of the responses. The purpose of going through this step is to simulate the demodulation process that is used in practice as part of MEMS-gyroscope signal processing elements. This approach aids in quantifying the variation of the mean values and the standard deviation of the steady state of time response along the sensing direction. After peak-picking and the removal of the transient part, the resulting response is used to characterize and predict response statistics via Monte Carlo method. The plot that represents this response is illustrated in Figure 2-7 where the last sample point which is approximately 13,000 coincides with 0.5 seconds. In the next sections, an attempt will be made to justify the prediction of responses via selection of suitable time/ensemble response statistics.
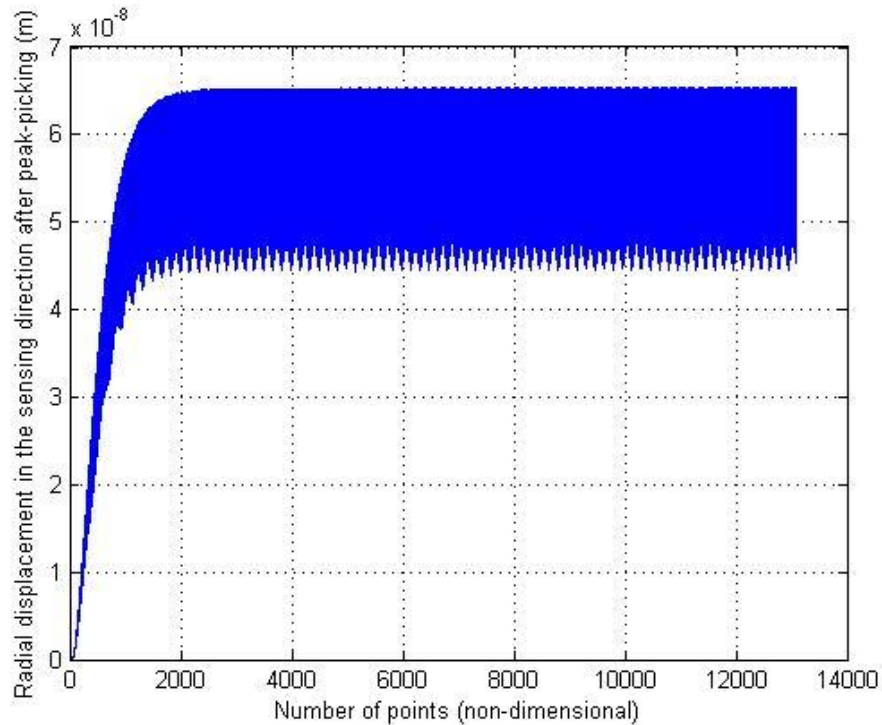
Figure 2-7. Time response after peak-picking for mass-spring gyroscope ($\Omega=2\pi$ rad/sec)

2.5.3.2. Optimal number of points along time response

Before performing the uncertainty quantification, it is important to come up with a suitable set of data that exhibits consistence and convergence for the response statistics. For this purpose, number of samples along the time axis as well number samples along the sample paths have been considered. In this chapter, various time data sets as well as ensemble data sets have been considered to establish a robust scheme for predicting useful response statistics. This has been achieved primarily via examining the temporal mean, temporal standard deviation, ensemble mean and ensemble standard deviation.

The ensemble average of a repetitive response is defined by defining a time for each path, creating the ensemble of time varying signals referenced to that time and then averaging across this ensemble at this time instant.

An attempt is made to define the number of points along the time axis which can be used for the application of Monte Carlo method based on the numerical simulation. After peak-picking and the removal of the transient, the first 100 points along the remaining steady state response shown in Figure 2-7 has been considered first. These 100 points have been used to determine the temporal mean and standard deviation. This process is considered with increments of 100 points up to 6000 points. This process is performed for cases without and with the drift, keeping the noise component the same.

Figures 2-8 and 2-9, respectively, illustrate the results for the temporal mean and the standard deviation. These figures also illustrate that, reasonable convergence will be achieved after 2000 points which are considered for further analysis in predicting mass-spring gyroscope response statistics. Figures 2-8 and 2-9 also illustrate the effect of increasing drift on the response statistics. Hence, an alternate approach is warranted for predicting the response statistics for highlighting the noise term.
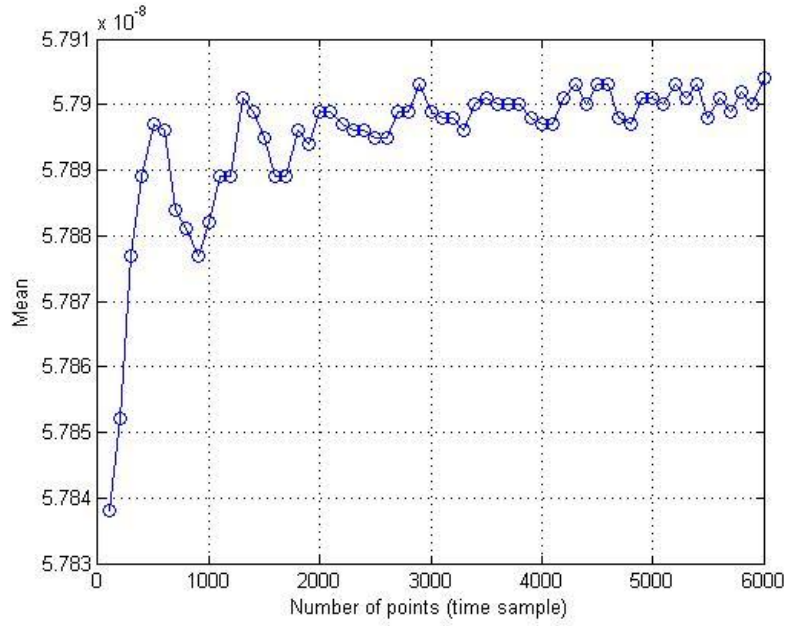
(a)
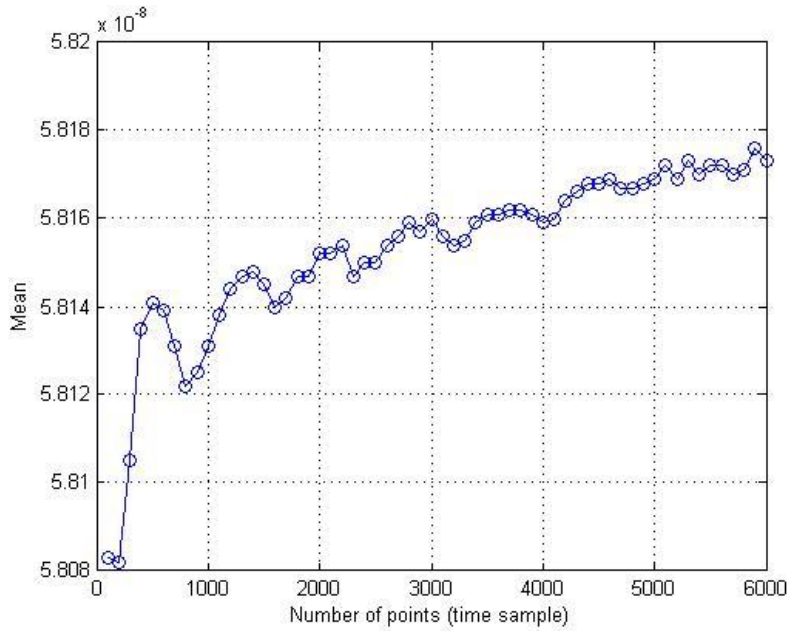
(b)

Figure 2-8. Number of points (time) vs. Mean along the time response for mass-spring gyroscope (a) without drift (b) with drift ($\Omega = 2\pi$ rad/sec)
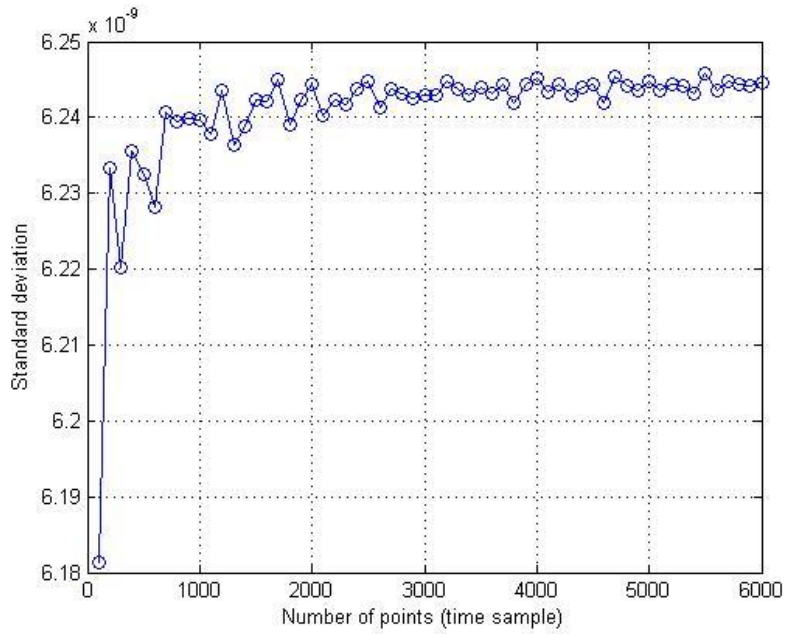
(a)
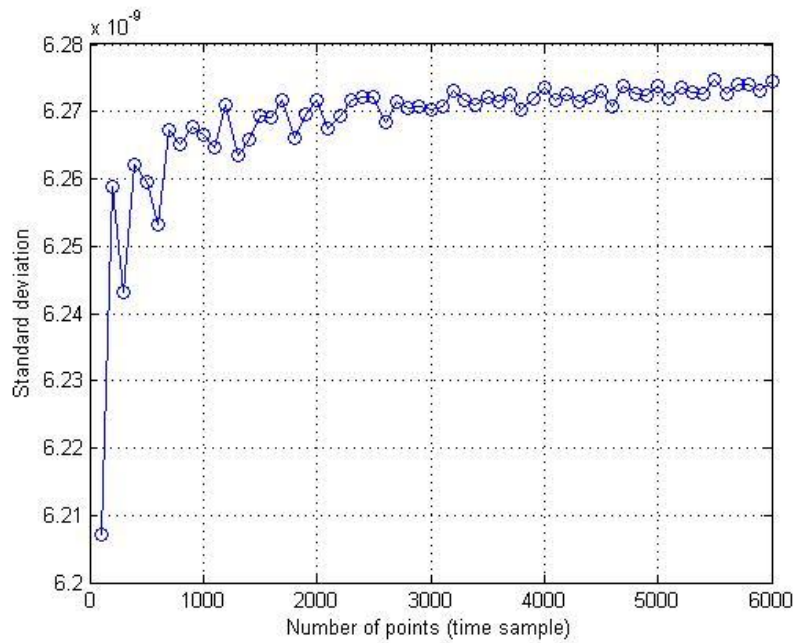
(b)

Figure 2-9. Number of points vs. standard deviation along the time response for mass-spring gyroscope (a) without drift (b) with drift ($\Omega=2\pi$ rad/sec)

The statistical response predictions performed in the previous section confirms the significance of considering time sample points past the 2000 points based on both the mean and standard deviation. In order to ascertain the predictions via the sample paths, 100 random samples have been employed. The sample paths are depicted in Figure 2-10.

Employing the 100 samples, the ensemble mean as well as the standard deviations are computed. Figures 2-11 (a) and (b), show the ensemble mean without and with drift. Figures 2-11 (a) and (b) show that reasonable consistency for ensemble mean without drift is obtained for any points after 3600 points and ensemble mean with drift shows no consistency. This may be attributed to the effect of increasing drift on the response. However, the predictions made for the standard deviations for the response are illustrated in Figures 2-12 (a) and (b). These figures demonstrate that after 3900 points in cases without and with drift standard deviation values show a converging trend and points past the 3900 mark may be considered suitable for further analysis in predicting response statistics.
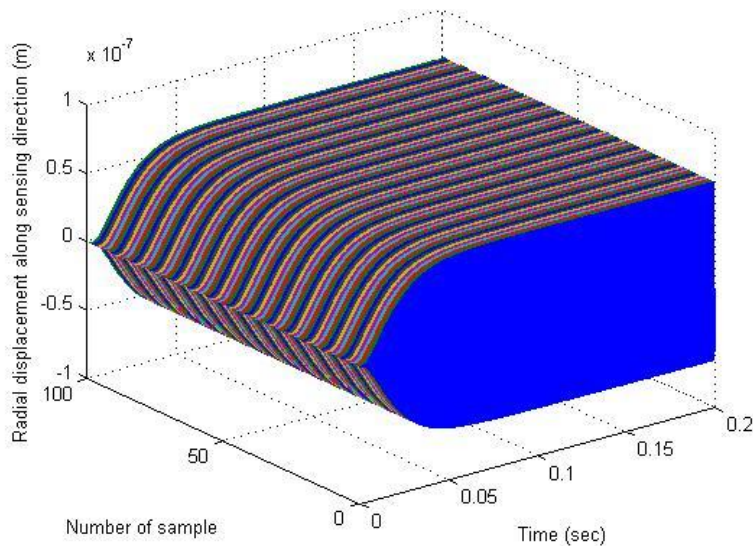
Figure 2-10. Radial displacement in the sensing direction with input angular rate (100 samples)
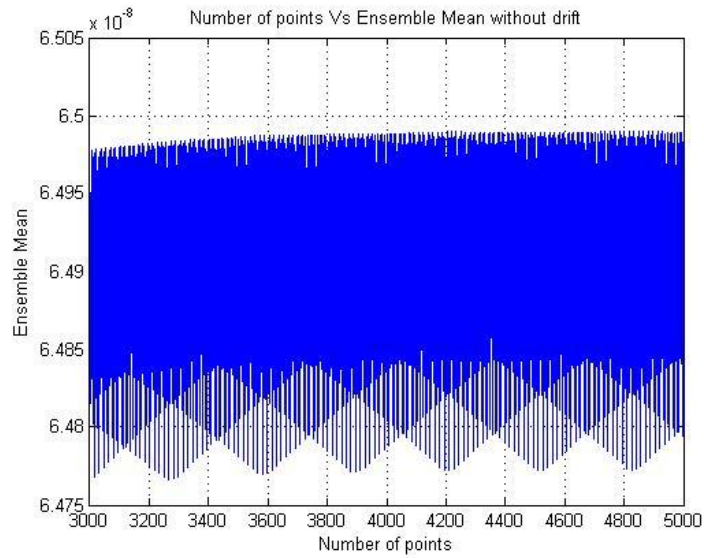
(a)
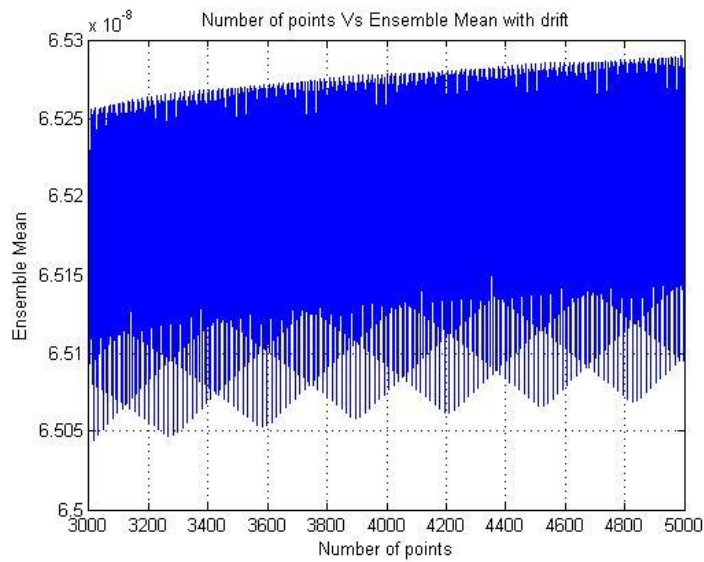
(b)

Figure 2-11. Number of samples vs. Ensemble Mean (a) without drift and (b) with drift (100 samples along path axis and $\Omega=2\pi$ rad/sec)
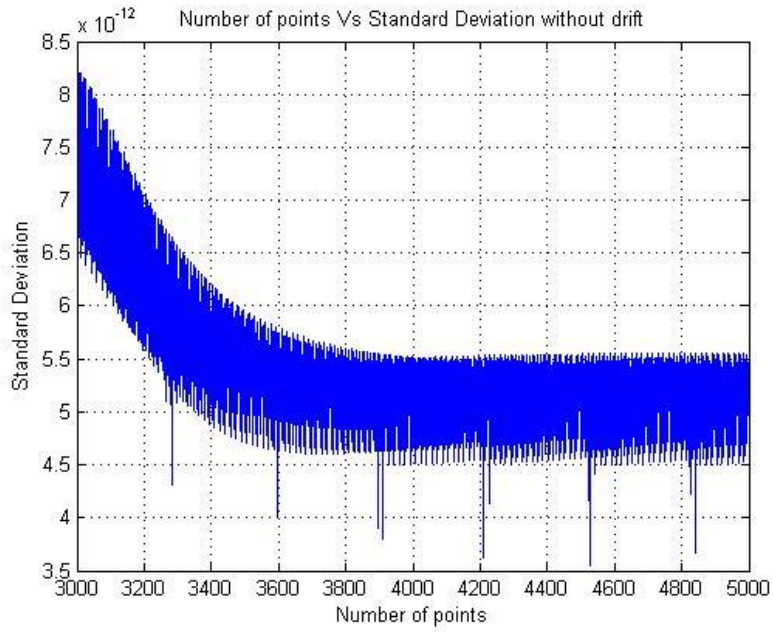
(a)
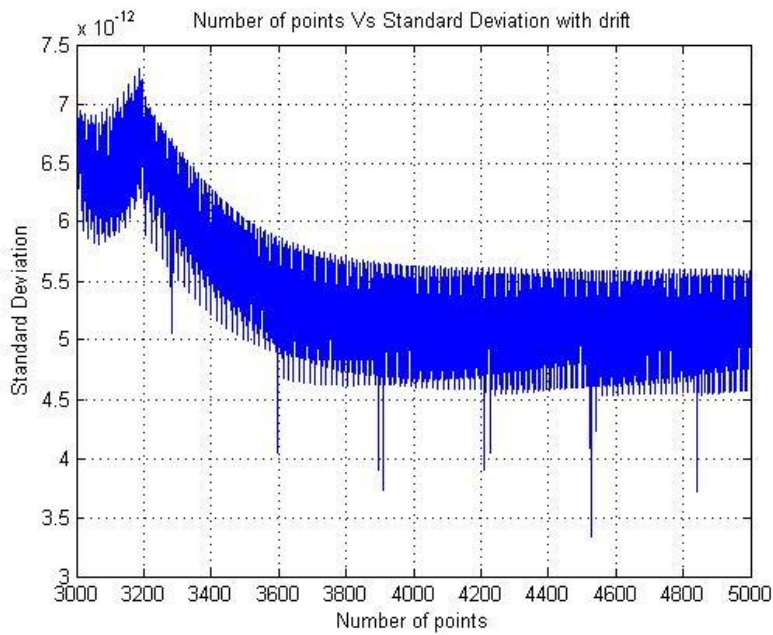
(b)

Figure 2-12. Number of points vs. Standard deviation (a) without drift and (b) with drift (100 samples along path axis and $\Omega = 2\pi$ rad/sec)

2.5.3.3.   Discrete time steps

It is known that time step size plays a significant role in the numerical simulation process. Obviously, smaller time steps results in more accurate predictions of the response along with increased computations costs. In order to find the optimal time step to achieve reasonably accurate results in moderate time, a suitable fixed step size is selected by running several simulations via the ODE45 integration routine within MATLAB. Based on the simulation trials the time step size has been chosen to be 0.000001 seconds. Further reduction in step size has been found to be unnecessary.

2.6.   Closure

A suitable numerical model is developed for investigating the dynamic response characteristics of a mass-spring element when the mass-spring gyroscope is subjected to an input angular rate. The natural frequency variations caused by gyroscopic coupling in the system matrix are investigated. Time and frequency responses of the mass-spring gyroscope are examined when it is excited by a harmonic external force while the sensor is subjected to an angular rate. Response amplitudes are obtained when parameters frequency mismatch are varied. It is found that the presence of noise and drift terms have effects on the mass-spring system. However, randomness is introduced in numerical model to get the stochastic response. Different methods are performed to achieve a robust scheme for predicting useful response statistics via Monte Carlo simulation. These optimized response statistics are used in uncertainty quantification of different parameters of mass-spring gyroscope in the next chapter.

Chapter 3

3. Uncertainty Quantification for Mass-spring Gyroscope

3.1. Introduction

In the previous chapter, a systematic numerical simulation procedure has been developed based on a mathematical model that represents the dynamical behavior of mass-spring type vibratory gyroscopes. In addition to determining the response due to changes in system parameters via a deterministic response analysis, predictions of response statistics due to random inputs have also been demonstrated. Suitable number of temporal points as well as sample paths have been selected and optimized for further analysis while a fixed optimal time step size has also been ascertained. In this chapter, attention is focused on examining the optimal number of sample paths for characterizing the response statistics via ensemble mean and standard deviations. Employing the optimal sample number, uncertainty quantification is performed for parameter uncertainties in input angular rate, frequency mismatch, and the quality factor. In addition, uncertainty quantification in the frequency domain has also been performed considering uncertainties in frequency mismatch.

3.2. Optimal number of Samples

When the system is subjected to harmonic excitation with input angular motion which contains noise and drift, the response along the sensing direction is achieved numerically and the results have been presented in Chapter 2. Optimal as well as robust sampling strategies have been

developed for mass-spring gyroscopes based on the simulated dynamic responses via peak-picking as illustrated in Figure 2-7. After eliminating the transient oscillatory motion, the Monte Carlo method is applied on the steady state part of the time response. Results for 50 samples, are depicted in Figure 3-2.
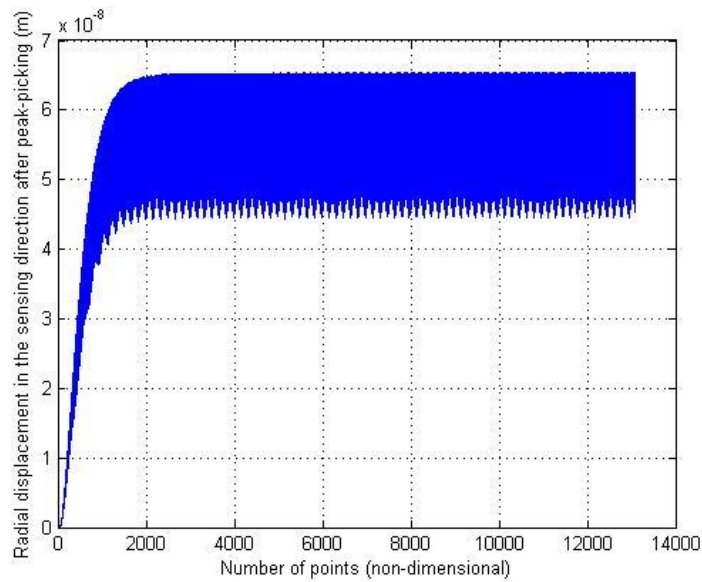
Figure 3-1. Time response after peak-picking for mass-spring gyroscope ($\Omega=2\pi$ rad/sec)
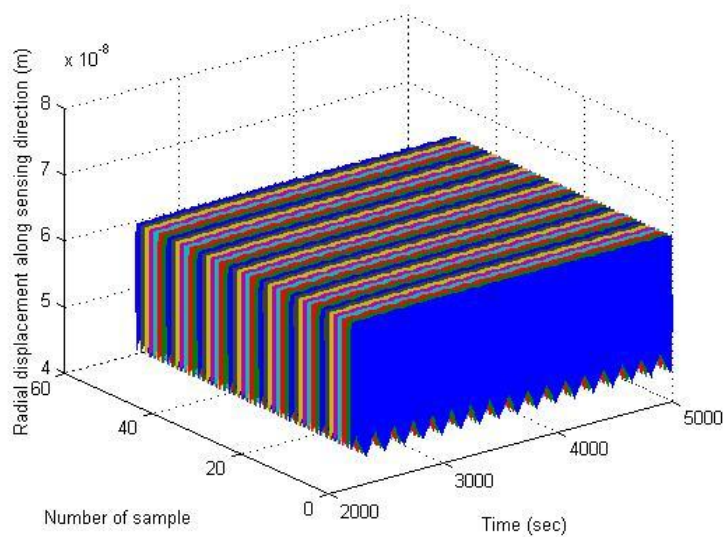
Figure 3-2. Radial displacement in the sensing direction after peak-picking (50 samples)

Optimization of the number of samples is an essential part for Monte Carlo method since use of larger number of samples increases the computational effort significantly. Following the pervious analysis, it has been determined that any point after 3900 points along the steady part of Figure 3-1 can be chosen for further analysis. In the present analysis five temporal points at 4501, 4502, 4503, 4504, 4505 have been considered for the application of Monte Carlo simulation. At these points, ensemble mean as well as standard deviation have been computed for varying sample numbers starting from 5 to 100 with an increment of 5 samples.

The computed ensemble mean for the cases of without and with consideration of drift, respectively, are illustrated in Figures 3-3 (a) and (b). The influence of drift is evident from the Figure 3-3 (b). The corresponding figures for the standard deviation as shown in Figures 3-4 demonstrate reasonable convergence after 30 samples. These figures also demonstrate the significance of drift that is evident from the order of magnitude of the standard deviation. Further these ensemble standard deviation predictions seem to be consistent at the 5 temporal points considered. Hence, it can be concluded that any of the 5 temporal points can be considered for the ensemble mean and standard deviation computations. For the present analysis, the point 4501 has been chosen while performing the computations employing 50 samples.
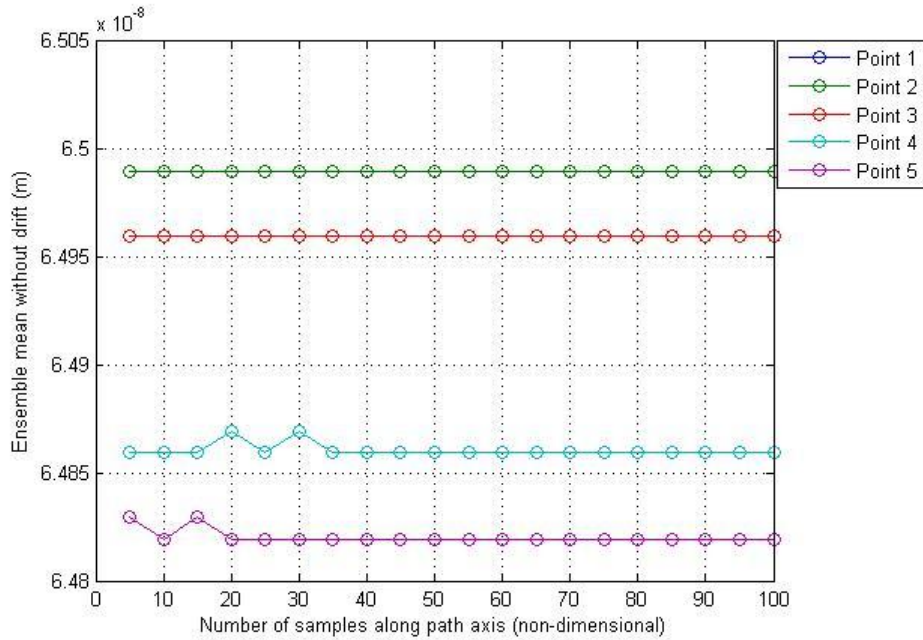
(a)
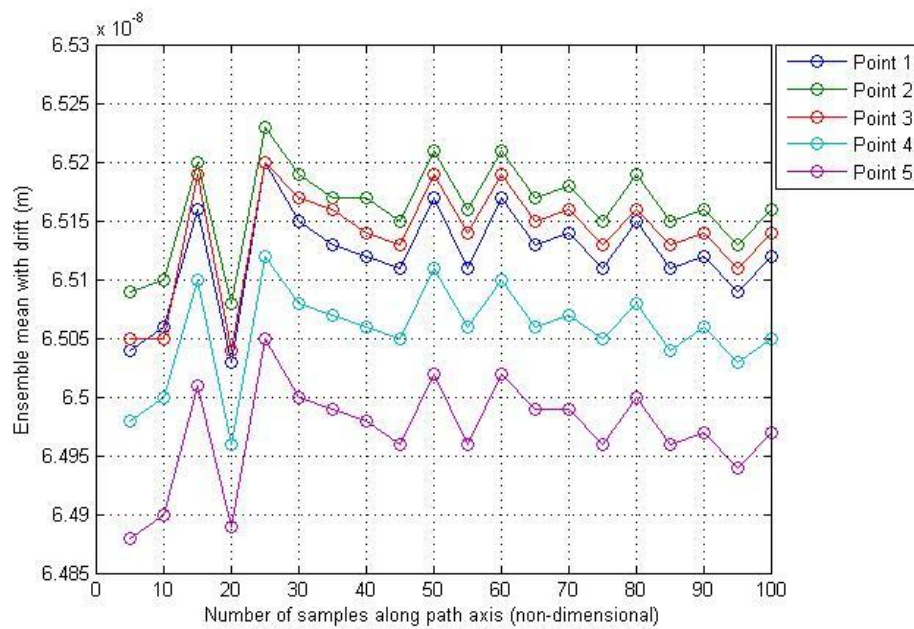
(b)

Figure 3-3.Number of samples along path axis vs. Ensemble mean (a) without drift and (b) with drift ($\Omega=2\pi$ rad/sec)
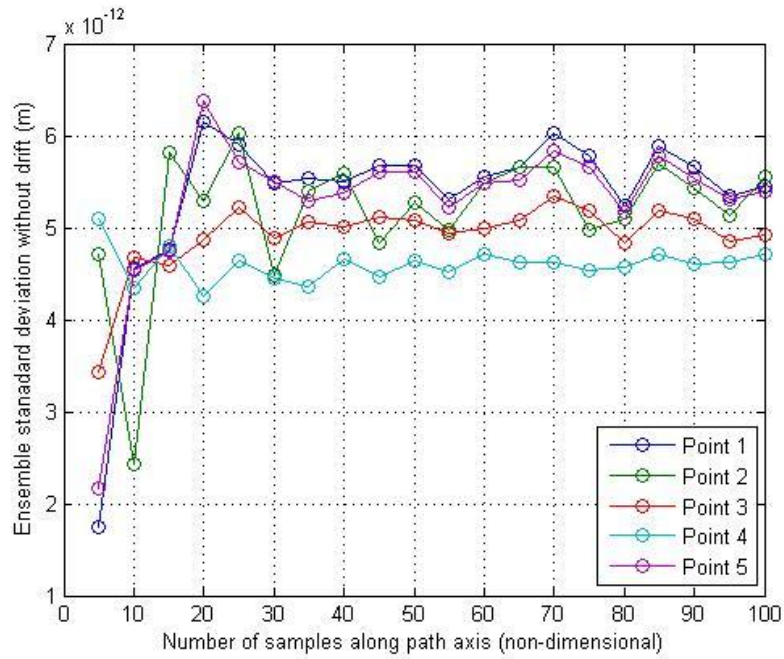
(a)
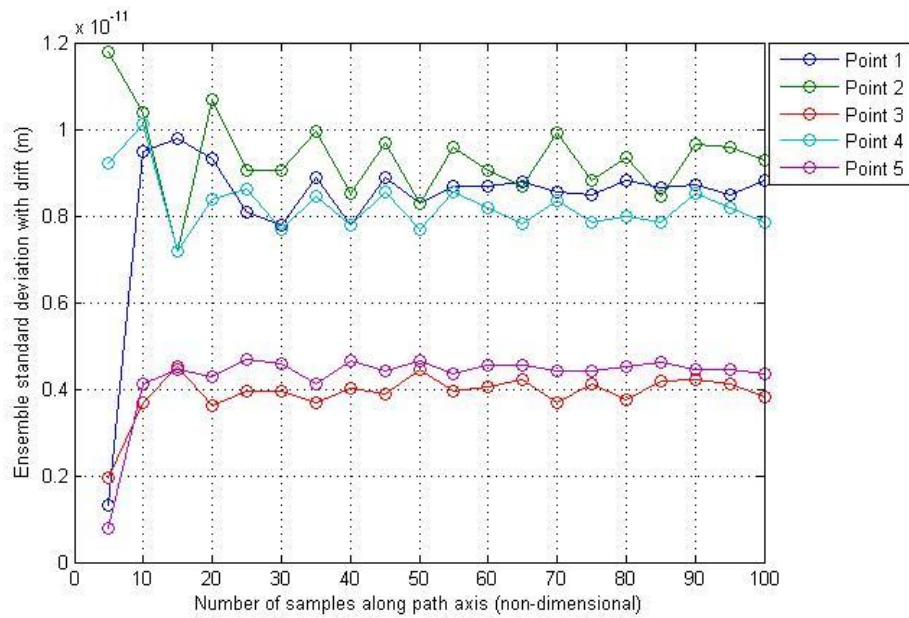
(b)

Figure 3-4. Number of samples along path axis vs. Standard deviation (a) without drift and (b) with drift (*Ω=2π rad/sec*)

The point 4501 has been singled out from Figure 3-2 and 50 samples are shown via the 3D plot for illustrative purposes. These 50 samples, when subjected to uncertainties in various system parameters are useful in estimating the response statistics via the uncertainty quantification process.
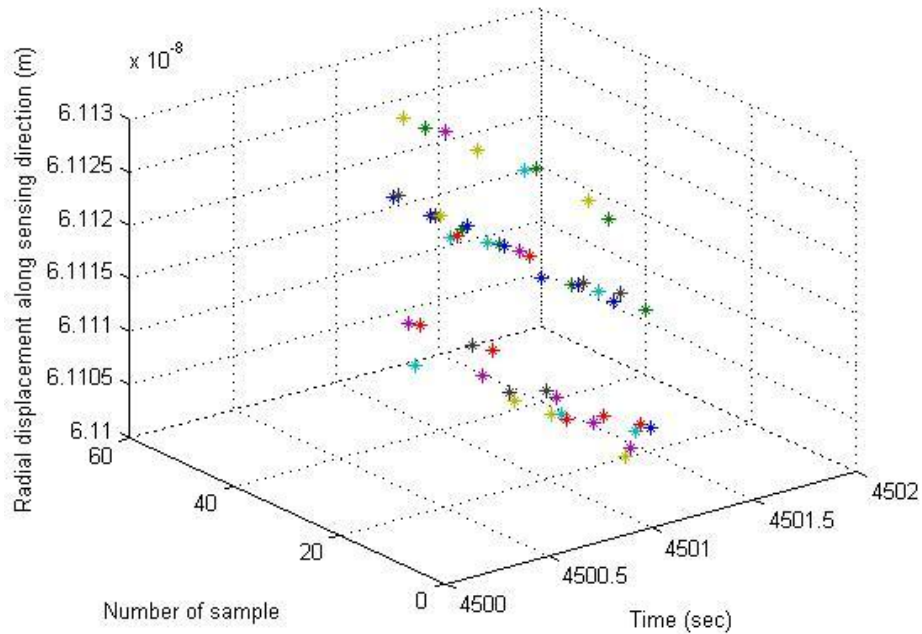
Figure 3-5. Radial displacement in the sensing direction with input angular rate at point 4501 (50 samples)

3.3. Uncertainty quantification

Uncertainty quantification (UQ) can be defined as it is the science of quantitative characterization and reduction of uncertainties in applications. It tries to determine how likely certain outcomes are if some aspects of the system are not exactly known.

In general, there are two distinct types of uncertainties present in physical models. One type is model uncertainty, also known as 'epistemic' uncertainty. This is the error that exists in the model, i.e., how close or far the model is from reality. The other is parameter uncertainty, also known as the 'aleatoric' uncertainty. This is associated with the lack of complete knowledge of input parameters, i.e., how far they are from nominal and what is the nature of their variability or uncertainty. This work is concerned only with the latter. Given some uncertainty in the model parameters, one needs to understand their effect on the predictions based on the model, and this is accomplished by propagating uncertainty through the model, i.e., developing the variability in the prediction (See e.g., Agarwal and Aluru, 2009).

The design methodologies for MEMS are based on deterministic approaches, where the input parameters as example geometrical and physical properties are assumed to be known precisely. For the given values of the input parameters, one can simply solve the coupled system for the field variables such as displacement and evaluate relevant quantities of interest such as input angular rate, resonant frequency, quality factor, frequency mismatch etc. Uncertainties can be described using stochastic quantities and uncertain parameters can be modeled using random variables, and uncertain spatial or temporal functions are represented as random fields or processes.

In order to correctly characterize the uncertain input parameters in terms of random variables with appropriate distribution, it is important to have convenient experimental data set regarding these parameters. Unfortunately, for most of the MEMS devices detailed experimental data are not available. Experiments do not provide sufficient information about the variation of certain parameters and in such a situation, the most straightforward way is to model the uncertain

parameter as normally distributed random variable over the given range and quantify the response statistics via numerical simulations based on the model.

Two major categories are available for computational methods to illustrate uncertainty propagation. One of the methods is based on a statistical approach and another is based on a non-statistical approach. The statistical approach includes methods such as Monte Carlo simulations and various sampling schemes. These can be computationally expensive, as their accuracy depends on the sample size. However, as demonstrated earlier, suitable procedures for optimizing the number of samples as well as the optimal temporal region can overcome the computational limitations. In the following sections, the effects on the response statistics due to uncertainties in the input angular rate as well as the frequency mismatch are examined.

3.4. Uncertainty Quantification Results and Discussion

Uncertainties in input angular speed are introduced in the mathematical model considering drift and noise terms and the resulting dynamic response simulations are used to obtain optimal number of points along time axis and optimal number of samples along path axis. This optimal configuration is also used for examining uncertainties in frequency mismatch. For the purposes of uncertainty quantification, the noise term in the model is introduced as a random variable with Normal (Gaussian) distribution. At a certain temporal point which lies after 3900 points along time sample, 50 samples are taken along sample path axis for the application of Monte Carlo simulation based on the dynamic response. This enables prediction of response statistics in the form of standard deviation of output response for different cases.

3.4.1. Uncertainty in Input Angular Rate

For this case the system is subjected to fixed frequency mismatch of 0.01%. In order to generate random input angular rate (Ω) within the MATLAB environment, mean of input angular rate is fixed at 2π rad/sec and the standard deviations are varied from 1% to 10% of fixed mean. By using mean and standard deviations different random samples are generated and these normally distributed random values are added to the nominal input angular rate to achieve a total angular rate. This total input angular rates are used in the simulation and the resulting responses are employed in the quantification of ensemble standard deviations. For each standard deviation of input angular rate, 50 random input samples are employed. In order to map curve, 10 different inputs standard deviation values are used to get 10 ensemble standard deviations of output responses. These curves are also investigated for varying fixed values of quality factors Q from 500 to 2500 with an increment of 500 as shown in Figure 3-6. It may be recalled that the nominal Q is 1000 and hence the choice of Q's represent above and below this nominal value.

It is evident from Figure 3-6 that the variation of input angular rate standard deviation does not have a significant effect on the output response standard deviation. It may attributed to the negligible effects that the input angular rate has on the natural frequencies. The increase in response standard deviation with increasing Q is also evident and justifiable since damping is inversely proportional to Q.
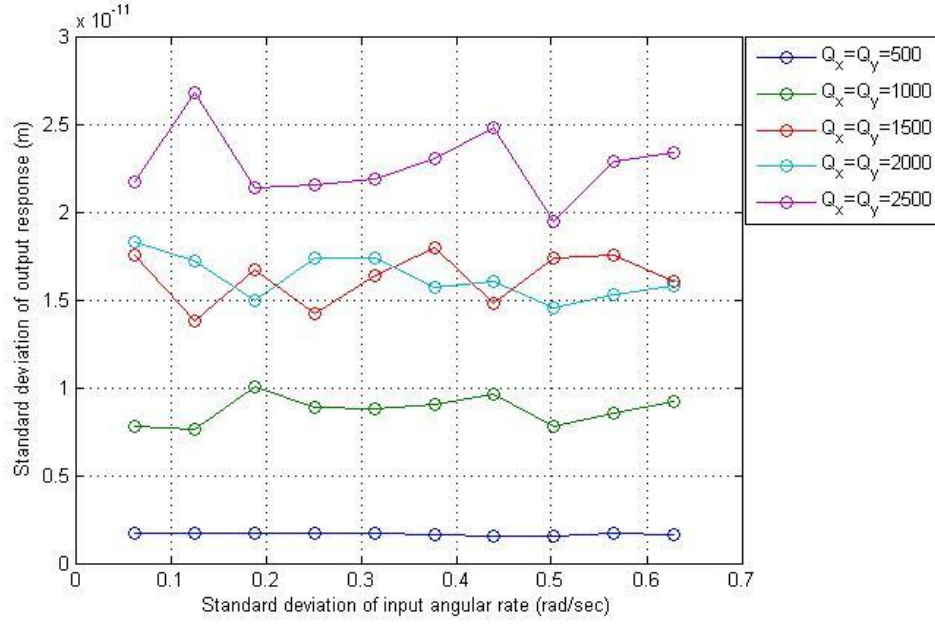
Figure 3- 6. Standard deviation of input angular rate vs. standard deviation of output response, (frequency mismatch is 0.01%)

3.4.2. Uncertainty in Frequency Mismatch

For the purposes of introducing frequency mismatch, Equation (2.5) given in chapter 2 is rewritten as

$$
\begin{bmatrix} 1 & 0 \\ 0 & 1 \end{bmatrix} \ddot{\boldsymbol{q}} + \begin{bmatrix} \frac{\omega_x}{Q_x} & -2\Omega \\ 2\Omega & \frac{\omega_y}{Q_y} \end{bmatrix} \dot{\boldsymbol{q}} + \begin{bmatrix} \omega_x^2 - \Omega^2 & 0 \\ 0 & \omega_y^2 - \Omega^2 \end{bmatrix} \boldsymbol{q} = \begin{bmatrix} \frac{F_0}{m_p} sin\, \omega_x\, t \\ 0 \end{bmatrix},
\tag{3.1}
$$

where $\boldsymbol{q} = [q_1\, q_2]^T$ represents a vector that contains the generalized coordinates and the elements of the system matrices are given in section 2.1.2 of chapter 2. In order to introduce frequency mismatch ϑ, the natural frequencies of the stationary gyroscope, namely ω_x and ω_y, are considered unequal and these frequencies are related via:

47

$$\omega_y = \omega_x(1 + \vartheta), \tag{3.2}$$

In this case, the system has a fixed input angular rate (Ω) of 2π rad/sec. In order to produce Gaussian distributed random number for frequency mismatch (ϑ), mean is fixed at 0.00001 and standard deviations are varied from 0.00001 with an increment of 0.00001 up to 0.0001. The above mean and standard deviation have been used for generating random numbers via MATLAB. For each input standard deviation 50 random samples of frequency mismatch are employed to get corresponding output response standard deviation and this procedure is repeated for 9 remaining input standard deviations to obtain corresponding output response standard deviations and is used in the plot 3-7. These predictions are also performed for varying fixed values of the quality factor Q and the results are presented in Figure 3-7. Standard deviations of the output response increases in a nonlinear fashion with the frequency mismatch and the magnitude of the output response standard deviation shows a diverging trend when the quality factor increases (i.e. damping ratio decreases).
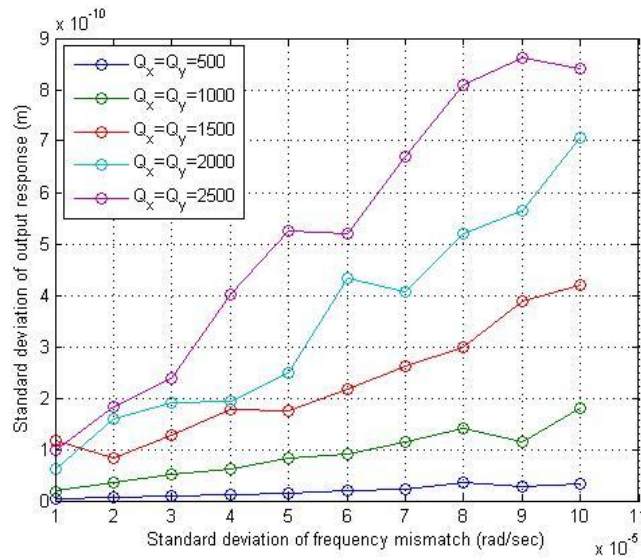
Figure 3-7. Standard deviation of frequency mismatch vs. standard deviation of output response, ($\Omega = 2\pi$ rad/sec)

In order to quantify the influence of uncertainty in frequency mismatch on the output response statistics considering a fixed quality factor of 1000, Least-square approach is employed on the resultant data to obtain a parametric relationship between the two relevant standard deviations. MATLAB command 'polyfit' with degree 2 is employed for this purpose as expressed below.

$$\sigma_{response} = 3.2 \times 10^{-3} \sigma^2_{f.mismatc\ h} + 1.2339 \times 10^{-6} \sigma_{f.mismatc\ h} + 8.8620 \times 10^{-12}, \qquad (3.3)$$

where $\sigma_{response}$ and $\sigma_{f.mismatc\ h}$ denote as standard deviations of the output response and frequency mismatch respectively. This process is illustrated in Figure 3-8.
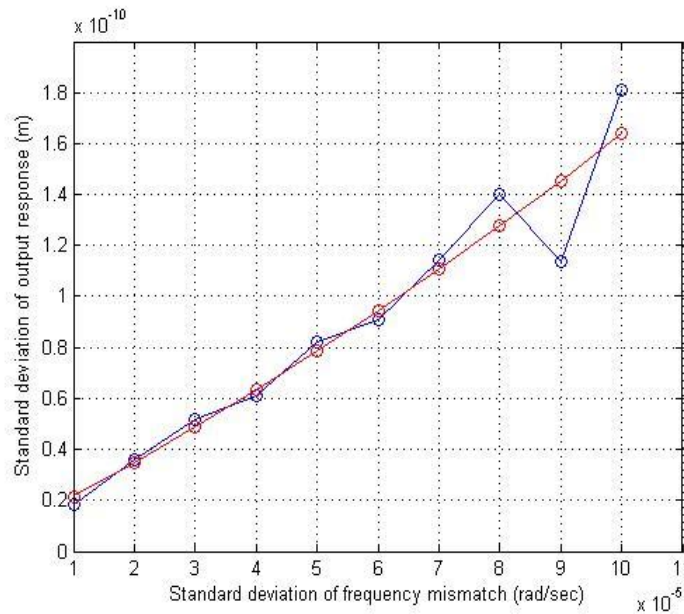
Figure 3- 8. Standard deviation of frequency mismatch vs. standard deviation of output response, $(\Omega = 2\pi \text{ rad/ sec and } Q = 1000)$

3.4.3. Uncertainty in Quality Factor

When the system is subjected to uncertainties in quality factor, input angular rate is fixed at 2π rad/sec and for random number generation mean of quality factor is fixed at 1000 and standard

deviations are varied from 50 with an increment of 50 up to 500 and employing 50 random samples to obtain corresponding ensemble output standard deviation for each input standard deviation and illustrated in Figure 3-9 for different frequency mismatch values. It is evident from Figure 3-9 that, for 0.01% and 0.02% frequency mismatch, output response statistics show a significantly different trend when compared with higher mismatch values. It may be attributed to the fact that for lower frequency mismatch the two natural frequencies are likely to be close to each other. The response statistics may take large values as a result of internal resonance. For the lower values of frequency mismatch, when the quality factor increases, the output standard deviations increase and seem to have a converging trend. Further, in order to illustrate the effect of large frequency mismatch on the performance of mass-spring gyroscope, 10% and 20% frequency mismatch are used in the numerical simulation. Figure 3-9 shows that, for large frequency mismatch, magnitudes of output standard deviations do not have notable variation as internal resonance may not play a significant role.
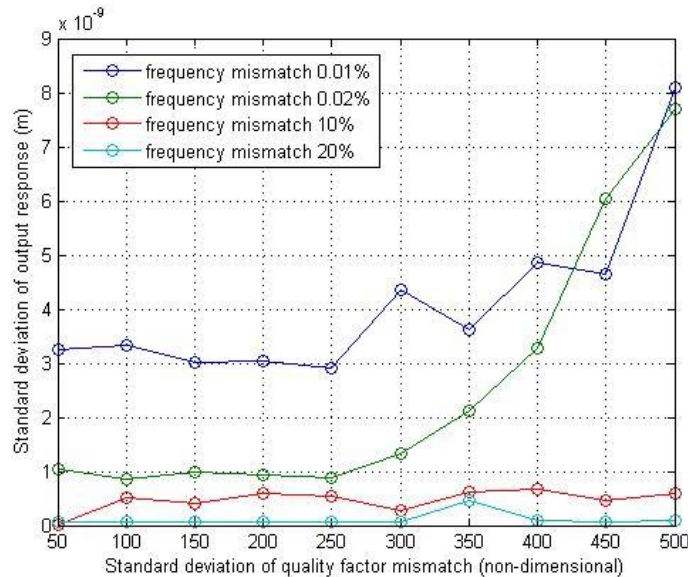
Figure 3-9. Standard deviation of quality factor mismatch vs. standard deviation of output response for different frequency mismatch ($\Omega = 2\pi$ rad/sec)

Least-square method is applied on resultant data to quantify the influence of uncertainty in quality factor mismatch on the output response statistics. For this purpose, the plot that correspond to 0.01% mismatch in Figure 3-9 is considered and redrawn in Figure 3-10. From the data set, a parametric relationship between the two relevant standard deviations can be extracted:

$$\sigma_{response} = 4.0960 \times 10^{-14} \sigma^2_{q.mismatch} - 1.4621 \times 10^{-11} \sigma_{q.mismatch} + 4.190 \times 10^{-9}, \quad (3.4)$$

where $\sigma_{response}$ and $\sigma_{q.mismatch}$, respectively, indicate as standard deviation of output response and standard deviation of quality factor mismatch.
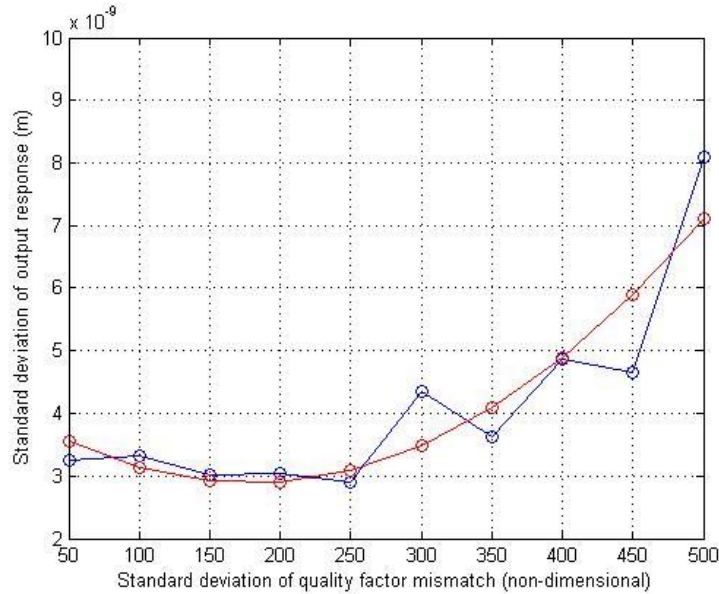
Figure 3-10. Standard deviation of quality factor (non-dimensional) vs. standard deviation of output response for fixed frequency mismatch ($\vartheta = 0.01\%$, $\Omega = 2\pi$ rad/sec)

3.5. Frequency response

In order to develop a stabilization system for MEMS gyroscope, it is important to understand the frequency response in the early stages of system design, since the frequency response for MEMS

gyroscope is likely to have a direct impact on the controller design and can help identify potential stability issues—especially when considering wider-bandwidth solutions for next generation designs. This information is also useful for predicting the gyroscopes' response to vibration (See e.g., Looney, July 2012).

Taking Laplace transformation of system equations (2.3) and (2.4) presented in Chapter 2, the equations in the *s* domain can be expressed as

$$s^2 Q_1(s) + \frac{\omega_x}{Q_x} s Q_1(s) - 2\Omega s Q_2(s) + (\omega_x^2 - \Omega^2) Q_1(s) = F_1(s) \tag{3.5}$$

$$s^2 Q_2(s) + 2\Omega s Q_1(s) + \frac{\omega_y}{Q_y} s Q_2(s) + (\omega_y^2 - \Omega^2) Q_2(s) = 0 \tag{3.6}$$

where $F_1(s), Q_1(s)$ and $Q_2(s)$ represent, respectively, the Laplace transform of $f_1(t), q_1(t)$ and $q_2(t)$.

From Equations (3.5) and (3.6), the amplitude ratio of the displacement in the sensing direction to the displacement in the driving direction (i.e.,$|Q2/Q1|$) is evaluated considering frequency mismatch. Similarly, the forced frequency response magnitude $|Q2/F1|$ is also evaluated. For this purpose, the magnitudes of

$$\frac{Q_2(s)}{Q_1(s)} = -\frac{2\Omega s}{s^2 + \frac{\omega_y}{Q_y} s + (\omega_y^2 - \Omega^2)} \quad , \quad \text{and} \tag{3.7}$$

$$\frac{Q_2(s)}{F_1(s)} = -\frac{2\Omega s}{As^4 + Bs^3 + Cs^2 + Ds + (\omega_x^2 - \Omega^2)(\omega_y^2 - \Omega^2)} \quad , \tag{3.8}$$

are used, where

$$A = 1, \tag{3.9a}$$

$$B = \frac{\omega_x}{Q_x} + \frac{\omega_y}{Q_y} \ , \tag{3.9b}$$

$$C = \frac{\omega_x}{Q_x}\frac{\omega_y}{Q_y} + \omega_x^2 - \Omega^2 + \omega_y^2 - \Omega^2 + 4\Omega^2, \tag{3.9c}$$

$$D = \frac{\omega_x}{Q_x}\left(\omega_y^2 - \Omega^2\right) + \frac{\omega_y}{Q_y}\left(\omega_x^2 - \Omega^2\right), \tag{3.9d}$$

The parameters given in Table 2-1 are used for the numerical calculations of the amplitude ratio as well as forced frequency responses. From Equation (3.6), the amplitude ratio of the displacement in the sensing direction to the displacement in the driving direction (i.e., $|Q2/Q1|$) is evaluated and depicted for quality factors 1×10^8 and 1000 in Figures 3-11 and Figure 3-12, respectively. The figures show that the amplitude ratio has the maximum value near the non-rotating mass-spring natural frequency ω_y and that the magnitude of the amplitude ratio increases with an increase in the input angular rate.

Similarly, the frequency response magnitude $|Q2/F1|$, evaluated from Equation (3.7), is illustrated for quality factor 1×10^8 and 1000, respectively, are in Figures 3-13 and 3-14. In addition, the magnitude of frequency response is shown to increase as the input angular rate increases.
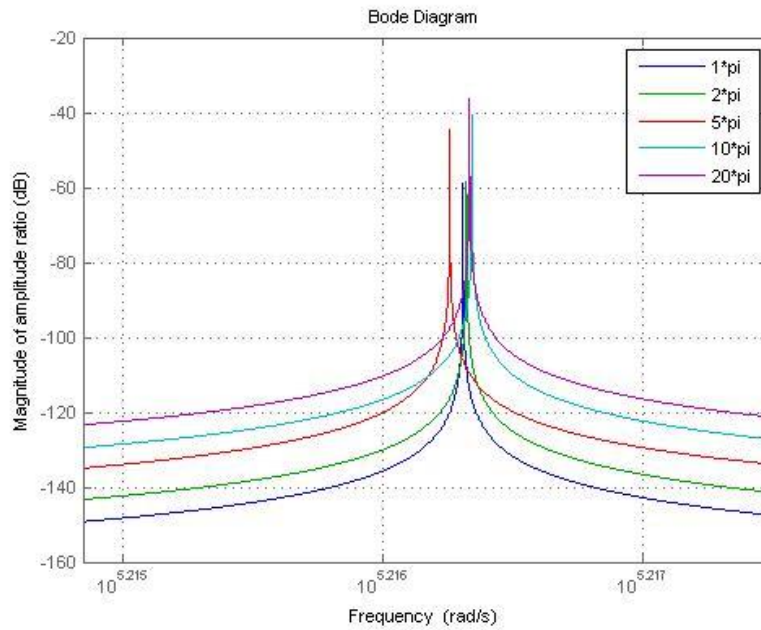
Figure 3-11. Variation of amplitude ratio for different input angular rates (frequency mismatch with 0.01%, Quality factor, $Q_x = Q_y = 1 \times 10^8$)
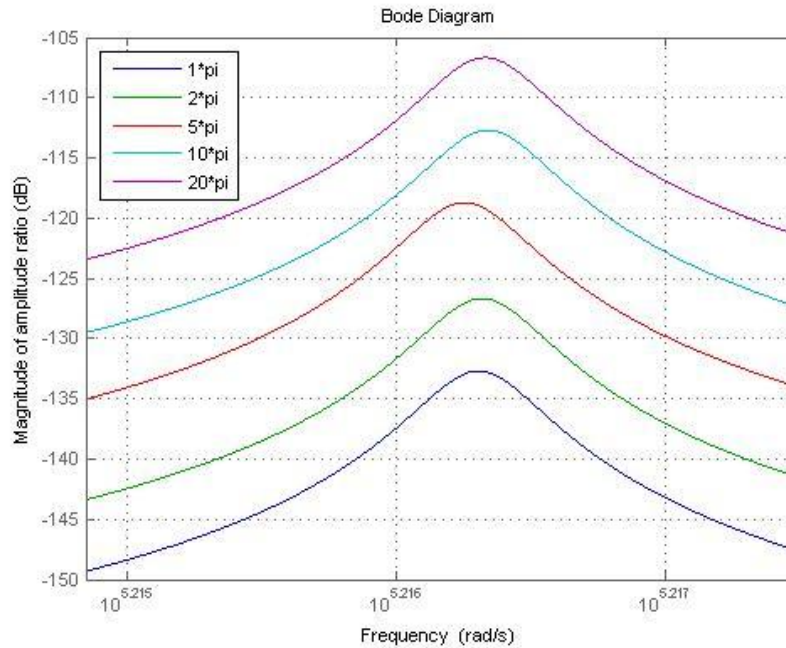
Figure 3-12. Variation of amplitude ratio for different input angular rates (frequency mismatch with 0.01% mismatch, Quality factor, $Q_x = Q_y = 1000$)
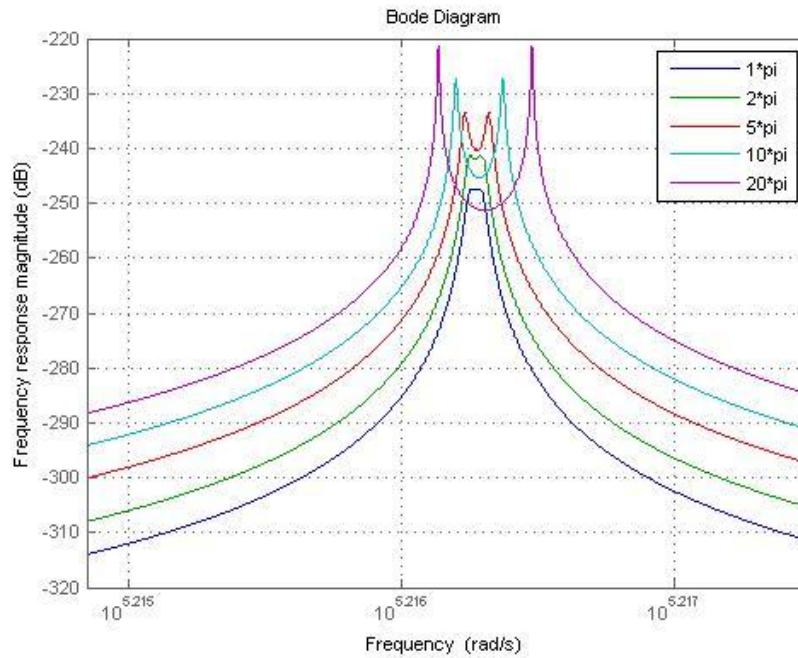
Figure 3-13. Variation of frequency response for different input angular rates (frequency mismatch with 0.01% mean, Quality factor, $Q_x = Q_y = 1 \times 10^8$)
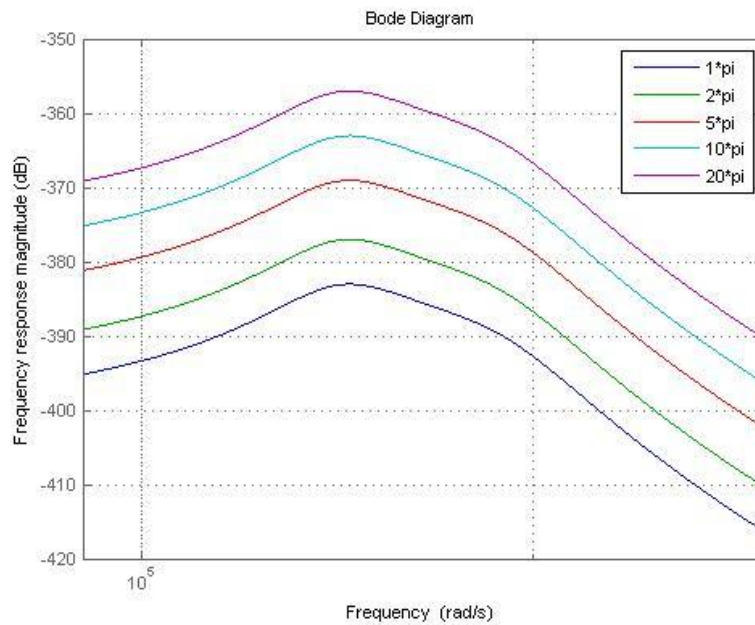
Figure 3-14. Variation of frequency response for different input angular rates (frequency mismatch with 0.01% mean, Quality factor, $Q_x = Q_y = 1000$)

In order to analyze the uncertainty quantification in the frequency domain with frequency mismatch, 50 random samples are employed in the numerical simulation and the resulting responses are demonstrated in Figure 3-15 where the input angular rate and quality factor are fixed at 2π rad/sec and 1000, respectively.
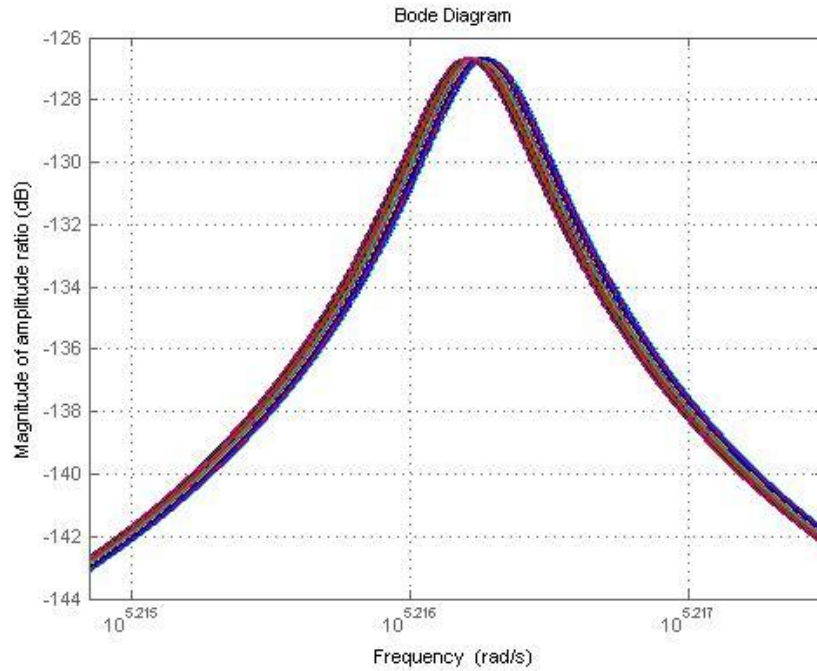
Figure 3-15. Variation of amplitude ratio for different samples (frequency mismatch with 0.01%, Quality factor, $Q_x = Q_y = 1000$, $\Omega = 2\pi$ rad/sec)

For the purposes of quantifying the effect of the uncertainty frequency mismatch, magnitudes of the amplitude ratio peaks are computed considering uncertainties in frequency mismatch. Figure 3-16 illustrates the gradually increasing nonlinear relationship between the standard deviation of frequency mismatch and standard deviation of magnitude of amplitude ratio $|Q2/Q1|$.
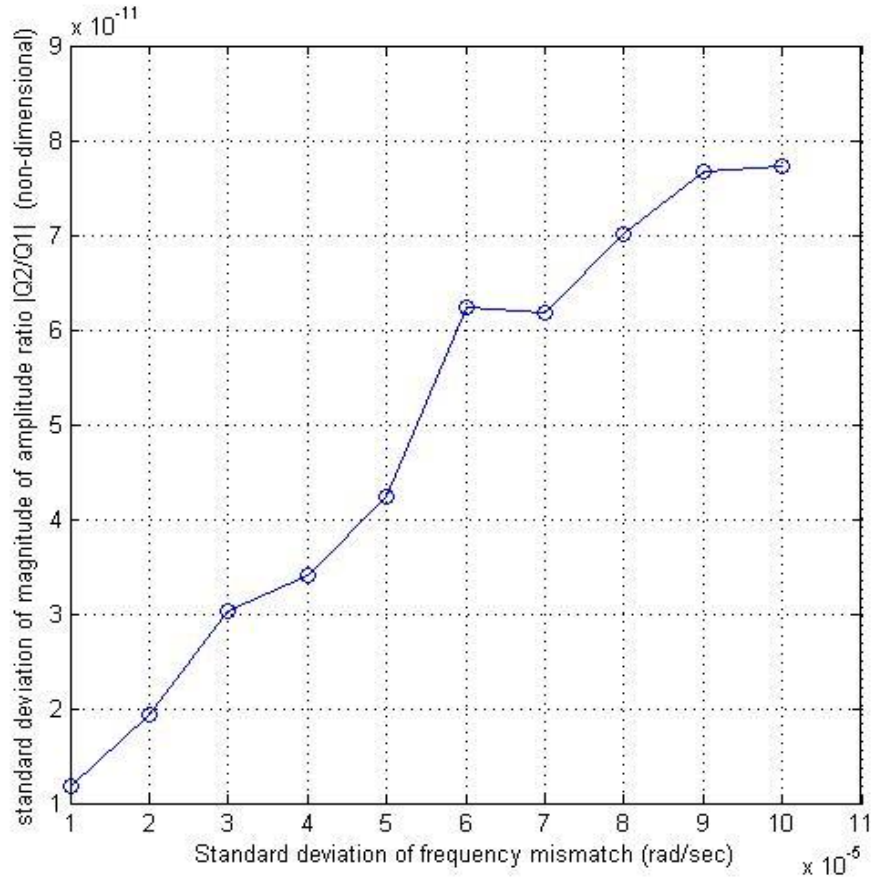
Figure 3-16. Standard deviation of frequency mismatch vs. standard deviation of magnitude of amplitude ratio $|Q2/Q1|$ ($\Omega = 2\pi$ rad/sec, Quality factor, $Q_x = Q_y = 1000$)

Least-square method is used to get a parametric relationship between two standard deviations using the MATLAB command 'polyfit' (degree 2) :

$$\sigma_{|Q2/Q1|} = -0.0030\sigma_{f.mismatc\ h}^2 + 1.1185 \times 10^{-6}\sigma_{f.mismatc\ h} - 1.2234 \times 10^{-12}, \qquad (3.10)$$

where $\sigma_{|Q2/Q1|}$ and $\sigma_{f.mismatc\ h}$, respectively, symbolize the standard deviation of magnitude of amplitude ratio $|Q2/Q1|$ and standard deviation of frequency mismatch. This process is illustrated in Figure 3-17.
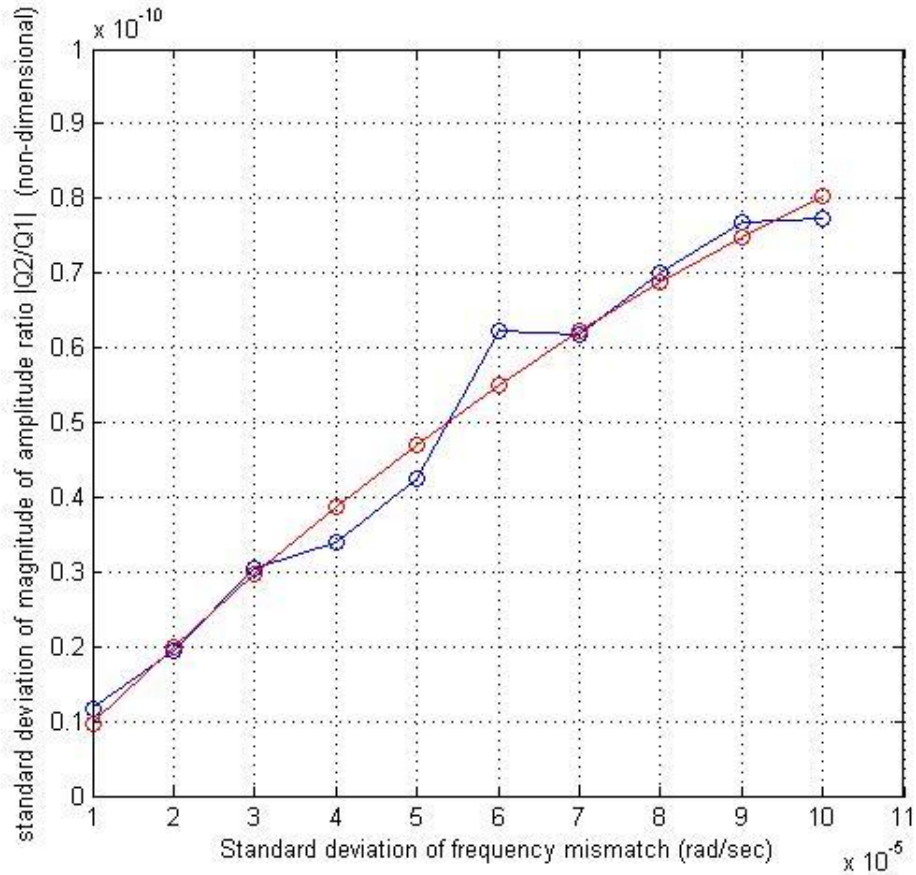
Figure 3-17. Standard deviation of frequency mismatch vs. standard deviation of magnitude of amplitude ratio $|Q2/Q1|$ ($\Omega = 2\pi$ rad/sec, Quality factor, $Q_x = Q_y = 1000$)

The standard deviation of frequency corresponding to the peak amplitude ratio is also evaluated for varying standard deviations of frequency mismatch and depicted in Figure 3-18 to illustrate that the frequency mismatch uncertainty has negligible influence.
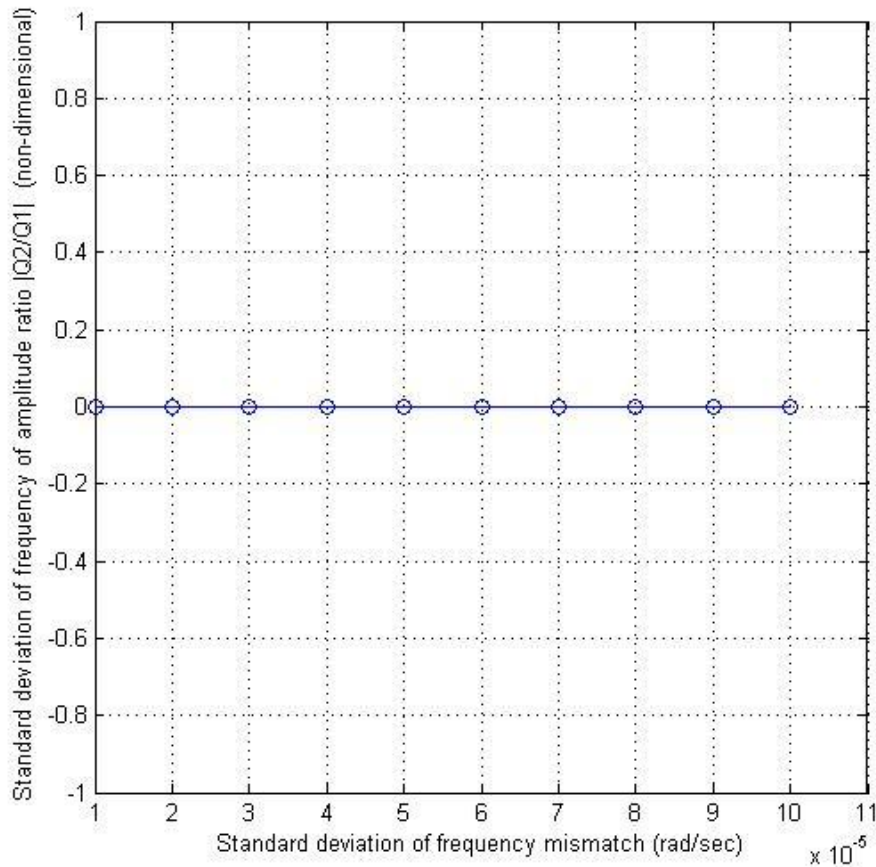
Figure 3-18. Standard deviation of frequency mismatch vs. standard deviation of frequency of peak amplitude ratio $|Q2/Q1|$ ($\Omega = 2\pi$ rad/sec, Quality factor, $Q_x = Q_y = 1000$)

With the intention of quantifying the effect of the uncertainty of peak frequency, magnitudes of the frequency response peaks are computed considering uncertainties in frequency mismatch. Figure 3-19 illustrates the gradually increasing nonlinear relationship between the Standard deviations of frequency mismatch and magnitude of frequency response $|Q2/F1|$. It is interesting to note that this variation has a similar pattern to that exhibited previously in Figure 3-17 for the case of peak amplitude ratio.
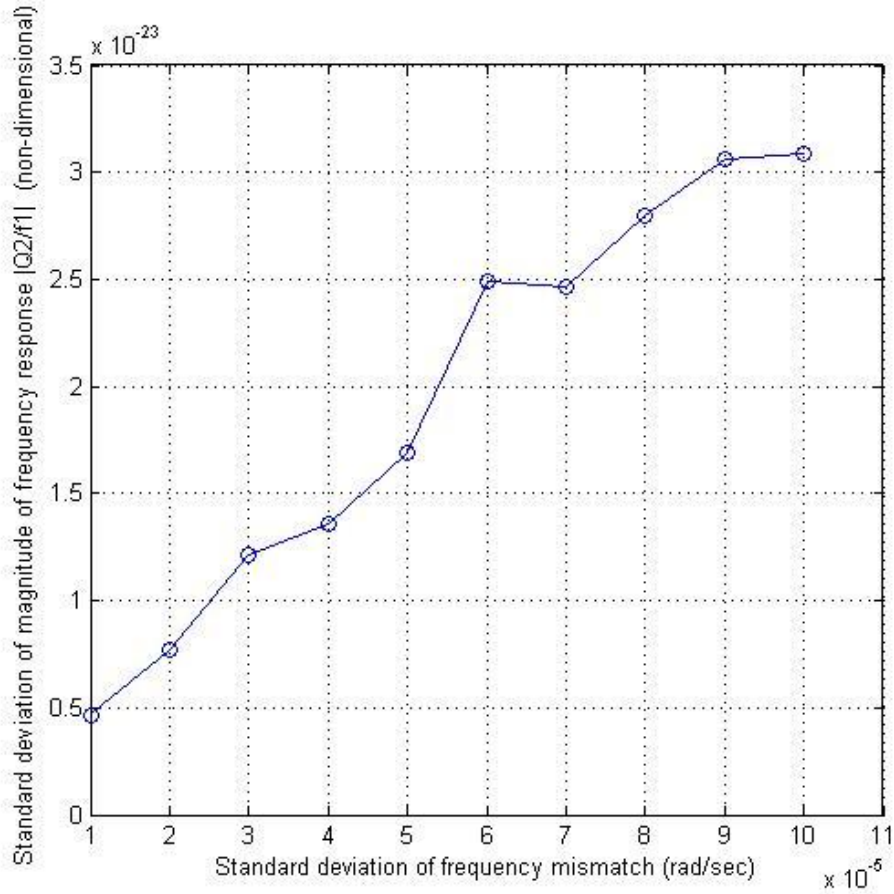
Figure 3-19. Standard deviation of input frequency mismatch vs. standard deviation of magnitude of frequency response $|Q2/F1|$ ($\Omega = 2\pi$ rad/sec, Quality factor, $Q_x = Q_y = 1000$)

Least-square method is used to get a parametric relationship between two standard deviations using the MATLAB command 'polyfit' (degree 2) :

$$\sigma_{|Q2/F1|} = -1.2121 \times 10^{-15}\sigma^2_{f.mismatc\ h} + 4.4624 \times 10^{-19}\sigma_{f.mismatc\ h} - 4.8745 \times 10^{-25},$$

(3.11)

where $\sigma_{|Q2/F1|}$ and $\sigma_{f.mismatc\ h}$, respectively, denote as standard deviation of magnitude of frequency response $|Q2/F1|$ and standard deviation of frequency mismatch. This process is depicted in Figure 3-20.

60
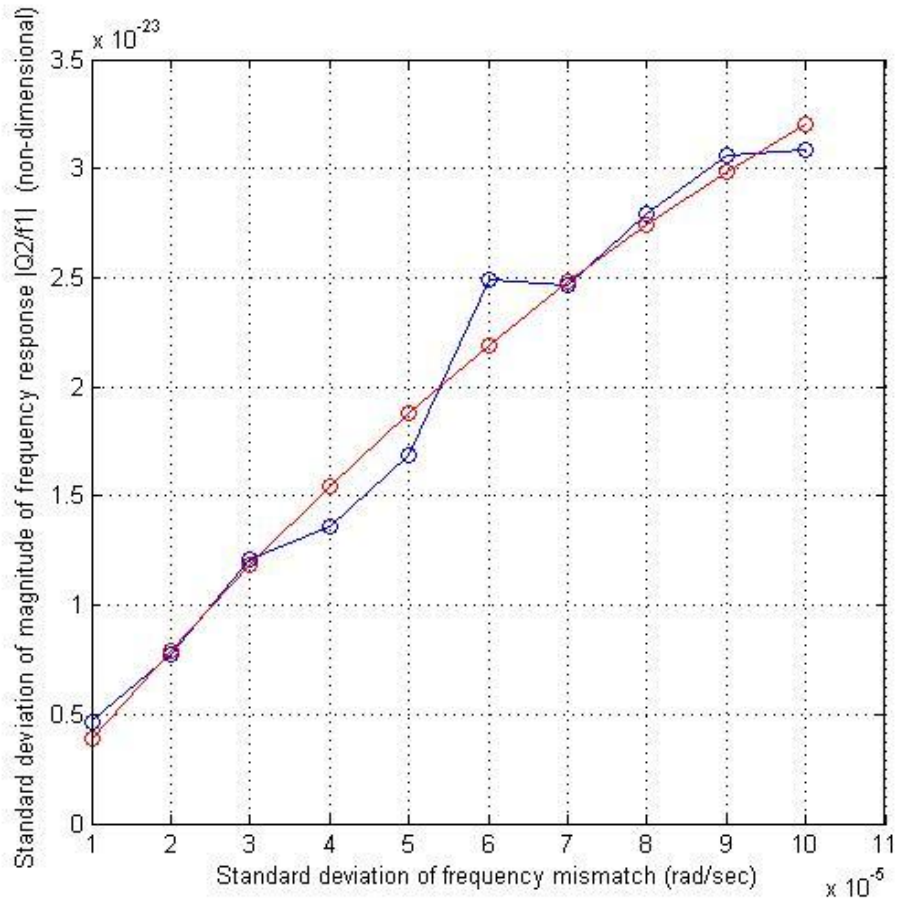
Figure 3-20. Standard deviation of frequency mismatch vs. standard deviation of magnitude of frequency response $|Q2/F1|$ ($\Omega = 2\pi$ rad/sec, Quality factor, $Q_x = Q_y = 1000$)

The standard deviation of frequency that corresponds to the magnitude of peak of frequency response is also evaluated for varying frequency mismatch standard deviation and depicted in Figure 3-21, which illustrates that the mismatch uncertainty has negligible influence as exhibited in the previous case.
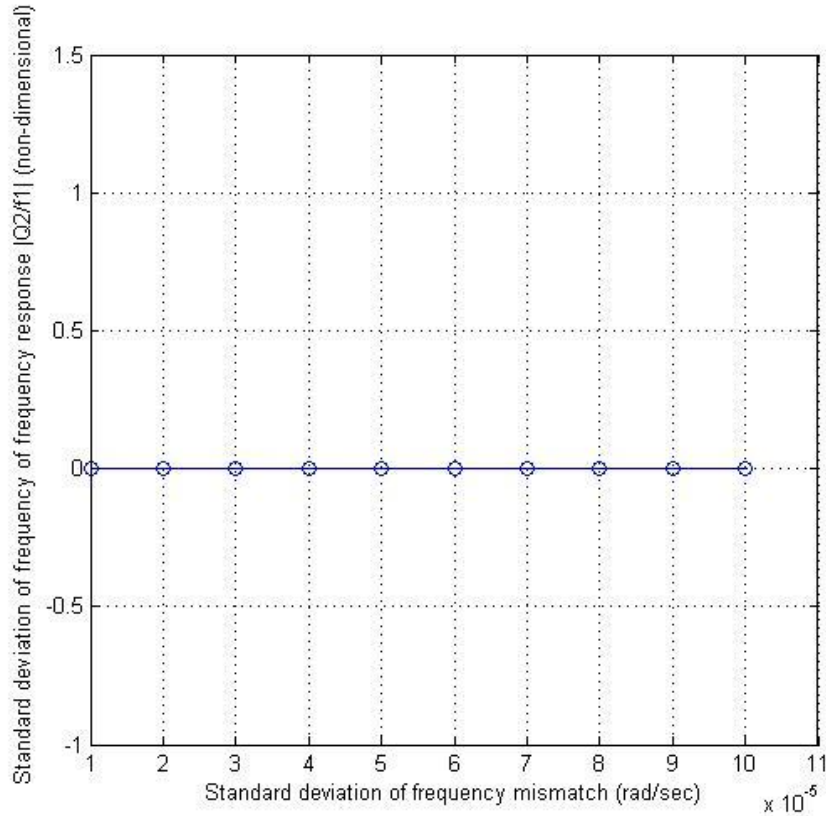
Figure 3-21. Standard deviation of frequency mismatch (rad/sec) vs. standard deviation of frequency of frequency response $|Q2/F1|$ (non-dimensional) ($\Omega = 2\pi$ rad/sec, Quality factor, $Q_x = Q_y = 1000$)

3.6. Closure

In this chapter, optimal temporal sample paths determined in Chapter 2 have been employed for uncertainty quantification for mass-spring gyroscope. In order to predict response statistics, dynamic response simulations have been used for quantifying standard deviation of output response when parameters such as input angular rate, frequency mismatch and quality factor are subjected to uncertainty. Uncertainty quantification in the frequency domain has also been demonstrated in terms of the standard deviations of the peak amplitude ratios and peak forced

response magnitudes. Least-square algorithm is used in both time and frequency domain in an effort to obtain a parametric relationship between the input and output parameter uncertainties.

Chapter 4

4. Dynamic Response Analysis for Ring-based Gyroscopes

4.1. Introduction

In this chapter, numerical schemes that are suitable for simulating the dynamic behavior of ring-based vibratory gyroscopes are developed. As discussed in Chapter 2, these schemes are intended for the purpose of uncertainty quantification and predicting the dynamic behavior of this class of devices under uncertain environment as well as system parameter uncertainties. Similar procedures have been followed for the purpose of characterizing the response to variation in system as well as environmental parameters. The dynamic behavior of ring-type vibratory angular rate sensors is presented via a mathematical model that has been derived by previous researchers. Further analysis associated with uncertainty quantification for this class of gyroscopes is presented in chapter 5.

4.2. Model description

In this chapter, ring gyroscope model is adopted from previous research performed by Cho (2004) who primarily employed this model for performing stability analysis of this class of vibratory gyroscopes. A body-fixed frame *x-y-z* has been used for representing the angular motion of the ring with respect to the inertial reference frame R. In Figure 4-1, *r* represents the mean radius of the ring, and u_r and u_θ represent, respectively, the radial and circumferential displacements. In addition, for the purposes supporting the ring, eight internal springs are employed, and it is assumed that the equivalent stiffness of these springs is low compared to that

of the ring. Hence, it can be assumed that the presence of these springs do not to have a significant effect on the ring dynamics.
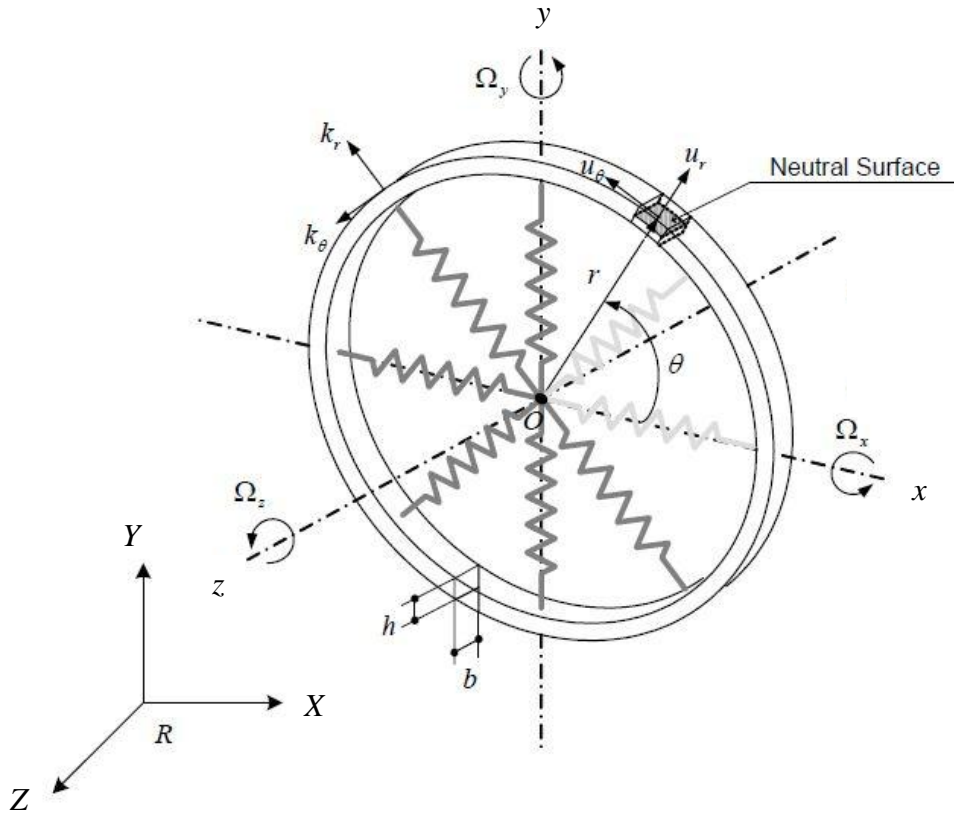
Figure 4-1. Schematic of a rotating ring with support springs

4.3. Equation of motion

For the purposes of deriving the governing equation different types of energy terms, namely kinetic energy, strain energy, potential energy, energy from external loads etc. are developed from deformation, internal and external loads and the vibratory and the rigid body motion of the ring. Hamilton's principle is then used to derive the governing equation of motion.

Natural Frequencies and Mode Shapes

When the ring is assumed to be symmetric, two identical modes having equal natural frequencies are found to exist. One of them is called the primary mode while other is referred to as the secondary mode. This set of modes are also known as degenerate modes (see e.g., Maluf, 2000). The mutual angle between the two degenerate modal configurations is $\theta = \frac{\pi}{2n}$ due to ring symmetry, where n is the mode number. This set of modes for different mode numbers are illustrated in Figure 4-2.

(a) $n = 2$

(b) $n = 3$

(c) $n = 4$
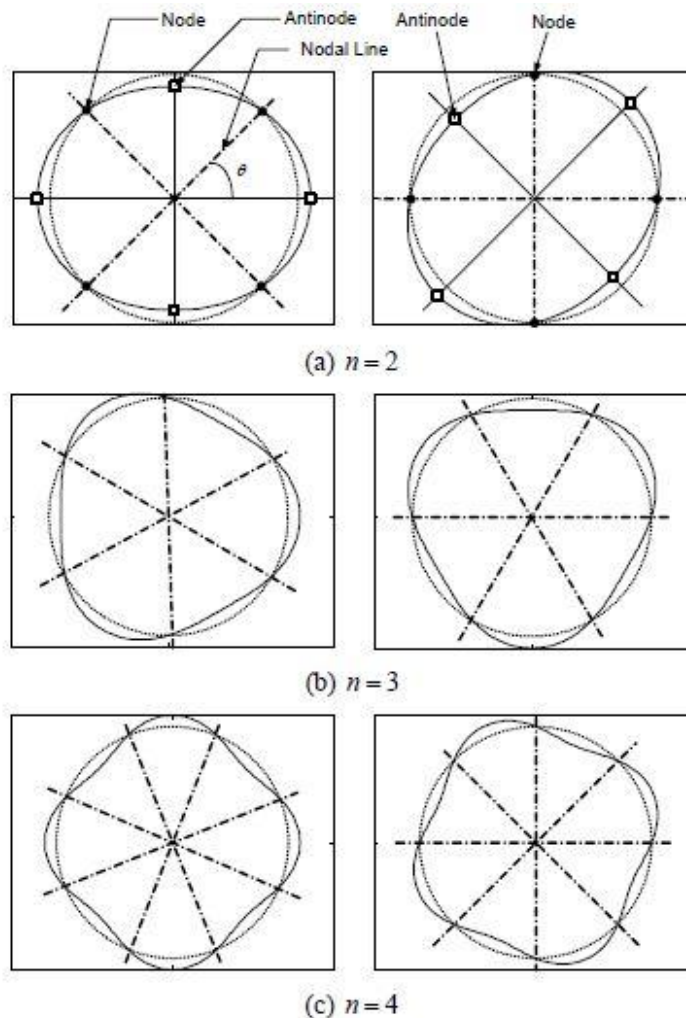
Figure 4-2. Stationary flexural modes of a rotating ring with n=2, 3, 4 nodal diameters

Normal Mode Equations of Motion

The vibratory ring-type gyroscope exploits the presence of these degenerate modes and, in particular, employs the second flexural mode. This mode is often popularly referred to as the "wine-glass" mode since one can easily shatter a wine glass, with relatively low amplitude sound signal that corresponds to this frequency. This feature demonstrates that this mode is easily excitable and hence employed in the gyroscope construction. When the ring is subjected to input angular rate Ω while the second flexural mode is excited, this mode attempts to move from one degenerate mode to another due to the Coriolis effect as shown in the Figure 4-3. The largest angular shift is achieved from secondary flexural modes when $n = 2$ due to external rate input which in turn provides the measurement signals that correspond to the input angular velocity. In accordance with the formula, $\theta = \dfrac{\pi}{2n}$ the angular separation between these modes become $\dfrac{\pi}{4}$ as seen from Figure 4-3.

(a) Primary mode   (b) Secondary mode
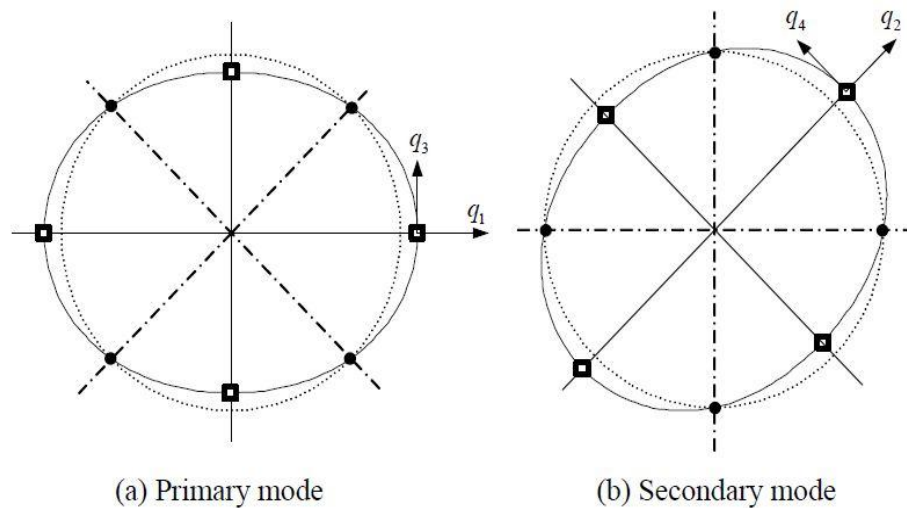
Figure 4-3. Second flexural modes used in the normal mode equations

A combination of excitation of the primary mode and an input angular rate results in Coriolis effect which trends to rotate the primary mode towards the secondary mode and hence the

resultant response consists of a combination of primary as well as the secondary modes. Hence, the radial and circumferential displacement can be written as a linear combination of the associated mode shapes:

$$u_r(\theta, t) = \sum_n^\infty [q_1(t)\cos(n\theta) + q_2(t)\sin(n\theta)], \qquad (4.1a)$$

$$u_\theta(\theta, t) = \sum_{n=0}^\infty [q_3(t)\cos(n\theta) + q_4(t)\sin(n\theta)], \qquad (4.1b)$$

where the generalized coordinates $q_1(t)$ and $q_2(t)$ correspond to the flexural mode while $q_3(t)$ and $q_4(t)$ correspond to the circumferential mode as displayed in Figure 4-3. Employing equation (4.1) in the system of equations described in the continuous form (See, Cho, 2004) the second order linear gyroscopic equations in discretized form can be derieved in terms of the generalized coordinate vector $\boldsymbol{q}$ and expressed as

$$\ddot{\boldsymbol{q}} + G\dot{\boldsymbol{q}} + K\boldsymbol{q} = F \quad , \qquad (4.2)$$

where $\boldsymbol{q} = [q_1\ q_2\ q_3\ q_4]^T$.

Equations of Motion

In the present thesis, it is assumed that the ring is symmetric. However, in practice, presence of geometric as well as structural imperfections are unavoidable due to the manufacturing process used in fabricating this class of devices (see, e.g., Eley et al., 2000). Hence, in the design of this class of devices, it is customary to incorporate this imperfection via a mass mismatch parameter. The equations of motion considering this imperfection as well as a relationship between the radial and the flexural modes (see, e.g., Cho, 2004) take the form:

$$M\ddot{\boldsymbol{q}} + (G + D)\dot{\boldsymbol{q}} + K\boldsymbol{q} = F \qquad , \qquad (4.3)$$

where $\boldsymbol{q} = [q_1\ q_2]^T$ represents generalized coordinate vector that consists of the radial components of the second flexural mode, and the system matrices are obtained as

$$M = \begin{bmatrix} 1 & 0 \\ 0 & 1 + \delta m \end{bmatrix}, G = \begin{bmatrix} 0 & -2\Omega\gamma \\ 2\Omega\gamma & 0 \end{bmatrix}, D = \begin{bmatrix} 2\xi\omega_{01} & 0 \\ 0 & 2\xi\omega_{02} \end{bmatrix},$$

$$K = \begin{bmatrix} \kappa_1 + \kappa_2\Omega^2 & -\dot{\Omega}\gamma \\ \dot{\Omega}\gamma & \kappa_1 + \kappa_2\Omega^2 \end{bmatrix}, F = \begin{bmatrix} \dfrac{F_1\hat{\hat{b}} - n\hat{\hat{a}}F_4}{\hat{\hat{a}} + \hat{\hat{b}}} \\ \dfrac{F_2\hat{\hat{b}} + n\hat{\hat{a}}F_3}{\hat{\hat{a}} + \hat{\hat{b}}} \end{bmatrix}, \quad\quad\quad \text{(4.4 a)}$$

where,

$$\gamma = \frac{\hat{\hat{b}} + n^2\hat{\hat{a}}}{n\left(\hat{\hat{a}} + \hat{\hat{b}}\right)}, \kappa_1 = \frac{\hat{\hat{b}}\hat{\hat{c}} - n^2\hat{\hat{a}}^2}{\rho A\left(\hat{\hat{a}} + \hat{\hat{b}}\right)}, \kappa_2 = \left[\frac{n^2\left(\hat{\hat{b}} + \hat{\hat{c}} - 4\hat{\hat{a}}\right)}{\hat{\hat{a}} + \hat{\hat{b}}} - \frac{(2 + n^2)\left(\hat{\hat{b}}\hat{\hat{c}} - n^2\hat{\hat{a}}\right)}{(\hat{\hat{a}} + \hat{\hat{b}})^2} \right],$$

$$\hat{\hat{a}} = n^2\frac{EI}{r^4} + \frac{EA}{r^2}, \hat{\hat{b}} = n^2\left(\frac{EI}{r^4} + \frac{EA}{r^2}\right), \hat{\hat{c}} = n^4\frac{EI}{r^4} + \frac{EA}{r^2} \quad\quad\quad \text{(4.4 b)}$$

Here, M is the mass matrix which also include the mass mismatch term δm, G represents the skew-symmetric gyroscopic matrix which results from the Coriolis acceleration while D represents the damping matrix, and K denotes the stiffness matrix. The matrices M, D, and K are symmetric. The approximated parameters γ, κ_1 and κ_2 take constant values that depend on the mode number n and the physical properties of a ring while vector F represents the generalized excitation force. In the damping matrix D, ξ is the damping ratio, and ω_{01} and ω_{02}, respectively, represent non-rotating ring natural frequencies that are associated with the flexural generalized coordinates q_1 and q_2.

Equations (4.2) are employed for the purposes simulating the time response of the ring-type gyroscope for fixed system parameter values which is described in the following section. In addition, these equations are also suitably modified to accommodate uncertainties via random variation of parameters to aid uncertainty quantification. The uncertainty results are presented partly in the present chapter and in detail in Chapter 5.

4.4. Simulation of Deterministic Time Response

4.4.1. Introduction

In the present chapter, for the purposes of investigating the dynamic characteristics of ring-based gyroscopes, time response analysis is performed considering the mathematical model derived in the previous section. The time response analysis is then performed assuming that the mass is excited with a periodic external force in which the excitation frequency is set to be same as the natural frequency associated with a non-rotating system so that the system gain can be maximized. It may be noted that the natural frequency variation with the input angular rate has been marginal and hence this choice for the excitation frequency is considered to have minimal influence on reduction of the resonant characteristics. The dynamic effects due to variation of typical parameters of a MEMS mass-spring gyroscope are examined via numerical simulations and are depicted via suitable transient response plots. The results for varying system parameters such as the input angular rate, damping and mass/stiffness mismatch are then presented.

4.4.2. Natural frequency variation

Typical parameters for a micromachined ring-type angular sensor is considered as shown in Table 4-1. In this thesis, ring is assumed to be fabricated from nickel which is known to have isotropic material properties. It is known that bifurcations of natural frequencies can take place because of the speed-dependent gyroscopic coupling and system stiffness (see e.g., Cho, 2004).

When there is no input angular motion of the ring, as expected, the two natural frequencies of the ring are identical as shown in the previous research by Cho (2004).

Table 4- 1. Ring Parameters for the Numerical Calculations

Density (Nickel)	$\rho = 8800\ (kg/m^3)$
Young's Modulus (Nickel)	$E = 210 \times 10^9 (N/m^2)$
Mean Radius	$r = 500\ (\mu m)$
Radial Thickness	$h = 12.5\ (\mu m)$
Axial Thickness	$b = 30\ (\mu m)$

It was demonstrated that the lower natural frequency decreases while the higher natural frequency increases with the input angular rate (Cho, 2004). It may be noted that for practical range of input angular speeds i.e., $0\sim2\pi$ (rad/sec) the difference between the two natural frequencies are negligible. However, when the mass mismatch is non-zero, the mismatch term δm contributes to the non-rotating ring natural frequencies as well as to the variation of the two natural frequencies as the input angular rate increases. Further, for the system parameters used in the present thesis, a mass mismatch of 0.01% , results in non-identical natural frequencies of $\omega_{01} = 1.89187 \times 10^5 (rad/sec)$ and $\omega_{02} = 1.89178 \times 10^5 (rad/sec)$ for the stationary ring.

4.4.3. Numerical simulation

In a ring gyroscope, it is assumed that the ring element is excited by a harmonic external force while the gyroscope as a whole is subjected to an angular rate. When the system is under the influence of typical input signals it is useful to perform a dynamic response analysis for the ring system. For this purpose, a numerical simulation procedure is developed. This procedure forms the basis of Uncertainty Quantification to be performed later in Chapter 5. The simulation is performed via the fourth-order Runge-Kutta scheme available within the MATLAB computing environment.

As discussed in section 4.1.2, considering the degenerate pair of modes associated with the second flexural mode, if a radial external excitation force of $f_r = \cos \omega_{01} t$ is used to excite the primary mode associated with the generalized coordinate q_1, the force vector in Equation 4.4a takes the form

$$F = \begin{bmatrix} f_1 \cos \omega_{01} t \\ 0 \end{bmatrix}, \quad f_1 = \frac{2 f_r \hat{b}}{\rho A (\hat{a} + \hat{b})}, \tag{4.5}$$

It may be noted that the sinusoidal external force attempts to excite the primary mode at resonance with a frequency close to ω_{01}, which coincides with the non-rotating ring natural frequency associated with the generalized coordinate q_1.

The equations of motion (4.4) are then written in the first order form that is suitable for numerical integration of the ODE's as follows:

$$\dot{q}_1 = q_3, \tag{4.6a}$$

$$\dot{q}_2 = q_4, \tag{4.6b}$$

$$\dot{q}_3 = -(\kappa_1 + \kappa_2 \Omega^2)q_1 + \dot{\Omega}\gamma q_2 - 2\xi\omega_{01}q_3 + 2\Omega\gamma q_4 + f_1 \cos\omega_{01}t, \tag{4.6c}$$

$$\dot{q}_4 = -\dot{\Omega}\gamma q_1 - (\kappa_1 + \kappa_2 \Omega^2)q_2 - 2\Omega\gamma q_3 - 2\xi\omega_{01}q_4, \tag{4.6d}$$

Equations (4.6) are implemented in MATLAB and fourth order Runge-Kutta scheme is employed for integrating the set of ODE's. System parameters listed in Table 4-1 have been used in the simulations while the two natural frequencies ω_{01} and ω_{02} are considered to be identical first to examine the behavior in the absence mass mismatch. The ODE45 integration routine has been found to be suitable for the numerical simulations, with initial conditions set to be zero and the value of time step set to 0.000001 seconds.

4.4.3.1.   Time response without input angular motion

When the ring gyroscope system is subjected to harmonic excitation without any input angular motion ($\Omega=0$ rad/sec), the response of the ring gyroscope along the driving direction is obtained numerically and illustrated in Figure 4-4 (a). It can be seen that the time response of the ring gyroscope reaches a state of steady-state after about 0.002 seconds from the commencement of the excitation. On the other hand, the response of the ring gyroscope along the sensing direction is zero as there is no input angular motion.

It may be noted that the gyroscopic coupling present in the system is the main reason for the transfer of energy between the modes when the sensor is subjected to an input angular rate. By

increasing excitation force magnitude, an increase in the sensitivity can be obtained while the larger deflection of the ring in the sensing direction indicates higher sensitivity for the sensors. However, larger deflection may cause fatigue in the ring and as a result can lead to reduction in life for the sensor.
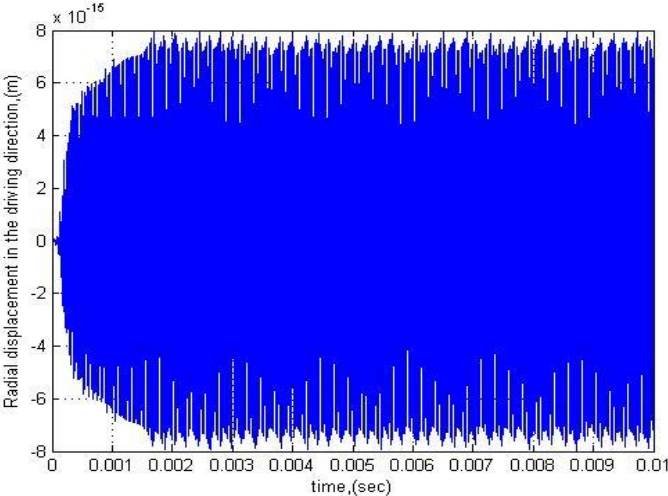
(a)
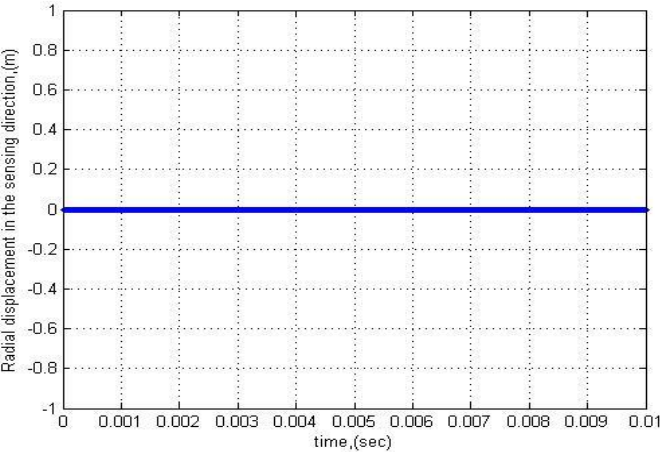
(b)

Figure 4-4. Radial displacement in the (a) driving direction and (b) sensing direction without input angular rate

4.4.3.2.　Time response with input angular motion

The variations of the natural frequencies are significantly small in the low speed range (i.e., less than 2π rad/sec) for which typical MEMS ring gyroscopes are designed, the excitation frequency can be assumed to be constant and made to coincide with the non-rotating natural frequency, ω_{01}, associated with the generalized coordinate q_1. In order to compensate for the increase in the first natural frequency with the angular speed, an excitation frequency of 1.89189×10^5 rad/sec which is slightly higher than the first natural frequency has been used for the simulations.

In order to examine the response of the ring gyroscope associated with the generalized coordinate q_2 (sensing direction), a suitable profile for the input angular rate must be applied. In the present analysis, this profile is assumed to start from a zero value and to reach a steady-state angular speed $\overline{\Omega}$ via a smooth increase in speed as depicted in Figure 4-5. The equation used to represent an angular rate profile that represents a smooth increase in the angular rate has been chosen to be

$$\Omega = \frac{n\pi}{2}\,\sin(\frac{\pi t}{0.005} - \frac{\pi}{2}) + \frac{n\pi}{2}\ \text{(rad/s)} \qquad\qquad \text{for } t < 0.005 \qquad\qquad (4.7)$$

At time $t = 0.005$ seconds the input angular rate time-profile is set to reach the steady-state of $n\pi$ rad/s. Different steady-state angular speeds such as $\overline{\Omega} = \pi, 2\pi, 5\pi, 8\pi, 10\pi$ as depicted in Figure 4-5 have been used to investigate the dynamic response.
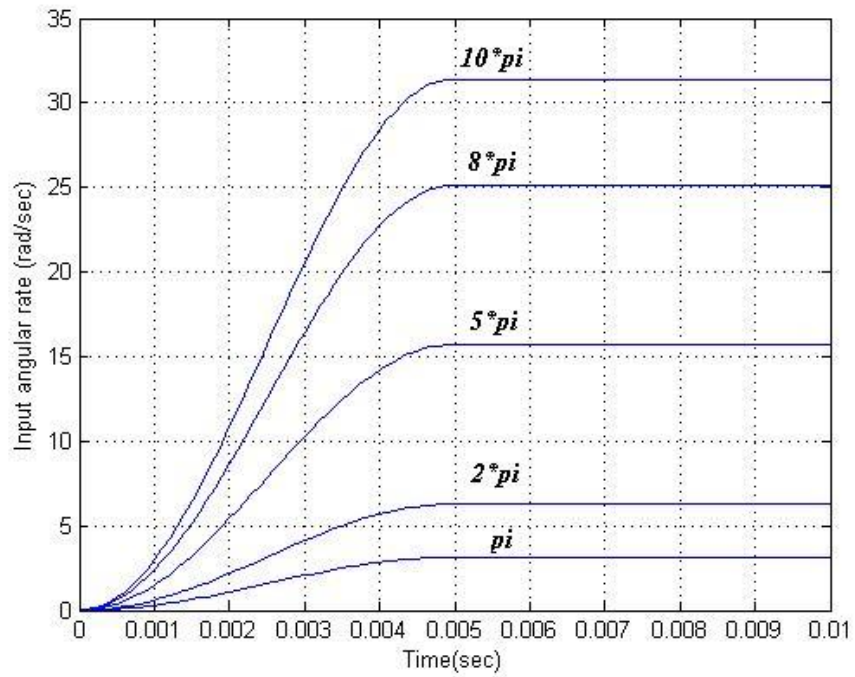
Figure 4-5. Input angular rate time-profile

In this chapter, a steady-state angular speed of $\overline{\Omega} = 2\pi$ rad/sec is considered for the purposes of

characterizing typical dynamic responses. When both the input angular motion and the harmonic

excitation are introduced simultaneously, the time responses of the system in the driving and the

sensing directions, respectively, are shown in Figures 4-6 (a) and (b).
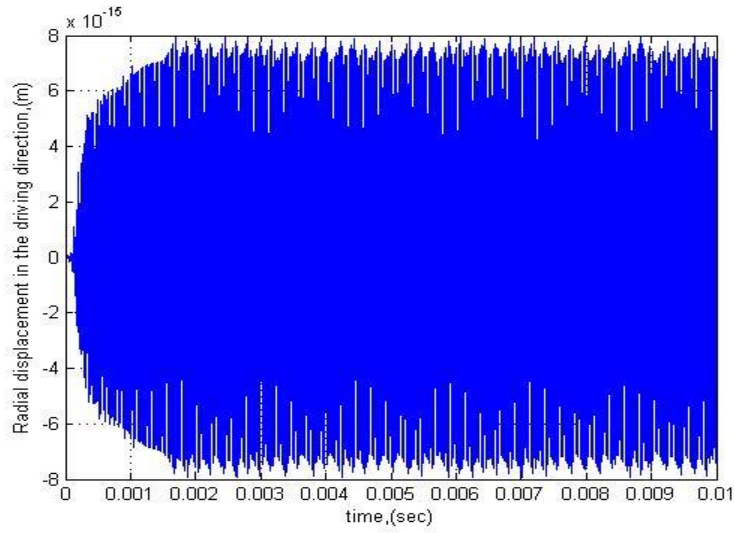
(a)
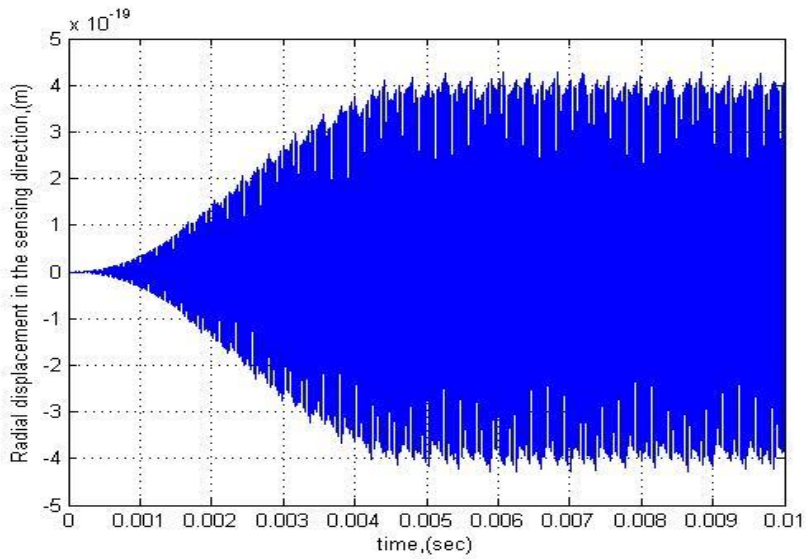
(b)

Figure 4-6. Radial displacement in the (a) driving direction and (b) sensing direction with input angular rate for $\overline{\Omega} = 2\pi$ rad/sec input angular rate

4.4.3.3.   Mass mismatch

It is known that due to uncertainties present in the MEMS fabrication process, it is impossible to obtain equal distribution of ring mass and uniformity of the suspension elements. This will manifest in the system as a frequency mismatch for the driving and the sensing motions. Hence, this form of mismatch is considered as one of the important parameters that affect the system dynamics. Hence, the effects of mass mismatch on the time response of the ring gyroscope are examined in this section. Figures 4-7 (a) and (b) show the response amplitudes for the ring system in the driving and sensing directions for time duration of 0.01 seconds. As illustrated in Figure 4-7 (b), a reduction in the response in the sensing direction is evident when the frequency mismatch of the vibratory system is increased. It may be noted that this reduction can be detrimental to the achievable performance of this forms of gyroscopes, for example, it can lead to lower sensitivity for the angular rate sensor. Further, uncertainty propagation due to this parameter can be considered important and forms a basis for one of the uncertainty quantification study presented in Chapter 5.
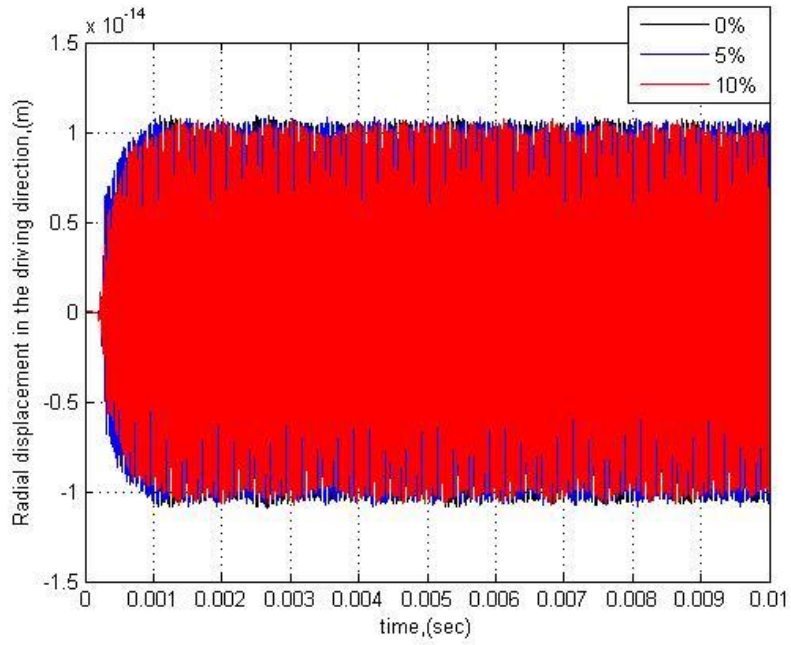
(a)
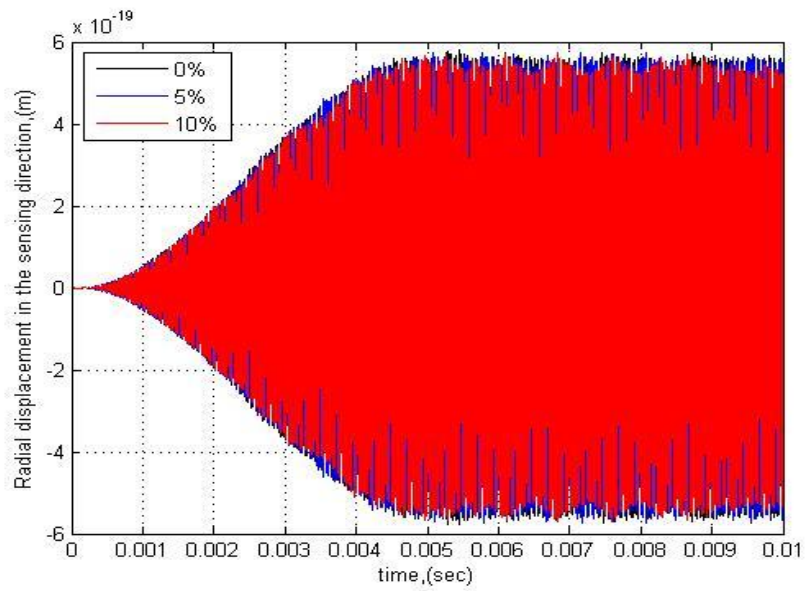
(b)

Figure 4-7. Variation of radial displacement in the driving (a) and sensing (b) directions for different mass mismatch values

4.5. Simulation of Random Time Response

4.5.1. Introduction

In present thesis, to see the effect of randomness and drift in MEMS mass-spring gyroscope model, a drift noise model is assumed in the following form:

$$d_d = \sigma_1(e^{a_d t} - 1) + \sigma_2 \zeta(t) \ . \tag{4.8}$$

This model consists of two parts. The first part represents the drift which is an exponential term, while the second part denotes the uncertainty which is introduced in the form of a random component.   In order to obtain the typical drift rate from Equation (4.8), the drift exponential coefficient a_d is set at a value 1.0 and the drift coefficient σ_1 is set at a value 0.0245. Uncertainty coefficient σ_2 is chosen to be 0.0001.

For the present study, the model presented via Equation (4.8) is to represent additive noise and drift to the nominal input angular rate Ω. Hence, the input angular rate takes the form:

$$\Omega = \overline{\Omega} + d_d \tag{4.9}$$

The drift/noise presented in Equation (4.8) is also used for representing uncertainties in other system parameters such as mass mismatch and damping ratio. As described the section 2.5.2 of Chapter 2 for the case of mass-spring gyroscope, Monte Carlo simulation method is used to predict the response statistics and uncertainty quantification. When the ring is subjected to uncertainties in input angular rate (Ω), mass (δ_m) and damping ratio (ξ), randomness is incorporated in the corresponding parameters and Monte Carlo simulation is used to generate multiple output samples.

4.5.2. Robustness of simulation

4.5.2.1. Stochastic response simulation after peak-picking

As shown in section 4.4.3.2, the output time response in the sensing direction contains two parts, known as transient and steady-state parts. The approach discussed in chapter 2 in the section 2.5.3.1 used in quantifying the variation of the mean values and the standard deviation of the steady state of time response along the sensing direction are employed here. After peak-picking and removal of the transient part, the resulting response is used to characterize and predict response statistics via Monte Carlo method. The plot that represents this response is illustrated in Figure 4-8 where the last sample point of approximately 7,500 coincides with 0.25 seconds. In the next sections, an attempt will be made to justify the prediction of responses via selection of suitable time/ensemble response statistics.
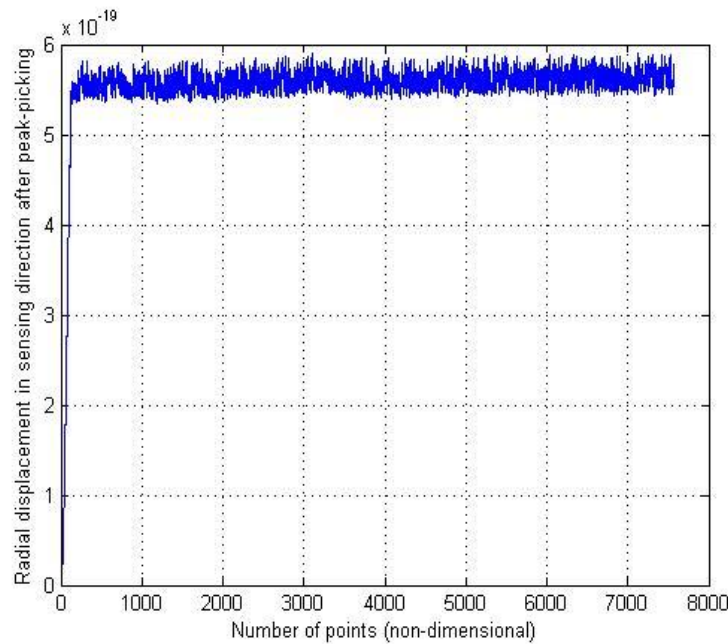
Figure 4-8. Time response after peaks-picking for ring gyroscope ($\Omega=2\pi$ rad/sec)

4.5.2.2.   Optimal number of points along time response

Before performing the uncertainty quantification, it is important to come up with a suitable set of data that exhibit consistence and convergence for the response statistics. For this purpose, number of samples along the time axis as well number of samples along the sample paths has been considered. This approach has been discussed in section 2.2.3.2 of chapter 2 and hence not presented in detail here.

An attempt is made to define the number of points along the time axis which can be used in the application of Monte Carlo method based on the numerical simulation. After peak-picking and the removal of the transient, the first 100 points along the remaining steady state response shown in Figure 4-10 have been considered first. These 100 points have been used to determine the temporal mean and standard deviation. This process is considered with increments of 100 points up to 6000 points and performed for cases without and with the drift, keeping the noise component the same.
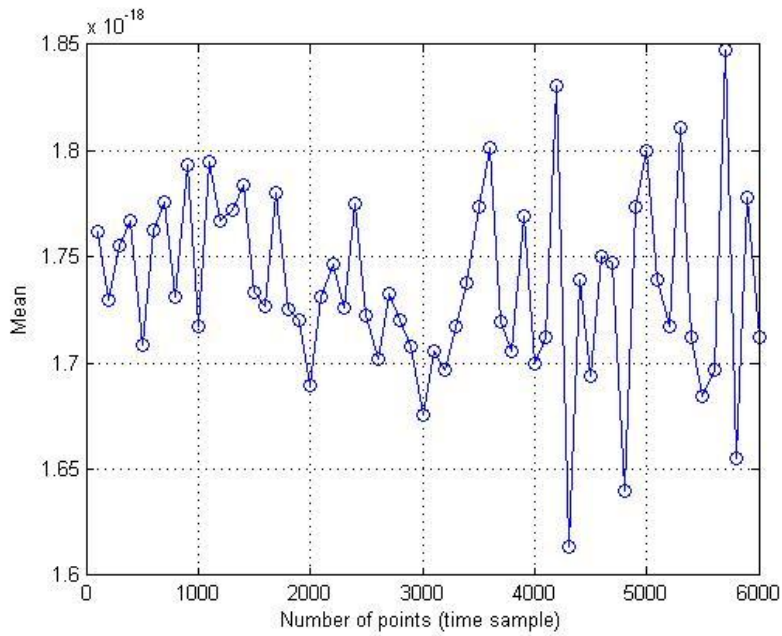
(a)
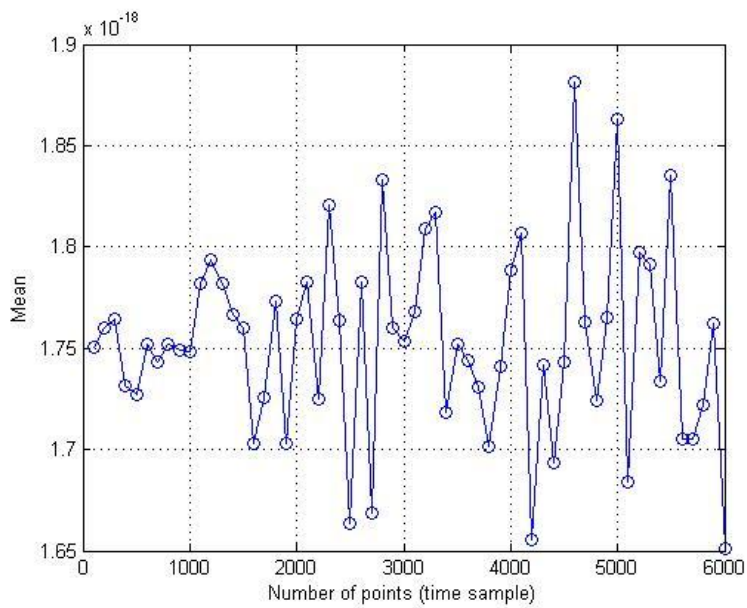
(b)

Figure 4-9. Number of points vs. Mean along the time response for ring gyroscope (a) without drift (b) with drift ($\Omega=2\pi$ rad/sec)
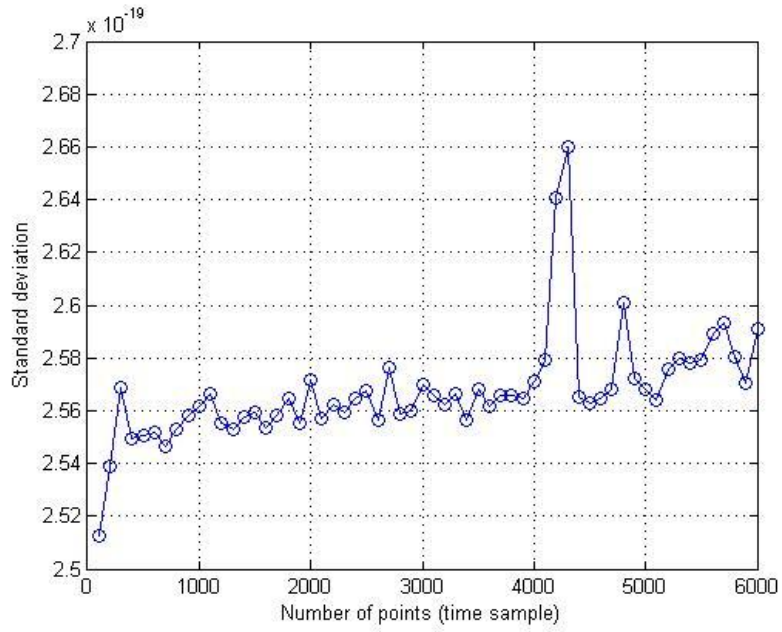
(a)
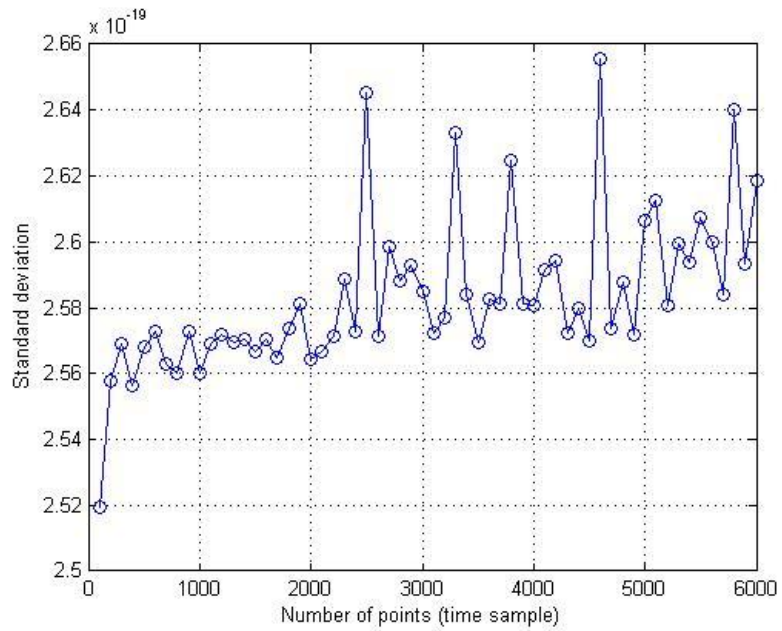
(b)

Figure 4-10. Number of points vs. standard deviation along the time response for ring gyroscope (a) without drift (b) with drift ($\Omega=2\pi$ rad/sec)

Figures 4-9 and 4-10, respectively, illustrate the results for the temporal mean and the standard deviation. These figures also illustrate that reasonable convergence will be achieved any point after 1000 points which are considered for further analysis in predicting ring gyroscope response statistics. Figures 4-9 and 4-10 also illustrate the effect of increasing drift on the response statistics. Hence, an alternate approach is warranted for predicting the response statistics for highlighting the noise term.

The statistical response predictions performed in the previous section confirms the significance of considering time sample points past the 1000 points based on both the mean and standard deviation. In order to ascertain the predictions via the sample paths, 100 random samples have been employed. The sample paths are depicted in Figure 4-11.
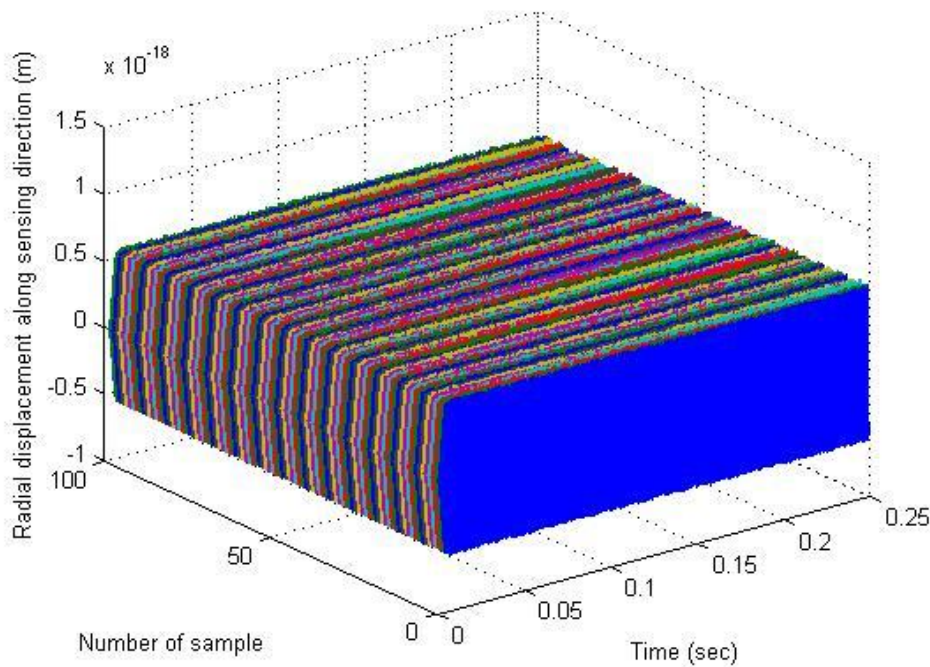
Figure 4-11. Radial displacement in the sensing direction with input angular rate (100 samples)
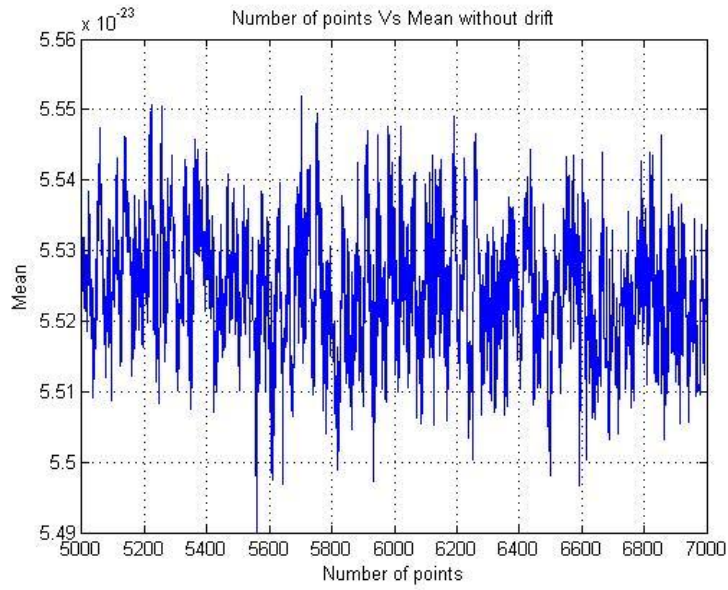
(a)
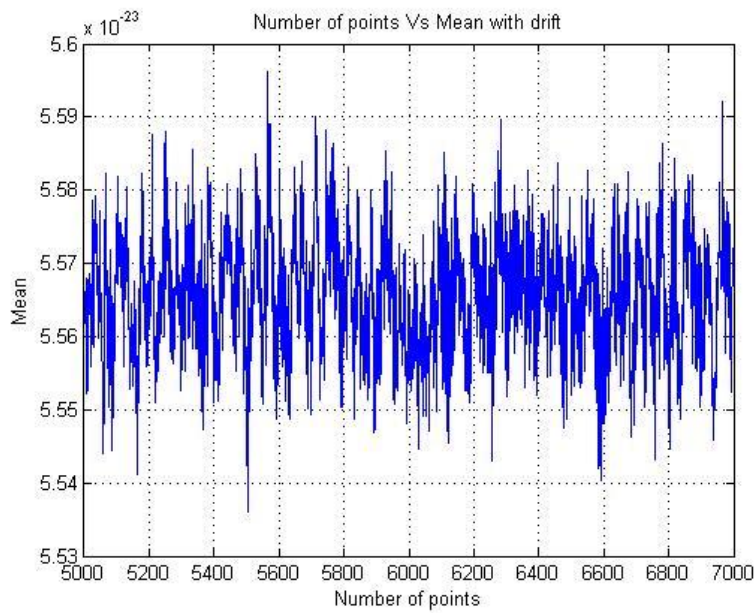
(b)

Figure 4-12. Number of points vs. Ensemble Mean (a) without drift and (b) with drift (100 samples along path axis and $\Omega=2\pi$ rad/sec)
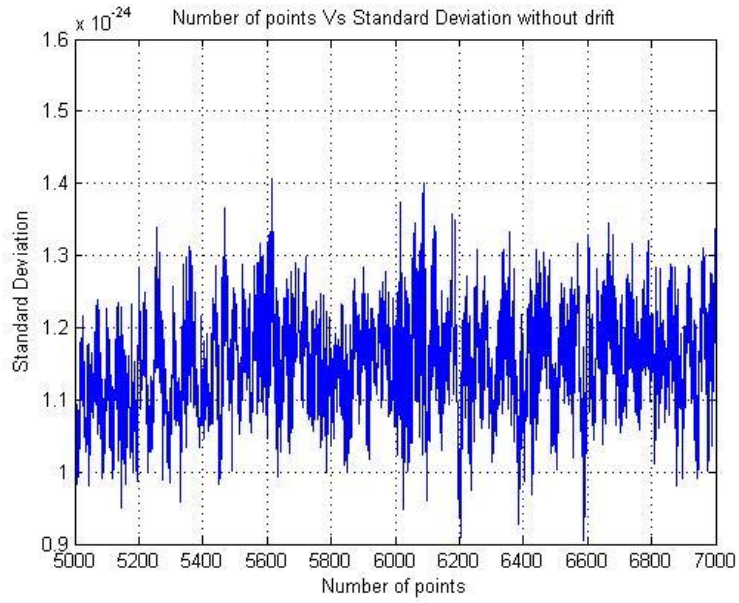
(a)
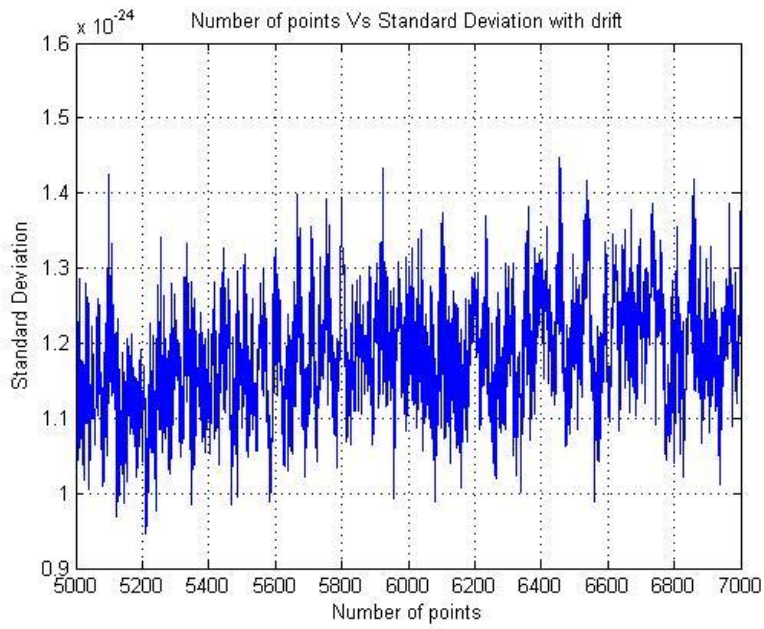
(b)

Figure 4- 13. Number of points vs. Standard deviation (a) without drift and (b) with drift (100 samples along path axis and $\Omega=2\pi$ rad/sec)

Employing the 100 samples, the ensemble mean as well as the standard deviations are computed. Figures 4-12 (a) and (b) show that reasonable consistency for ensemble mean without and with drift is obtained for any points after 5800 points. However, the predictions made for the standard deviations for the response are illustrated in Figures 4-13 (a) and (b). These figures demonstrate that after 5800 points in cases without and with drift, the standard deviation values show a converging trend and points past the 5800 mark may be considered suitable for further analysis in predicting response statistics.

4.5.2.3. Discrete time steps

It is known that time step size plays a significant role in the numerical simulation process. Obviously, smaller time steps results in more accurate predictions of the response along with increased computations costs. In order to find the optimal time step to achieve reasonably accurate results in moderate computational costs, a suitable fixed step size is selected by running several simulations via the ODE45 integration routine within MATLAB. Based on the simulation trials, a time step size of 0.000001 seconds has been chosen to be adequate. Further reduction in step size has been found to be unnecessary.

4.6. Closure

A numerical simulation scheme has been developed for characterizing the dynamic response of ring-based gyroscopes. This scheme is based on a two-mode discredited mathematical model

and has been used for investigating the dynamic response characteristics of a ring element when the ring gyroscope is subjected to an input angular rate. Response amplitudes are obtained when parameters mass mismatch are varied. Both noise and drift terms have been incorporated in the model for the purposes predicting the response under system parameter uncertainties. Both time based and sample based data analysis has been formed to achieve a robust scheme for predicting useful response statistics via Monte Carlo simulation. This robust scheme forms the basis of a detailed uncertainty quantification study to be performed for ring-based gyroscopes.

Chapter 5

5. Uncertainty Quantification for Ring-based Gyroscopes

5.1. Introduction

In the previous chapter, a systematic numerical simulation procedure has been developed based on a mathematical model that represents the dynamical behavior of ring type vibratory gyroscopes. In addition to determining the response due to changes in system parameters via a deterministic response analysis, predictions of response statistics due to random inputs have also been illustrated.   Suitable number of temporal points as well as sample paths have been selected and optimized for further analysis while a fixed optimal time step size has also been ascertained. In this chapter, attention is focused on examining the optimal number of sample paths for characterizing the response statistics via ensemble mean and standard deviations. Employing the optimal sample number, uncertainty quantification is performed for parameter uncertainties in input angular rate, mass mismatch, and the quality factor. In addition, uncertainty quantification in the frequency domain has also been performed considering uncertainties in mass mismatch.

5.2. Optimal number of Samples

When the system is subjected to harmonic excitation with input angular motion which contains noise and drift, the response along the sensing direction is achieved numerically and the results have been presented in Chapter 4. Optimal as well as robust sampling strategies are developed for ring gyroscopes based on the simulated dynamic responses via peak-picking as illustrated in

Figure 5-1. After eliminating the transient oscillatory motion, the Monte Carlo method is applied

on the steady state part of the time response. Results for 70 samples, are depicted in Figure 5-2

and it may be noted that a suitable *y*-axis scale has been chosen for clarity.
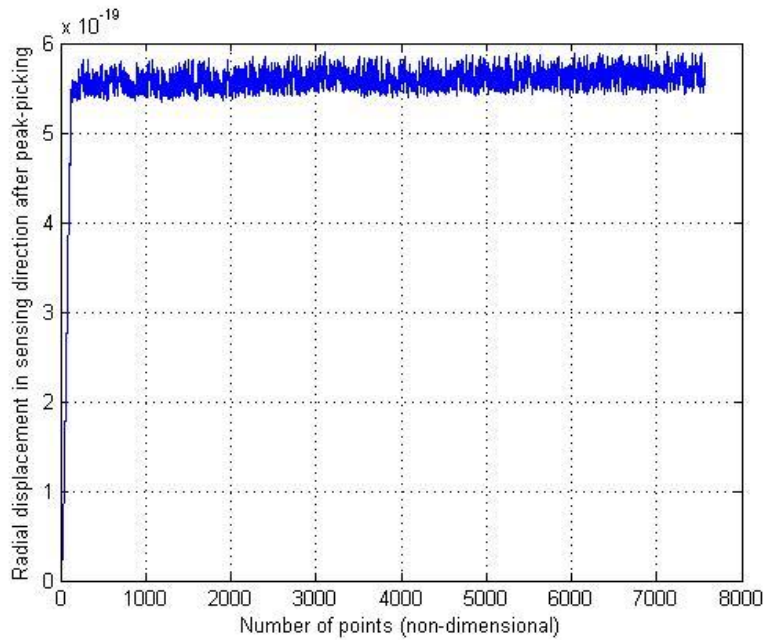
Figure 5-1. Time response after peak-picking for ring gyroscope (Ω=2π rad/sec)
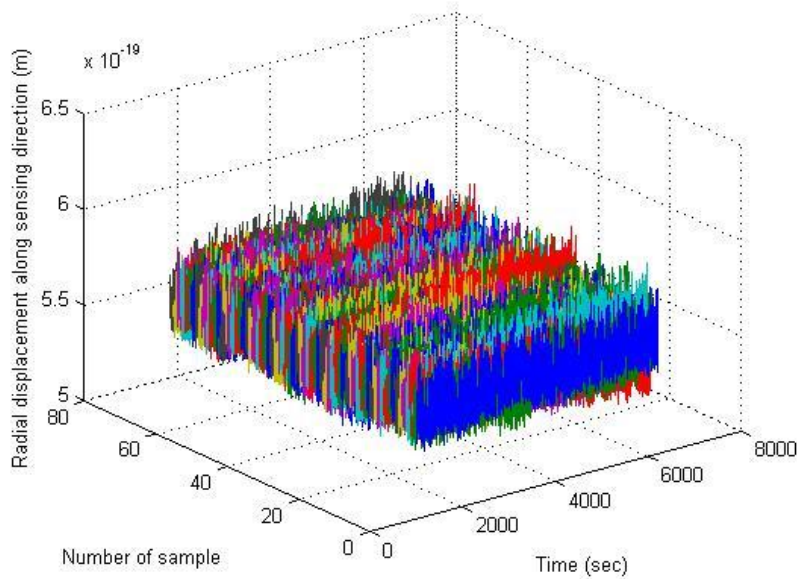
Figure 5-2. Radial displacement in the sensing direction after peak-picking (70 samples)

Optimization of the number of samples is an essential part for Monte Carlo method since use of larger number of samples increases the computational effort significantly. Following the analysis presented in the Chapter 4, it has been determined that any point after 5800 points along the steady part of Figure 5-1 can be chosen for further analysis. In the present analysis five temporal points at 6201, 6202, 6203, 6204, 6205 have been considered for the application of Monte Carlo simulation. At these points, ensemble mean as well as standard deviation have been computed for varying sample numbers starting from 5 to 100 with an increment of 5 samples.

The computed ensemble mean for the cases of without consideration of drift and with drift, respectively, are illustrated in Figures 5-3 (a) and (b). The corresponding figures for the standard deviation as shown in Figures 5-4 demonstrate reasonable convergence after 30 samples. Further, these ensemble standard deviation predictions seem to be consistent at the 5 temporal points considered. Hence, it can be concluded that any of the 5 temporal points can be considered for the ensemble mean and standard deviation computations. For the present analysis, the point 6201 has been chosen with computations employing 70 samples.
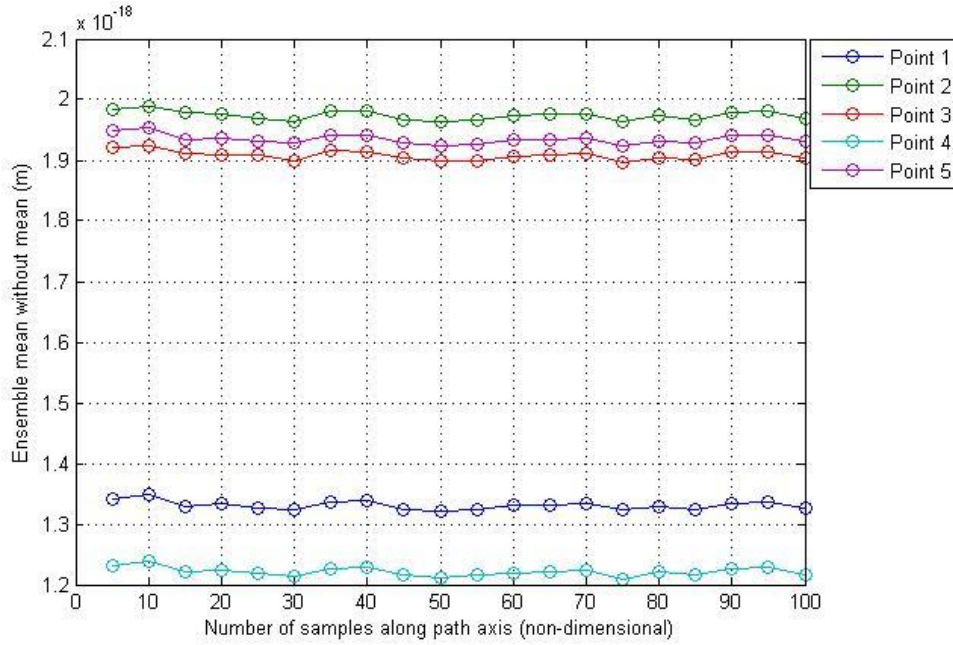
(a)
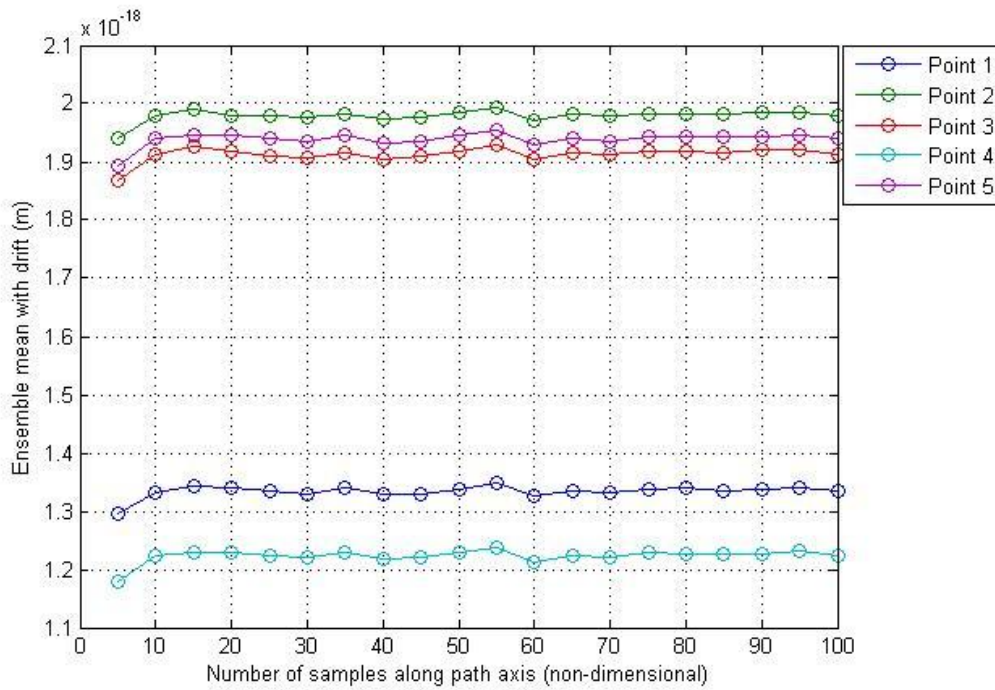
(b)

Figure 5-3. Number of samples along path axis vs. Ensemble mean (a) without drift and (b) with drift ($\Omega=2\pi$ rad/sec)
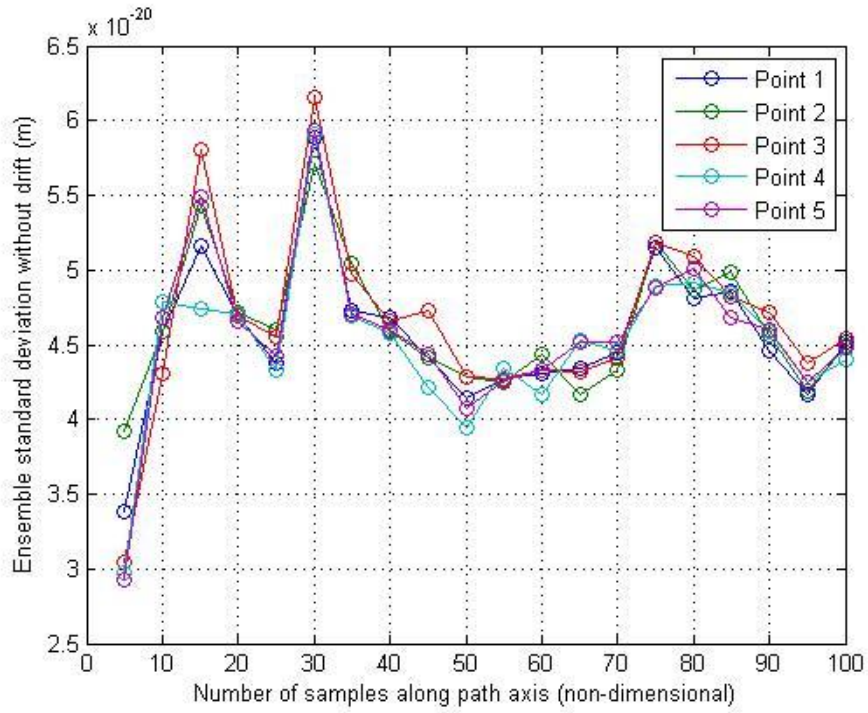
(a)
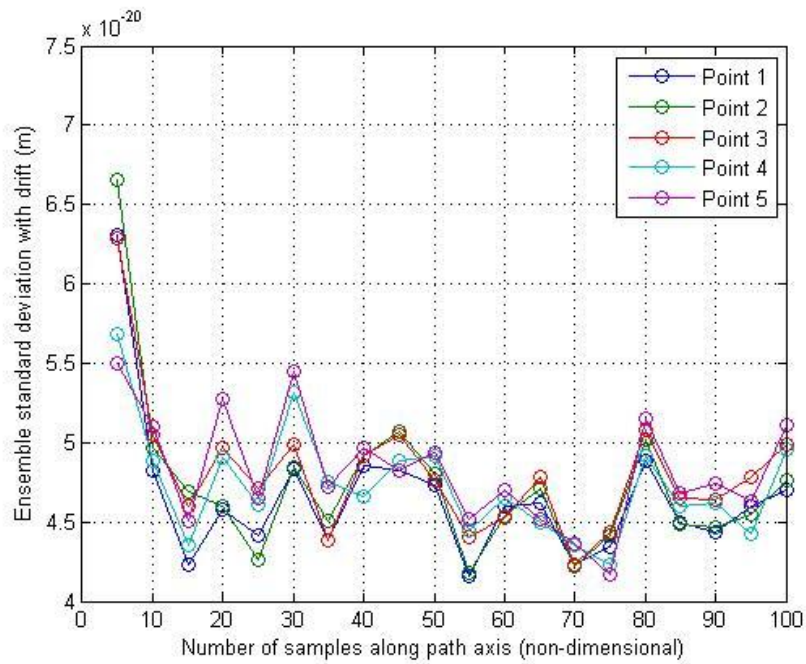
(b)

Figure 5-4. Number of samples along path axis vs. Standard deviation (a) without drift and (b) with drift ($\Omega=2\pi$ rad/sec)

The point 6201 has been singled out from Figure 5-2 and 70 samples are shown via the 3D plot for illustrative purposes. These 70 samples, when subjected to uncertainties in various system parameters are useful in estimating the response statistics via the uncertainty quantification process.
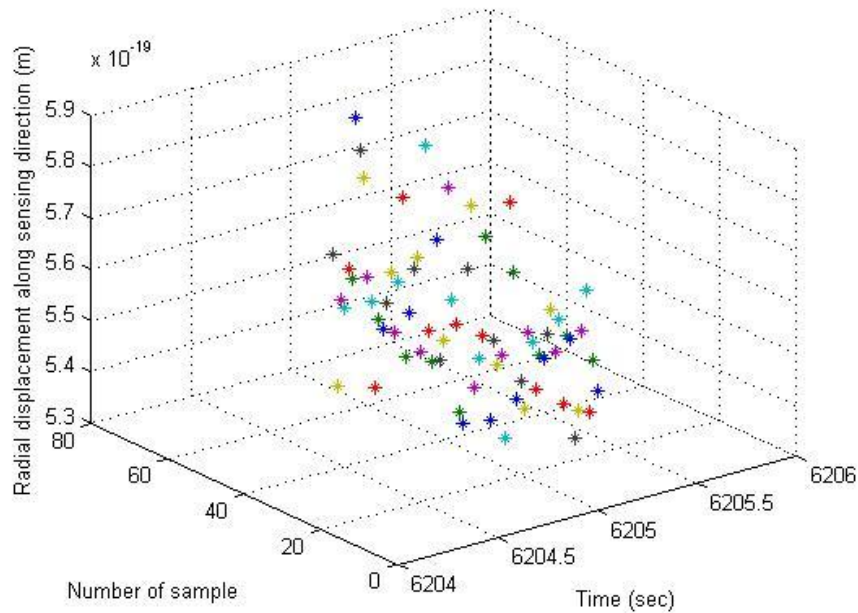
Figure 5-5. Radial displacement in the sensing direction with input angular rate at point 6201 (70 samples)

5.3. Uncertainty Quantification Results and Discussion

Uncertainties in input angular speed are introduced in the mathematical model considering drift and noise terms and the resulting dynamic response simulations are used to obtain optimal number of points along time axis and optimal number of samples along path axis. This optimal configuration is also used for examining uncertainties in mass mismatch. For the purposes of uncertainty quantification, the noise term in the model is introduced as a random variable with

Normal (Gaussian) distribution. At a certain temporal point 6201 which lies after 5800 points along time sample, 70 samples are taken along sample path axis for the application of Monte Carlo simulation based on the dynamic response. This enables prediction of response statistics in the form of standard deviation of output response for different cases.

5.3.1. Uncertainty in Input Angular Rate

For this case, when the mass mismatch for ring is fixed at 0.01% and for the purpose of generating random numbers having Gaussian distribution, mean input angular rate (Ω) is fixed at 2π rad/sec and standard deviations are varied from 1% to 10% of 2π rad/sec. Employing this mean and standard deviations random numbers are generated within the MATLAB environment and these random inputs are considered in the simulation process and corresponding output standard deviations are obtained. 70 random samples are taken for each input standard deviation in order to achieve corresponding ensemble output standard deviation. To demonstrate the relation between input and output standard deviation via continuous curve 10 input standard deviations are considered. These curves are also investigated for varying fixed values of damping ratio ξ values from 0.01 to 0.05 with an increment of 0.01 as shown in Figure 5-5. It may be recalled that the nominal ξ is 0.01 and hence the choice of ξ's represent above and below this nominal value.

Curves shown in Figure 5-6 reveal that variation of input angular rate standard deviation does not have a significant effect on the output response standard deviation. It may be attributed to the negligible effects that the input angular rate has on the natural frequencies. The increase in

response standard deviation with increasing ξ values up to 0.03 also evident in the Figure 5-6. When the damping ratio ξ is further increased the response standard deviations decrease and then again tends to increase. It may be noted that a damping ratio of 0.03 appears to form a threshold value in the case of a ring gyroscope. This prediction suggests careful consideration of damping ratios in the design of this form of gyroscopes when uncertainties in angular rate are dominant.
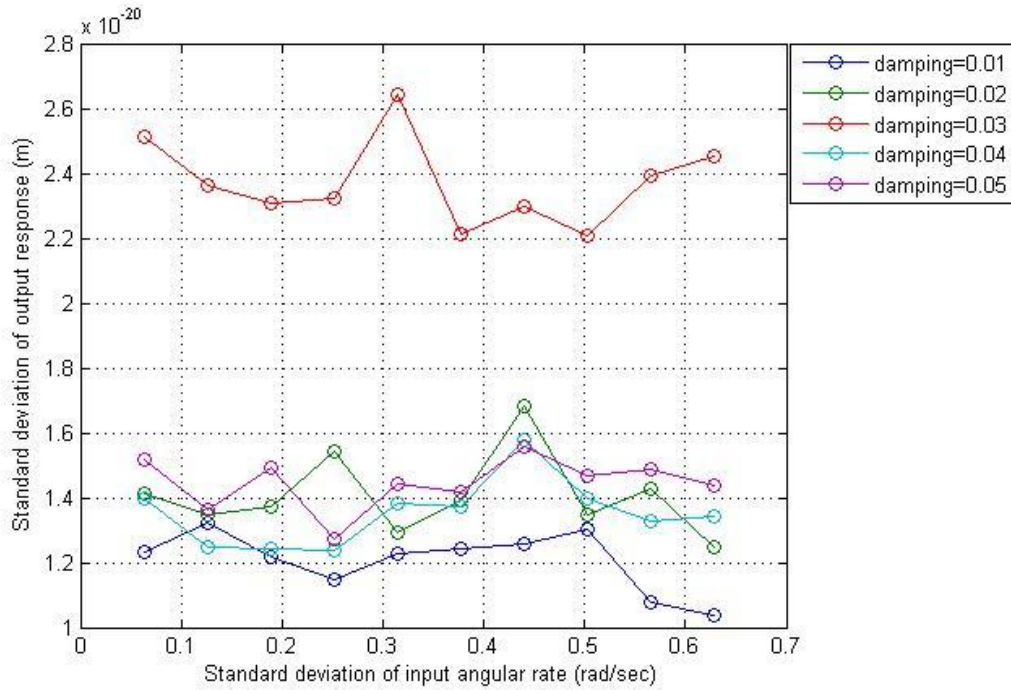
Figure 5-6. Standard deviation of input angular rate vs. standard deviation of output response, (mass mismatch is 0.01%)

5.3.2. Uncertainty in Mass Mismatch

For the purposes of introducing mass mismatch, Equation (4.2) which is given in chapter 4 can be rewritten as

$$\begin{bmatrix} 1 & 0 \\ 0 & 1+\delta_m \end{bmatrix} \ddot{q} + \begin{bmatrix} 2\xi\omega_{01} & -2\Omega\gamma \\ 2\Omega\gamma & 2\xi\omega_{02} \end{bmatrix} \dot{q} + \begin{bmatrix} \kappa_1 + \kappa_2\Omega^2 & -\dot{\Omega}\gamma \\ \dot{\Omega}\gamma & \kappa_1 + \kappa_2\Omega^2 \end{bmatrix} q = \begin{bmatrix} f_1 \cos \omega_{01} t \\ 0 \end{bmatrix}, \qquad (5.1)$$

where $\boldsymbol{q} = [q_1 \ q_2]^T$ represents a vector that contains the generalized coordinates, δm is the mass mismatch and the elements of the system matrices are given in section 4.1.2 of chapter 4.

In this case, for a fixed input angular rate (Ω) of 2π rad/sec, standard deviations of mass mismatch are varied from 0.00001 with an increment of 0.00001 up to 0.0001 while the mean is fixed at 0.0001. The above mean and standard deviation values are employed for generating normally distributed random numbers via MATLAB and for each input standard deviation 70 samples are employed within the simulation in order to get corresponding ensemble standard deviation of output response. 10 different standard deviations for mass mismatch and corresponding output standard deviations are generated and illustrated in Figure 5-7. In this Figure, this predictions are also performed for different fixed values of damping ratio ξ. It is interesting to note that, as in the case of uncertainty in input angular rate, a threshold value of 0.03 for the damping ratio exists in this case.
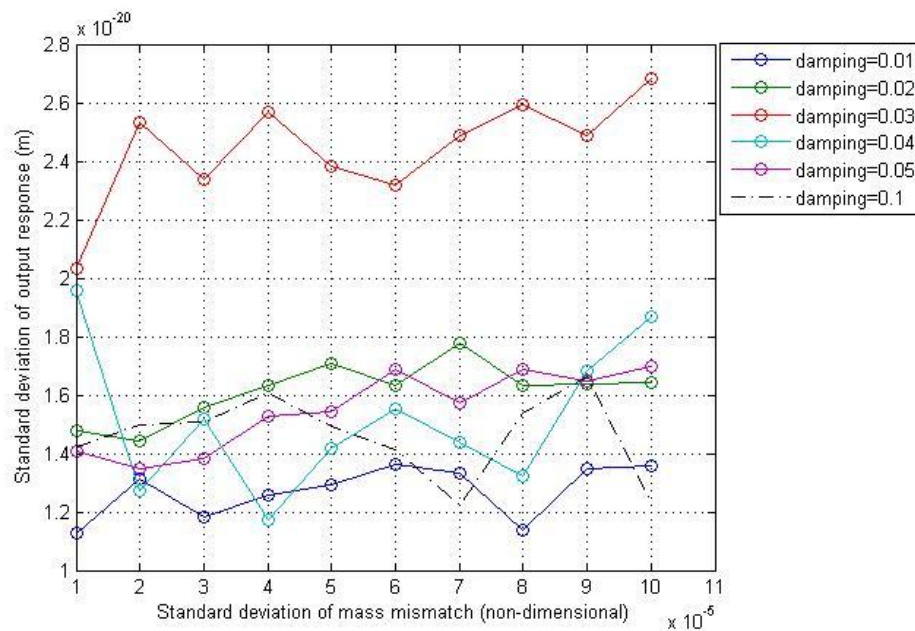
Figure 5-7. Standard deviation of mass mismatch vs. standard deviation of output response, ($\Omega = 2\pi \ rad/sec$)

In order to quantify the influence of uncertainty in mass mismatch on the output response statistics, Least-square approach is employed on the resultant data to obtain a parametric relationship between the two relevant standard deviations. MATLAB command 'polyfit' with degree 2 is employed for this purpose to obtain this parametric relationship:

$$\sigma_{response} = -1.8379 \times 10^{-13} \sigma_{m.mismatch}^2 + 3.4748 \times 10^{-17} \sigma_{m.mismatch} + 1.1503 \times 10^{-20},$$

(5.2)

where $\sigma_{response}$ and $\sigma_{m.mismatch}$ denote standard deviations of output response and mass mismatch respectively. This process is illustrated in Figure 5-8.
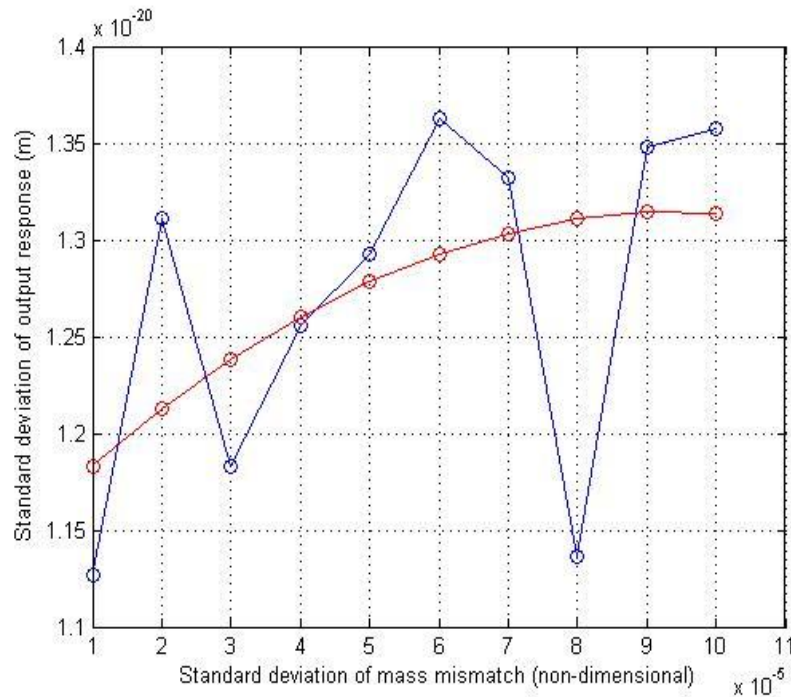
Figure 5-8. Standard deviation of mass mismatch vs. standard deviation of output response, $(\Omega = 2\pi \ rad/sec)$

5.3.3. Uncertainty in Damping Ratio

In this case, for fixed value of input angular rate ($2\pi \ rad/sec$) when normally distributed random numbers are generated with mean damping ratio value of 0.0001 and the standard deviations are varied from 0.00001 with an increment of 0.00001 up to 0.0001. For each standard deviation of damping ratio uncertainty, 70 random samples are utilized to acquire corresponding ensemble standard deviation of output response. 10 standard deviation values of damping ratio uncertainty are chosen to generate curves which represent a relationship between input and output standard deviations. These curves are also generated for different fixed mass mismatch values. It is evident from Figure 5-9, that for 0.01% and 0.02% mass mismatch the standard deviations of output response have significantly different trend when compared with those obtained for higher mismatch values. It may be attributed to the fact that for lower mass mismatch the two natural frequencies are likely to be close to each other. The response statistics may take large values as a result of internal resonance. For the lower values of mass mismatch, when the damping ratio increases, the output standard deviations increase and seems to converge. Further, in order to illustrate the effect of large mass mismatch on the performance of ring gyroscope, 10% and 20% mass mismatch are used in the numerical simulation. Figure 5-9 shows that, for large mass mismatch, magnitudes of output standard deviations do not have notable variation as internal resonance may not play a significant role.
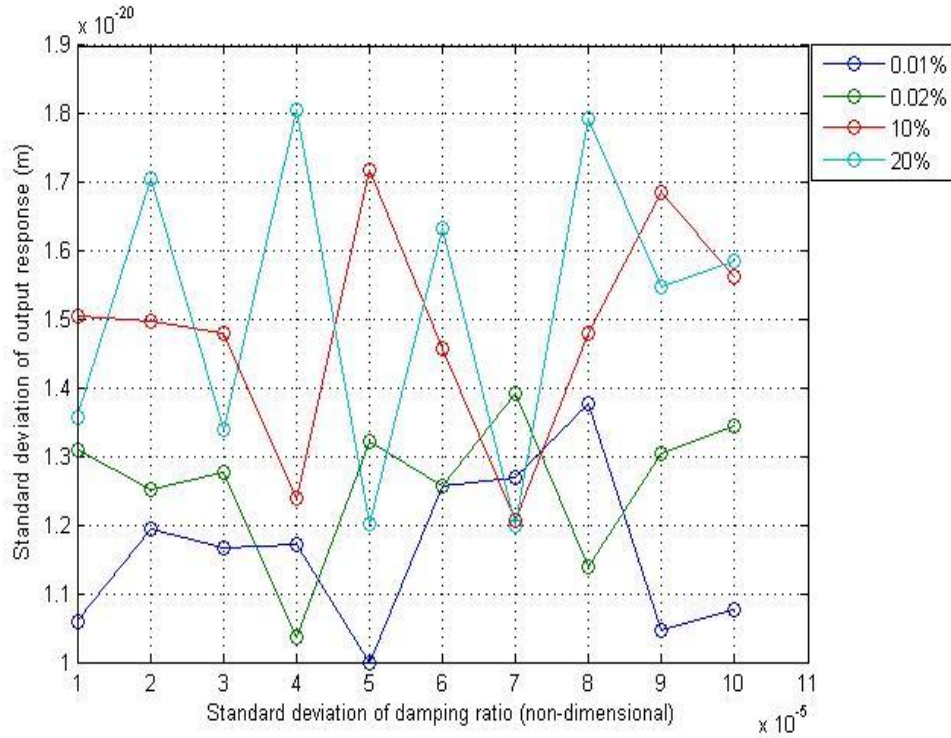
Figure 5-9. Standard deviation of damping ratio mismatch vs. standard deviation of output response for different mass mismatch ($\Omega = 2\pi \ rad/sec, \xi = 0.01$)

Least-square method is applied on resultant data to quantify the influence of uncertainty in damping ratio mismatch on the output response statistics. For this purpose, the plot that correspond to 0.01% mismatch in Figure 5-9 is considered and redrawn in Figure 5-10. From the data set, a parametric relationship between the two relevant standard deviations can be extracted:

$$\sigma_{response} = -6.0530 \times 10^{-13} \sigma_{d.mismatc\ h}^2 + 7.0788 \times 10^{-17} \sigma_{d.mismatc\ h} + 1.0078 \times 10^{-20},$$

(5.3)

where $\sigma_{response}$ and $\sigma_{d.mismatc\ h}$ indicate as standard deviations of output response and damping ratio mismatch respectively.
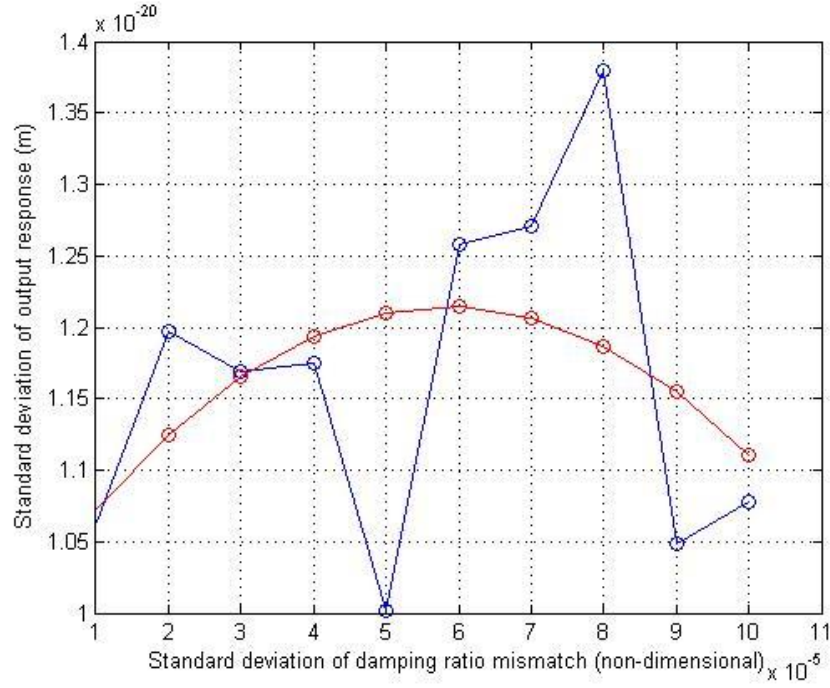
Figure 5-10. Standard deviation of damping ratio vs. standard deviation of output response for different mass mismatch ($\Omega = 2\pi\ rad/sec,\ \xi = 0.01$)

5.4. Frequency response

In this section an attempt is made for formulating a systematic procedure for performing uncertainty quantification in the frequency domain. On order to illustrate this procedure, uncertainty in mass mismatch has been chosen.

Taking Laplace transformation of system equations (5.1), the equations in the *s* domain can be expressed as

$$s^2 Q_1(s) + 2\xi\omega_{01}sQ_1(s) - 2\gamma\Omega sQ_2(s) + (\kappa_1 + \kappa_2\Omega^2)Q_1(s) = F_1(s)\ , \qquad (5.4)$$

$$(1 + \delta m)s^2 Q_2(s) + 2\xi\omega_{02}sQ_2(s) + 2\gamma\Omega sQ_1(s) + (\kappa_1 + \kappa_2\Omega^2)Q_2(s) = 0\ , \qquad (5.5)$$

102

where $F_1(s), Q_1(s)$ and $Q_2(s)$ represent, respectively, the Laplace transform of $f_1(t), q_1(t)$ and $q_2(t)$.

From Equations (5.4) and (5.5), the amplitude ratio of the displacement in the sensing direction to the displacement in the driving direction (i.e., $|Q2/Q1|$) is evaluated considering mass mismatch. Similarly, the forced frequency response magnitude $|Q2/F1|$ is also evaluated. For this purpose, the magnitudes of

$$\frac{Q_2(s)}{Q_1(s)} = -\frac{2\gamma\Omega s}{(1+\delta m)s^2 + 2\xi\omega_{02}s + (\kappa_1 + \kappa_2\Omega^2)} \,, \tag{5.6}$$

$$\frac{Q_2(s)}{F_1(s)} = -\frac{2\gamma\Omega s}{As^4 + Bs^3 + Cs^2 + Ds + (\kappa_1 + \kappa_2\Omega^2)^2} \,, \tag{5.7}$$

where

$$A = 1 + \delta m \,, \tag{5.8a}$$

$$B = 2\{\xi\omega_{02} + (1 + \delta m)\xi\omega_{01}\} \,, \tag{5.8b}$$

$$C = (1 + \delta m)\{2(\kappa_1 + \kappa_2\Omega^2) + 4\xi^2\omega_{01}\omega_{02} + 4\gamma^2\Omega^2\} \,, \tag{5.8c}$$

$$D = 2(\xi\omega_{01} + \xi\omega_{02})(\kappa_1 + \kappa_2\Omega^2) \,, \tag{5.8d}$$

The parameters given in Table 4-1 are used for the numerical calculations that are used in the evaluation of the amplitude ratio and the forced frequency response. From Equation (5.6), the amplitude ratio of the displacement in the sensing direction to the displacement in the driving direction (i.e., $|Q2/Q1|$) is evaluated and depicted for damping ratio 1×10^{-9} and 1000 in Figures 5-11 and 5-12, respectively. The figures show that the amplitude ratio has the maximum

value near the non-rotating ring natural frequency ω_{02} and that the magnitude of the amplitude

ratio increases with an increase in the input angular rate.

Similarly, the frequency response magnitude $|Q2/F1|$, evaluated from Equation (5.7), is

illustrated for damping ratio 1×10^{-9} and 1000, respectively, in Figures 5-13 and 5-14. In

addition, the magnitude of frequency response is shown to increase as the input angular rate

increases.
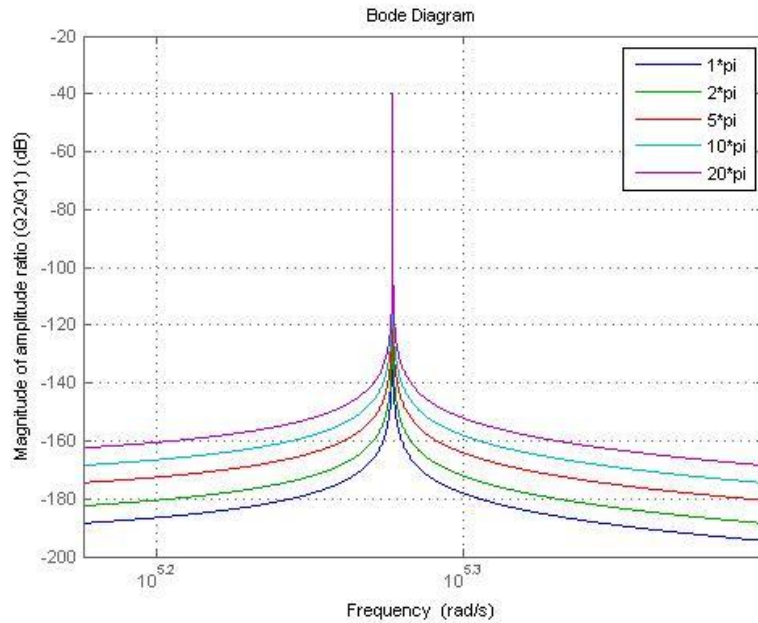
Figure 5-11. Variation of amplitude ratio for different input angular rates (mass mismatch with 0.01%, damping ratio, $\xi = 1 \times 10^{-9}$)
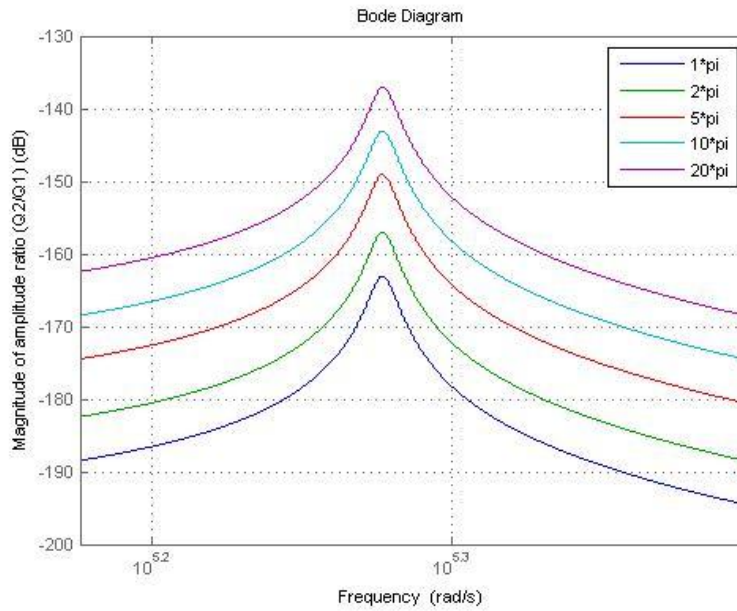
Figure 5-12. Variation of amplitude ratio for different input angular rates (mass mismatch with 0.01% mismatch, damping ratio, ξ=0.01)
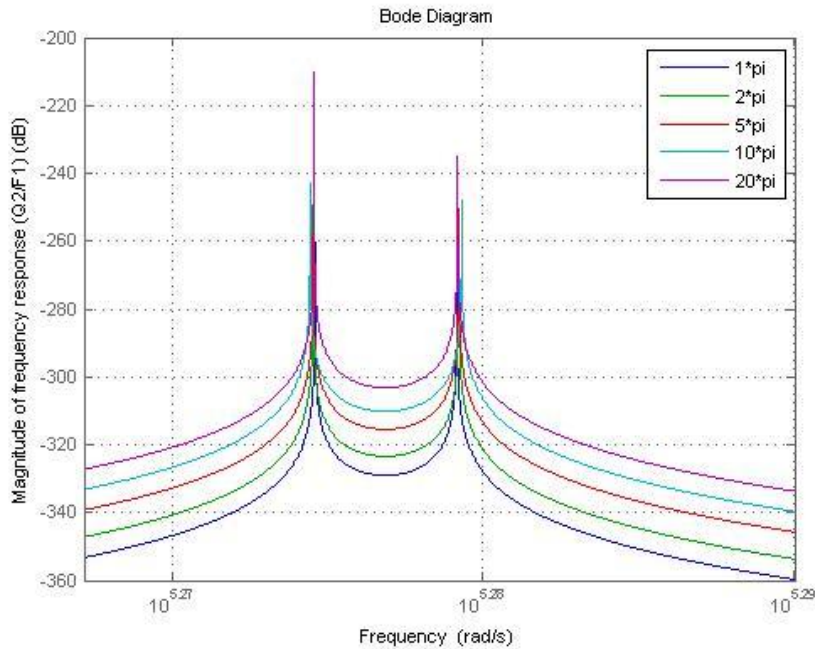
Figure 5-13. Variation of frequency response for different input angular rates (mass mismatch with 0.01% mean, damping ratio, ξ=1× 10^{-9})
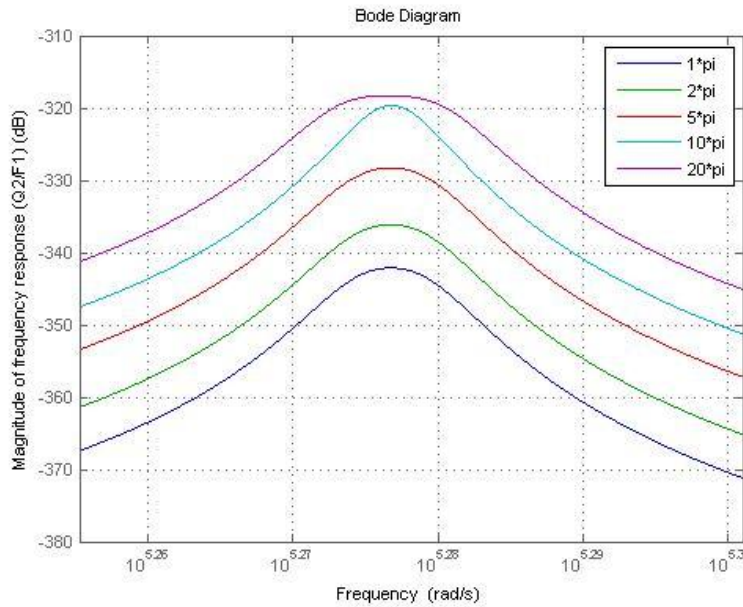
Figure 5-14. Variation of frequency response for different input angular rates (mass mismatch with 0.01% mean, damping ratio, ξ=0.01)

In order to analyze the uncertainty quantification in the frequency domain with frequency mismatch, 70 random samples are employed in the numerical simulation which is demonstrated in Figure 5-15 while the input angular rate and damping ratio are, respectively, fixed at 2π rad/sec and 0.01.
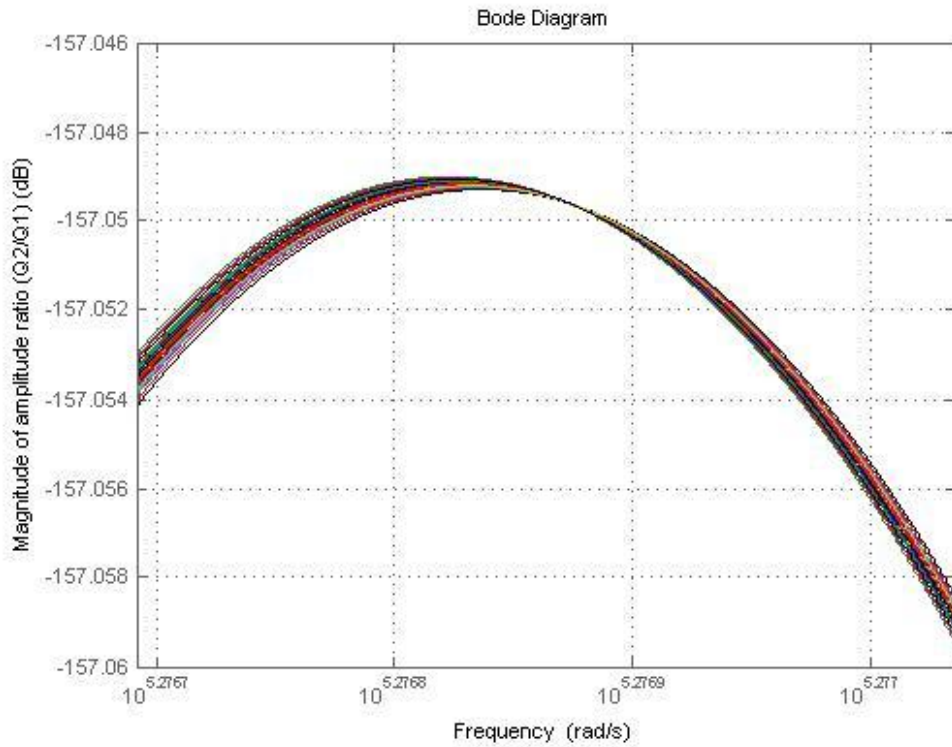
Figure 5-15. Variation of amplitude ratio for different samples (frequency mismatch with 0.01%, damping ratio, ξ=0.01, $\Omega = 2\pi\ rad/sec$)

For the purposes of quantifying the effect of the uncertainty mass mismatch, magnitudes of the amplitude ratio peaks are computed considering uncertainties in frequency mismatch. Figure 5-16 illustrates the gradually increasing nonlinear relationship between the Standard deviation of mass mismatch and standard deviation of magnitude of amplitude ratio $|Q2/Q1|$.
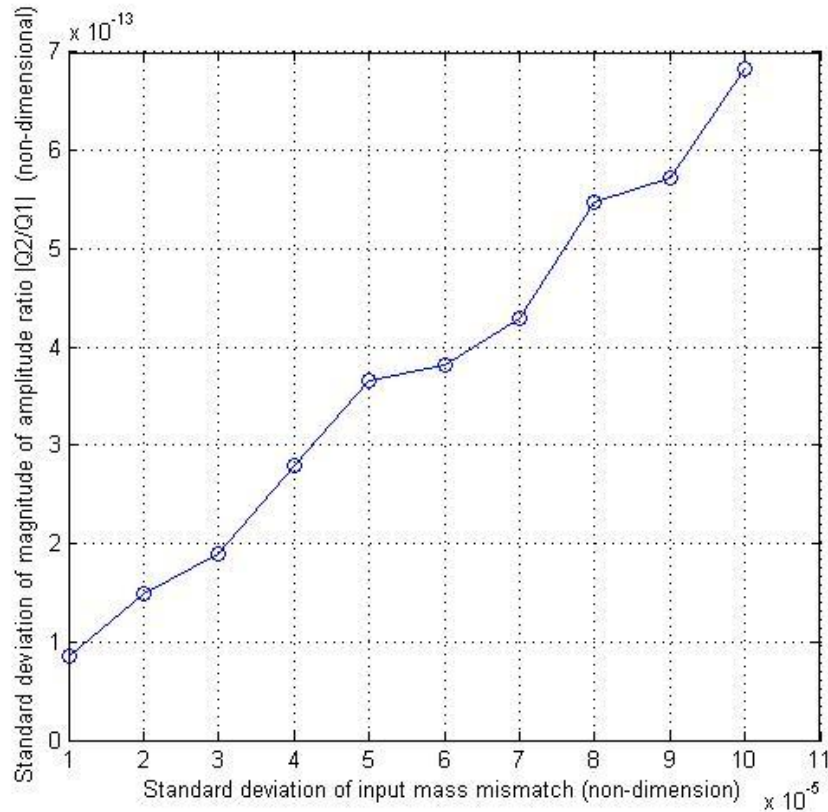
Figure 5-16. Standard deviation of mass mismatch vs. standard deviation of magnitude of amplitude ratio $|Q2/Q1|$ ($\Omega = 2\pi \ rad/sec$, damping ratio, ξ=0.01)

Least-square method is used to get a parametric relationship between two standard deviations using the MATLAB command 'polyfit' (degree 2) :

$$\sigma_{|Q2/Q1|} = 7.6506 \times 10^{-6}\sigma^2_{m.mismatc\ h} + 5.5835 \times 10^{-9}\sigma_{m.mis\ matc\ h} + 3.1808 \times 10^{-14}, \quad (5.9)$$

where $\sigma_{|Q2/Q1|}$ and $\sigma_{m.mismatc\ h}$, respectively, symbolize as standard deviation of magnitude of amplitude ratio $|Q2/Q1|$ and standard deviation of mass mismatch. This process is illustrated in Figure 5-17.
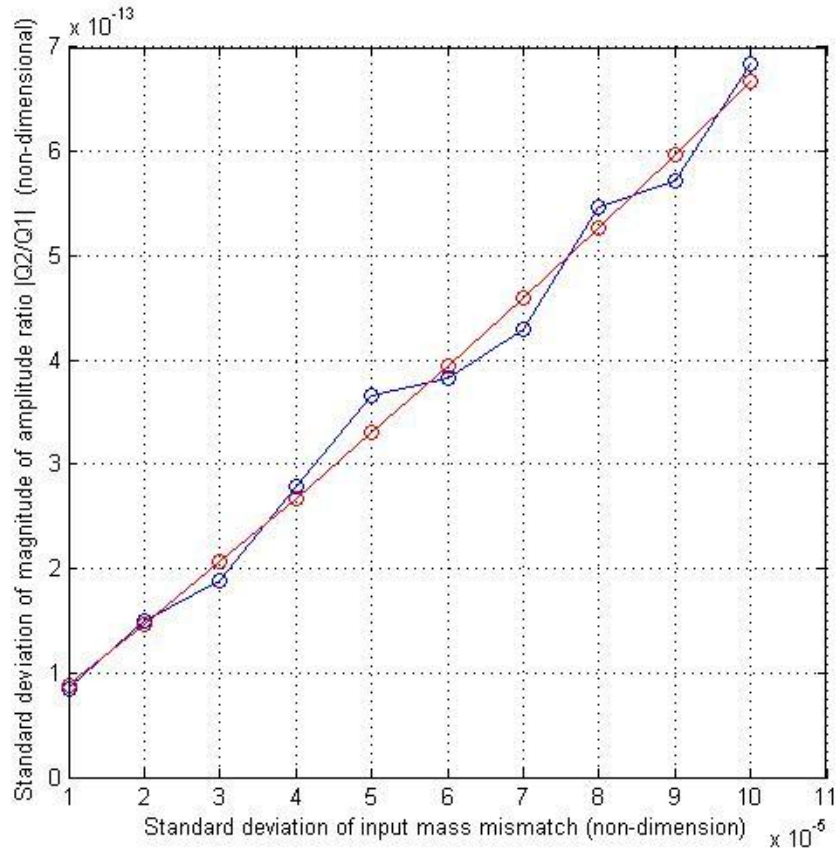
Figure 5-17. Standard deviation of mass mismatch (non-dimensional) vs. standard deviation of magnitude of amplitude ratio $|Q2/Q1|$ ($\Omega = 2\pi\ rad/sec$, damping ratio, ξ=0.01)

The standard deviation of frequency that corresponds to the peak of amplitude ratio is also evaluated for varying mass mismatch standard deviation and depicted in Figure 5-18 which illustrates that the mismatch uncertainty has negligible influence.
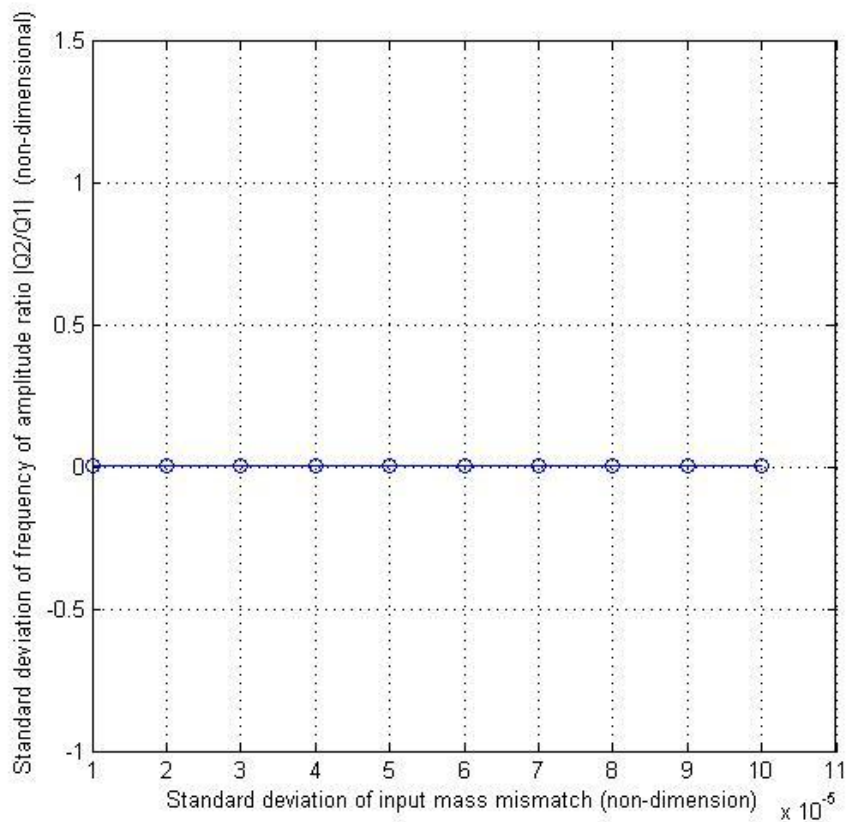
Figure 5-18. Standard deviation of mass mismatch vs. standard deviation of frequency of amplitude ratio $|Q2/Q1|$ ($\Omega = 2\pi \ rad/sec$, damping ratio, ξ=0.01)

With the intention of quantifying the effect of the uncertainty mass mismatch, magnitudes of the frequency response peaks are computed considering uncertainties in mass mismatch. Figure 5-19 illustrates the gradually increasing nonlinear relationship between the Standard deviation of mass mismatch and standard deviation of magnitude of frequency response $|Q2/F1|$.
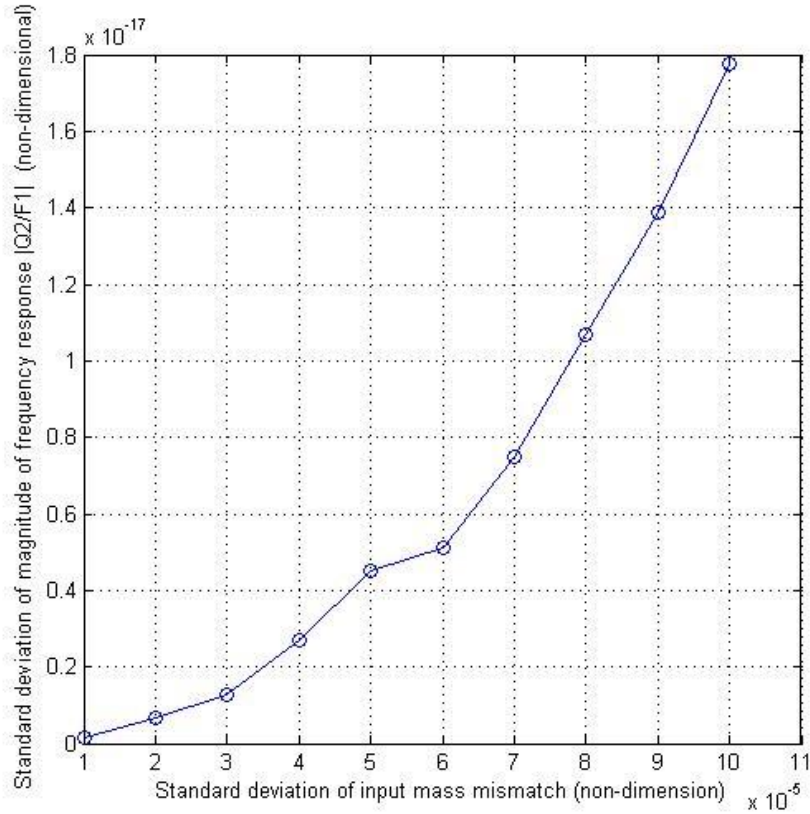
Figure 5-19. Standard deviation of input mass mismatch vs. standard deviation of magnitude of frequency response $|Q2/F1|$ ($\Omega = 2\pi\ rad/sec$, damping ratio, ξ=0.01)

Least-square method is used to get a parametric relationship between two standard deviations using the MATLAB command 'polyfit' (degree 2) :

$$\sigma_{|Q2/F1|} = 2.1099 \times 10^{-9}\sigma_{m.mismatc\ h}^2 - 4.2494 \times 10^{-14}\sigma_{m.mismatc\ h} + 6.3565 \times 10^{-19},$$

(5.10)

where $\sigma_{|Q2/F1|}$ and $\sigma_{m.mismatc\ h}$, respectively, denote as standard deviation of magnitude of frequency response $|Q2/F1|$ and standard deviation of mass mismatch. This process is illustrated in Figure 5-20.

111
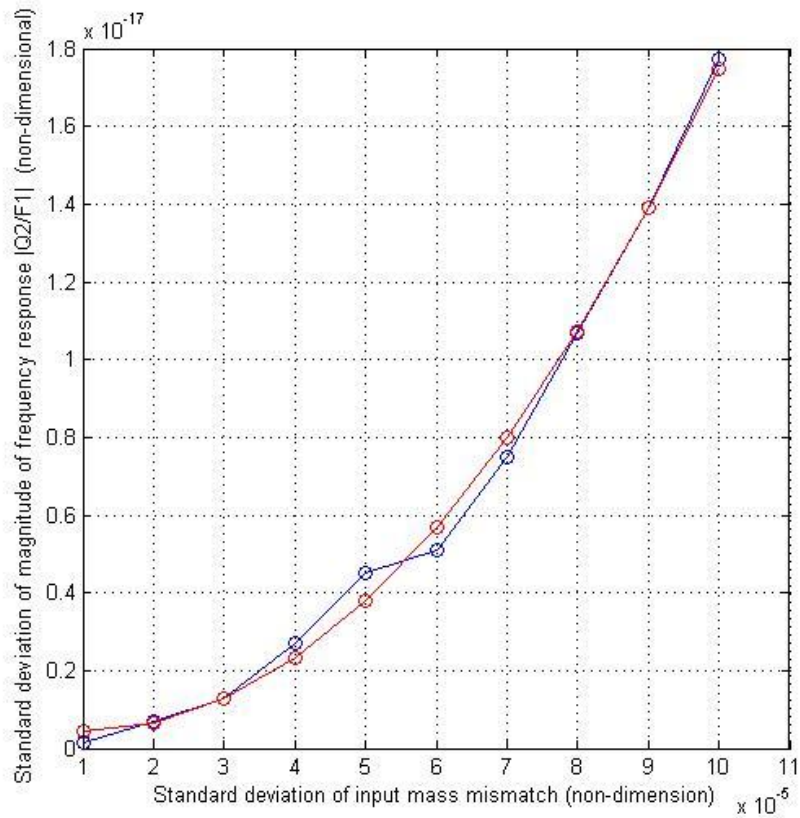
Figure 5-20. Standard deviation of input mass mismatch vs. standard deviation of magnitude of frequency response $|Q2/F1|$ ($\Omega = 2\pi\ rad/sec$, damping ratio, ξ=0.01)

The standard deviation of frequency that corresponds to the magnitude of peak of frequency response is also evaluated for varying mass mismatch standard deviation and depicted in Figure 5-21 which illustrates that the mismatch uncertainty has negligible influence, as in the previous case.
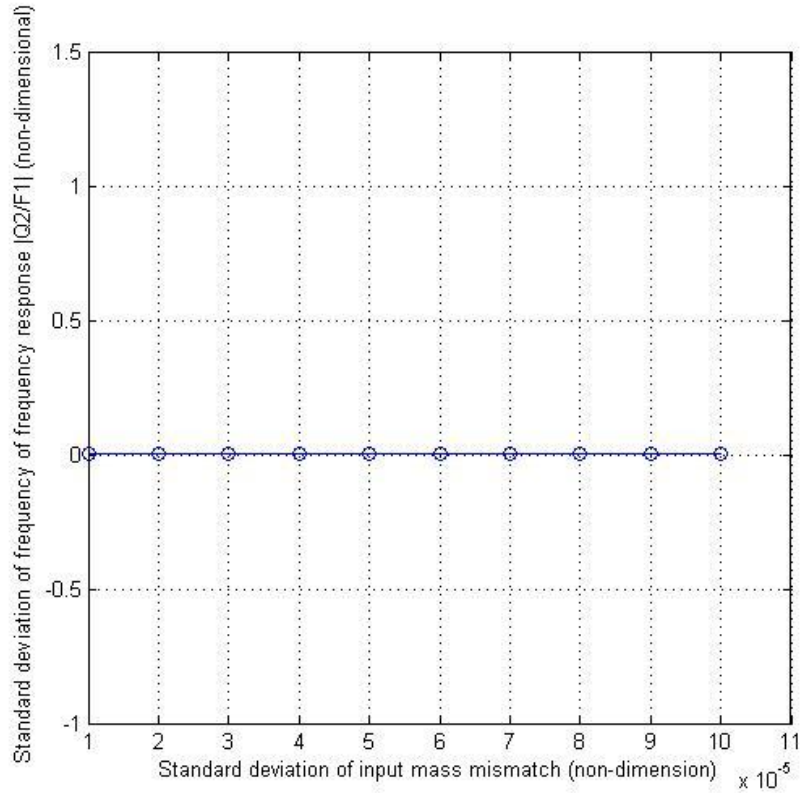
Figure 5-21. Standard deviation of mass mismatch vs. standard deviation of frequency of frequency response $|Q2/F1|$ ($\Omega = 2\pi\ rad/sec$, damping ratio, ξ=0.01)

5.5. Closure

In this chapter, for a ring-based gyroscope, optimal temporal sample paths have been determined via Monte Carlo simulation method. In order to predict response statistics, dynamic response simulations have been used for quantifying standard deviation of output response when the parameters such as input angular rate, mass mismatch and damping ratio are subjected to uncertainty. Uncertainty quantification in the frequency domain has also been demonstrated in terms of the standard deviations of the peak amplitude ratios and peak forced response

magnitudes. Least-square algorithm is used in both time and frequency domain in an effort to

obtain a parametric relationship between the input and output parameter uncertainties.

Chapter 6

6. Conclusions

6.1. Summary of the thesis

Numerical schemes that are suitable for predicting response statistics of mass-spring and ring gyroscopes are developed when this class of vibratory gyroscopes are subjected to parameter as well as environment uncertainties. In particular, emphasis is placed on examining uncertainties in input angular rate, mass/frequency mismatch and quality factor (measure of damping). Responses have been computed in the time domain as well as in the frequency domain while the system is subjected external excitation and body rotation.

Appropriate mathematical models suitable for the proposed simulation study are chosen first. Equations that govern the motion of a linear gyroscopic system with a suitable external harmonic excitation are employed for this purpose. In both cases, in an effort to maximize the gyroscope gain and hence the sensitivity, external excitation frequency was chosen to be close to one of the natural frequencies. Responses of input angular rates of varying magnitudes were simulated first for both types of gyroscopes. Responses under frequency mismatch of different percentages have been considered for mass-spring gyroscope while mass mismatch of various percentages have been considered for ring gyroscope. In order to examine the effect of randomness on output responses, random inputs have been introduced in the numerical schemes in the form of noise and drift terms. The emphasis is placed on the steady-state part of the response since it is more critical to the operation of a gyroscope. A peak-picking approach which simulates the demodulation process which is used in practice is employed first before applying the Monte

Carlo simulation method to predict the response statistics. A number of simulation trials to predict response statistics have been performed for both types of gyroscopes in an effort to ascertain the optimal temporal points as well as sample paths for the impending uncertainty quantification study.

In the interest of quantifying parameter uncertainties in gyroscopes, various system as well as environmental parameters have been chosen. The statistical analyses that have been performed to predict response statistics, helped to quantify standard deviation of output response when input angular rate, frequency/mass mismatch have been taken as parameter uncertainties. Further, the uncertainty quantification is also performed in the frequency domain to the effects of the above parameters on the peak response magnitude ratio as well as the forced frequency response. The predictions are quantified in the form of the standard deviation of the peak ratios and response magnitudes. In order to quantify the statistical predictions using the time as well as the frequency domain simulations, an attempt is also made to obtain relations that map the input and the output uncertainties via a least-square algorithm.

To the best of author's knowledge, this systematic approach for predicting the dynamic response statistics have not been performed for this class of gyroscopes and it is hoped that this approach paves the way for performing uncertainty quantification when these system are subjected to various other uncertainties that may be present in practice.

It is envisaged that the predictions made from the output response statistics and uncertainty quantification analyses of the present study can lead to significant performance improvements in the design of this class of micro-machined mass-spring and ring type vibrating angular rate sensors.

6.2. Thesis contributions

The original contributions arising from the present study may be summarized as follows:

- Suitable numerical schemes have been developed for systematic characterization of a class of vibratory gyroscopes giving emphasis to uncertainty quantification. Application of these schemes to both mass-spring type as well as ring-type gyroscopes has been demonstrated.

- For the predictions using the Monte Carlo simulations in the time-domain, a systematic process for determining the optimal temporal as well as sample paths has been developed so that the computational effort can be minimized.

- The applicability of the Uncertainty quantification analysis has been demonstrated via examining response statistics when the gyroscopes are subjected to uncertainties in input angular rate, frequency/mass mismatch and quality factor.

- An uncertainty quantification process in the frequency domain is developed to systematically examine the above uncertainties and suitable measures for quantifying the response uncertainties have been identified.

6.3. Recommendations for future research

This thesis attempted to present a systematic approach for the uncertainty quantification of a class of vibratory gyroscopes for the first time based on the dynamic response via the Monte Carlo Approach. The analysis presented in this thesis provides confidence in applying these

schemes in practice. However, before this method can be applied for the design of gyroscopes, further research is warranted in the following areas:

- The present study employed linear models in general and in the case of the ring-type gyroscope employed a discretized model for predicting the response statistics via numerical simulations. More accurate predictions considering multi mode as well as non-linear models could be used to improve the quantification.

- Present study focussed primarily on quantifying the effects of input angular rate, frequency/stiffness mismatch and quality factor. Other important parameters such as temperature could be studied using the approach developed in the present thesis by suitably modifying the mathematical model to incorporate thermal effects.

- Also, experimental response of commercial gyroscopes could be used to validate the theoretical predictions. However, exact parameters of commercial products are often not revealed by the manufactures and hence could only be performed by the respective manufacturers. Results from this thesis could provide a basis for the experimental quantification and could lead to validation of the predictions made in the present thesis.

References

Agarwal, N., Aluru, N., R., December 2009, "Stochastic Analysis of Electrostatic MEMS Subjected to Parameter Variations", *Journal of Microelectrical System,* Vol. 18, No. 6.

Bickford, W., B., Reddy, E., S., 1985, "On the in-plane vibrations of rotating rings", *Journal of Sound and Vibration*, Vol. 101(1), pp. 13-22.

Cho, J., 2004, Dynamic Response and Stability of Ring-based Vibratory Angular Rate Sensors, Master's thesis, University of Western Ontario, London, ON, Canada.

Davis, W. O., 2001, Mechanical Analysis and Design of Vibratory Micromachined Gyroscopes, Ph.D. Thesis, University of California, Berkeley, USA.

Eley, R., Fox, C., H., J., and McWilliam, S., 2000, "Coriolis coupling effects on the vibration of rotating rings", Journal of sound and vibration, Vol. 238(3), pp. 459-480.

Geen, J., A., Sherman, S.J., Chang, J.F., Lewis, S.R., 2002, "Single-chip surface micromachined integrated gyroscope with 50°/h Allan Deviation. IEEE J. Solid-State Circuits", Vol. 37, pp. 1860–1866.

Ghanem, R., G., Spanos, P., D., 2012, Stochastic finite Elements A Spectral Approach, Revised Edition, Springer-Verlag New York, New York, USA.

Giunta, A., A., McFarland, J., M., Swiler, L., P., Eldred, M. S., 2006, "The promise and peril of uncertainty quantification using response surface approximations", Structure and Infrastructure Engineering: Maintenance, Management, Life-Cycle Design and Performance, Vol. 2, pp. 175–189.

Huang, S., C., Soedel, W., 1987, "Effect of Coriolis acceleration on the free and forced in-plane vibrations of rotating rings on elastic foundation", *Journal of Sound and Vibration*, Vol. 115(2), pp. 253-274.

Lai, S., Kiang, J., 21–23 October 2009, "A CMOS-MEMS Single-Chip Dual-Axis Gyroscope", 4th IEEE International Conference on Microsystems, Packaging, Assembly and Circuits Technology, Taipei, Taiwan, pp. 305–307.

Looney, M., July 2012, "Analyzing Frequency Response of Inertial MEMS in Stabilization Systems", Analog Dialogue, Volume 46.

Mochida, Y., Tamura, M. and Ohwada, K., 2000, "A Micromachined Vibrating Rate Gyroscope with Independent Beams for the Drive and Detection Modes", Sensors and Actuators, Vol. 80, pp. 170 – 178.

N. Maluf, 2000, An introduction to Microelectromechanical system engineering, Artech house Inc., Boston and London.

Patel C. and McCluskey P., October 2012, "A Characterization of the Performance of MEMS Vibratory Gyroscope in Temperature and Humidity Environments", Transaction on control and mechanical systems, Vol. 1, N0. 6, PP. 239-244.

Putty, M. W., and Najafi, K., 1994, ''A micromachined vibrating ring gyroscope.'', Technical Digest, Solid-State Sensor and Actuator Workshop, Hilton Head Island, S.C., June 13–16, Transducers Research Found., pp. 213–220.

Shinozuka, M., Jan, C., M., 1972, "Digital simulation of random processes and its applications", Journal of sound and vibratio, Vol. 25, No. 1.

Snow, M., Bajaj, A., 2010, Uncertainty Quantification Study for a Comprehensive Electrostatic MEMS Switch Model, PRISM: NNSA Center of Prediction of Reliability, Integrity and Survivability of Microsystems, Paper 20.

Sparks, D., Slaughter, D., Beni, R., Jordan, L., Chia, M., Rich, D., Johnson, J., and Vas, T., 1999, ''Chip-scale packaging of a gyroscope using wafer bonding,'' Sens. Mater., 11 (4), pp. 97–207.

Technology Trends for Inertial MEMS,YOLE Development, January 2012.

Wang, T., 2009, Nonlinear And Stochastic Dynamics Of MEMS Based Angular Rate Sensing And Switching Systems, Ph.D Thesis, University of Western Ontario, London, Ontario, Canada.

Woodman, O. J., 2007, An introduction to inertial navigation, University of Cambridge, Cambridge, UK

Appendices

Appendix A1: MATLAB Routine for Mass-spring Gyroscope

This programme build for obtaining input angular rate time profile. This same profile has been used in ring gyroscope simulations.

```
% Capital omega(OMEGA)(Angular rate, rad/sec)
clear all;
clc; clf;
n=[1 2 5 8 10];
t1=0.0; t2=0.005; % Time for the transient part of the angular speed
for i=1:5
    y1= n(i)*pi; % Steady state part of the angular speed
    i=0.0;
    t=0.0;
    while t<0.1

        if t<t1
            y=0.0;
        elseif t<t2
            y = y1/2*sin(3.14159*(t-t1)/(t2-t1)-0.5*3.14159)+y1/2; %Transient
part of the angular speed
        else
            y = y1; % Steady state of the angular speed
        end

        i=i+1;
        time(i)=t;
        OMEGA(i)=y;
        t=t+0.0001;
    end
    plot(time,OMEGA,'-');
    hold on; grid on;
end
xlabel('Time(sec)');
ylabel('Input angular rate (rad/sec)');
```

MATLAB Routine for output time response (Radial displacement in the driving and sensing direction)

Driving Direction

```
clc; clf; clear all;
[T,Q]=ode45(@(t,q) mass_s(t,q),0.0:0.00001:0.1,[0.0;0.0;0.0;0.0]);% ordinary
differential equation solver(initial value problem)(calling function, range,
initial value q1,q2,q1_dot,q2_dot)
plot(T,Q(:,1),'-'); % displacement at driving direction vs time curve
grid on; hold on;
xlabel('time,(sec)');
ylabel('Radial displacement in the driving direction,(m)');
```

```matlab
function [Q_dot] = mass_s(t,q)

Q_dot=(zeros(size(q)));
omega=164536;
m_p = 0.00000000036;        %kg Gyroscope proof mass
omega_x = 164536;       %rad/sec Nominal X-Axis natural frequency
omega_y = 164536;       %rad/sec Nominal Y-Axis natural frequency
q_x = 1000;       % X-Axis quality factor
q_y = 1000;       % Y-Axis quality factor
f = 0.00000001;     %N amplitude of X-Axis drive force

% Capital omega(OMEGA)(Angular rate, rad/sec)
t1=0.0; t2=0.005; % Time for the transient part of the angular speed
y1=2*pi; % Steady state part of the angular speed
if t==t1
    y=0.0;
elseif t<t2
    y=y1/2*sin(3.14159*(t-t1)/(t2-t1)-0.5*3.14159)+y1/2; % Transient part of
the angular speed
else
    y=y1; % Steady state of the angular speed
end
OMEGA=y; % Input angular rate (rad/sec)
%-------------------------------------------------------------------------
-------------------------------------------
% Derivative of Capital omega(OMEGA_dot)
if t==t1
    y_dot=0.0;
elseif t<t2
    y_dot=y1/2*cos(3.14159*(t-t1)/(t2-t1)-0.5*3.14159)*(3.14159/(t2-t1)); %
Transiant part of the angular speed
else
    y_dot=0.0; % Steady state of the angular speed
end
OMEGA_dot=y_dot;

Q_dot(1)=q(3);
Q_dot(2)=q(4);
Q_dot(3)=((OMEGA).^2-(omega_x)^2)*q(1)+(OMEGA_dot)*q(2)+(-
(omega_x)/(q_x))*q(3)+(2.*OMEGA)*q(4)+(f/m_p)*sin(omega*t);
Q_dot(4)=-(OMEGA_dot)*q(1)+((OMEGA).^2-(omega_x)^2)*q(2)+(-2.*OMEGA)*q(3)+(-
(omega_x)/(q_x))*q(4);

end
```

Sensing Direction

```matlab
clc; clf; clear all;
[T,Q]=ode45(@(t,q) mass_s(t,q),0.0:0.00001:0.1,[0.0;0.0;0.0;0.0]);% ordinary
differential equation solver(initial value problem)(calling function, range,
initial value q1,q2,q1_dot,q2_dot)
plot(T,Q(:,2),'-'); % displacement at sensing direction vs time curve
grid on; hold on;
xlabel('time,(sec)');
```

```
ylabel('Radial displacement in the sensing direction,(m)');


function [Q_dot] = mass_s(t,q)

Q_dot=(zeros(size(q)));
omega=164536;
m_p = 0.00000000036;        %kg Gyroscope proof mass
omega_x = 164536;      %rad/sec Nominal X-Axis natural frequency
omega_y = 164536;      %rad/sec Nominal Y-Axis natural frequency
q_x = 1000;      % X-Axis quality factor
q_y = 1000;      % Y-Axis quality factor
f = 0.00000001;    %N amplitude of X-Axis drive force

% Capital omega(OMEGA)(Angular rate, rad/sec)
t1=0.0; t2=0.005; % Time for the transient part of the angular speed
y1=2*pi; % Steady state part of the angular speed
if t==t1
    y=0.0;
elseif t<t2
    y=y1/2*sin(3.14159*(t-t1)/(t2-t1)-0.5*3.14159)+y1/2; % Transient part of
the angular speed
else
    y=y1; % Steady state of the angular speed
end
OMEGA=y; % Input angular rate (rad/sec)
%------------------------------------------------------------------------
-------------------------------------------
% Derivative of Capital omega(OMEGA_dot)
if t==t1
    y_dot=0.0;
elseif t<t2
    y_dot=y1/2*cos(3.14159*(t-t1)/(t2-t1)-0.5*3.14159)*(3.14159/(t2-t1)); %
Transiant part of the angular speed
else
    y_dot=0.0; % Steady state of the angular speed
end
OMEGA_dot=y_dot;

Q_dot(1)=q(3);
Q_dot(2)=q(4);
Q_dot(3)=((OMEGA).^2-(omega_x)^2)*q(1)+(OMEGA_dot)*q(2)+(-
(omega_x)/(q_x))*q(3)+(2.*OMEGA)*q(4)+(f/m_p)*sin(omega*t);
Q_dot(4)=-(OMEGA_dot)*q(1)+((OMEGA).^2-(omega_x)^2)*q(2)+(-2.*OMEGA)*q(3)+(-
(omega_x)/(q_x))*q(4);

end
```

A Sample of MATLAB Routine for output time response with frequency mismatch

```
clc; clf; clear all;
N=[0.0 1.0 3.0];
col_or=['k' 'b' 'r'];
for i=1.0:1.0:3.0
    n=N(i);
```

```matlab
    [T,Q]=ode45(@(t,q) mass_s(t,q,n),0.0:0.00001:0.1,[0.0;0.0;0.0;0.0]);%
ordinary differential equation solver(initial value problem)(calling
function, range, initial value q1,q2,q1_dot,q2_dot)
    plot(T,Q(:,2),col_or(i)); % displacement at sensing direction vs time
curve
    grid on; hold on;
end
xlabel('time,(sec)');
ylabel('Radial displacement in the sensing direction,(m)');


function [Q_dot] = mass_s(t,q,n)

Q_dot=(zeros(size(q)));
omega=164536;
m_p = 0.00000000036;        %kg Gyroscope proof mass
omega_x = 164536*(1+n*0.0001);      %rad/sec Nominal X-Axis natural frequency
omega_y = 164536;      %rad/sec Nominal Y-Axis natural frequency
q_x = 1000;      % X-Axis quality factor
q_y = 1000;       % Y-Axis quality factor
f = 0.00000001;     %N amplitude of X-Axis drive force

% Capital omega(OMEGA)(Angular rate, rad/sec)
t1=0.0; t2=0.005; % Time for the transient part of the angular speed
y1=2*pi; % Steady state part of the angular speed
if t==t1
    y=0.0;
elseif t<t2
    y=y1/2*sin(3.14159*(t-t1)/(t2-t1)-0.5*3.14159)+y1/2; % Transient part of
the angular speed
else
    y=y1; % Steady state of the angular speed
end
OMEGA=y; % Input angular rate (rad/sec)
%------------------------------------------------------------------------
------------------------------------------
% Derivative of Capital omega(OMEGA_dot)
if t==t1
    y_dot=0.0;
elseif t<t2
    y_dot=y1/2*cos(3.14159*(t-t1)/(t2-t1)-0.5*3.14159)*(3.14159/(t2-t1)); %
Transiant part of the angular speed
else
    y_dot=0.0; % Steady state of the angular speed
end
OMEGA_dot=y_dot;

Q_dot(1)=q(3);
Q_dot(2)=q(4);
Q_dot(3)=((OMEGA).^2-(omega_x)^2)*q(1)+(OMEGA_dot)*q(2)+(-
(omega_x)/(q_x))*q(3)+(2.*OMEGA)*q(4)+(f/m_p)*sin(omega*t);
Q_dot(4)=-(OMEGA_dot)*q(1)+((OMEGA).^2-(omega_x)^2)*q(2)+(-2.*OMEGA)*q(3)+(-
(omega_x)/(q_x))*q(4);

end
```

A Sample of MATLAB Routine for output time response without and with randomness (Radial displacement in the driving and sensing direction). In order to achieve the responses without drift, drift term sigma1*(exp(a_d*t)) is considered to be zero.

```
clc; clear all;
for i=1:1
    N1=1.0:1.0:5.0;
    n=N1(i);
    for i1=1:5
        [T,Q]=ode45(@(t,q)
mass_s2(t,q,n),0.0:0.00001:0.2,[0.0;0.0;0.0;0.0]);% ordinary differential
equation solver(initial value problem)(calling function, range, initial value
q1,q2,q1_dot,q2_dot)
        P=findpeaks(Q(:,2));
        for i2=1:length(P)
            A(i2)=P(i2);
        end
        nc=1.0;
        for j=4501:4505
            B(nc)=A(j);
            nc=nc+1;
        end
        a=T;
        X(:,:,i1)=a';
        Y(:,:,i1)=B;
        meanY(i1)=mean(Y(:,:,i1));
        stdY(i1)=std(Y(:,:,i1));
    end
    X1(:,:,i)=X;
    X2(:,:,i)=(X1(:,:,i))';
    Y1(:,:,i)=Y;
    Y2(:,:,i)=(Y1(:,:,i))';
    meanX2(:,:,i)=mean(X2(:,:,i)); % Ensemble mean
    meanY2(:,:,i)=mean(Y2(:,:,i)); % Ensemble mean
    stdY2(:,:,i)=std(Y2(:,:,i)); % Ensemble standard deviation
    ensemble_mean=mean(meanY2(:,:,i)); % Mean of ensemble mean
    mean_stdY2(i)=mean(stdY2(:,:,i)); % Mean of ensemble standard deviation
end


function [Q_dot] = mass_s2(t,q,n)

Q_dot=(zeros(size(q)));
omega=164536;
m_p = 0.00000000036;       %kg Gyroscope proof mass
omega_x = 164536;     %rad/sec Nominal X-Axis natural frequency
omega_y = 164536;     %rad/sec Nominal Y-Axis natural frequency
q_x = 1000;     % X-Axis quality factor
q_y = 1000;     % Y-Axis quality factor
f = 0.00000001;    %N amplitude of X-Axis drive force
% Capital omega(OMEGA)(Angular rate, rad/sec)
t1=0.0; t2=0.005; % Time for the transient part of the angular speed
y1=2*pi; % Steady state part of the angular speed
if t==t1
    y=0.0;
```

```
elseif t<t2
    y=y1/2*sin(3.14159*(t-t1)/(t2-t1)-0.5*3.14159)+y1/2; % Transient part of
the angular speed
else
    y=y1; % Steady state of the angular speed
end
Omega=y;
%------------------------------------------------------------------------
-------------------------------------------
% Noise and Drift
sigma1=0.0245; sigma2=0.001;
a_d=1.0;
std_dev=(n/100)*Omega;
xi=normrnd(Omega,std_dev);
d_d=sigma1*(exp(a_d*t))+sigma2*xi; % equation for noise and drift
OMEGA=Omega+d_d; % Capital OMEGA with noise and drift
%------------------------------------------------------------------------
-------------------------------------------
% Derivative of Capital omega(OMEGA_dot)
if t==t1
    y_dot=0.0;
elseif t<t2
    y_dot=y1/2*cos(3.14159*(t-t1)/(t2-t1)-0.5*3.14159)*(3.14159/(t2-t1)); %
Transient part of the angular speed
else
    y_dot=0.0; % Steady state of the angular speed
end
OMEGA_dot=y_dot;

Q_dot(1)=q(3);
Q_dot(2)=q(4);
Q_dot(3)=((OMEGA).^2-(omega_x)^2)*q(1)+(OMEGA_dot)*q(2)+(-
(omega_x)/(q_x))*q(3)+(2.*OMEGA)*q(4)+(f/m_p)*sin(omega*t);
Q_dot(4)=-(OMEGA_dot)*q(1)+((OMEGA).^2-(omega_x)^2)*q(2)+(-2.*OMEGA)*q(3)+(-
(omega_x)/(q_x))*q(4);

end
```

A Sample of MATLAB Routine for output time response for 100 samples (3D plot)

```
clc; clear all;
for i=1:1
    N1=1.0:1.0:50.0;
    n=N1(i);
    for i1=1:100
        [T,Q]=ode45(@(t,q)
mass_s2(t,q,n),0.0:0.00001:0.2,[0.0;0.0;0.0;0.0]);% ordinary differential
equation solver(initial value problem)(calling function, range, initial value
q1,q2,q1_dot,q2_dot)
        a=T;
        B=Q(:,2);
        X(:,:,i1)=a';
        Y(:,:,i1)=B;
        d=1:100;
        c(i1)=d(i1)-1;
        e=(ones(size(a)))*c(i1);
        Z(:,:,i1)=e';
    end
    plot3(X(:,:,1),Z(:,:,1),Y(:,:,1),'-',X(:,:,2),Z(:,:,2),Y(:,:,2),'-
',X(:,:,3),Z(:,:,3),Y(:,:,3),'-',X(:,:,4),Z(:,:,4),Y(:,:,4),'-
',X(:,:,5),Z(:,:,5),Y(:,:,5),'-',X(:,:,6),Z(:,:,6),Y(:,:,6),'-
',X(:,:,7),Z(:,:,7),Y(:,:,7),'-',X(:,:,8),Z(:,:,8),Y(:,:,8),'-
',X(:,:,9),Z(:,:,9),Y(:,:,9),'-',X(:,:,10),Z(:,:,10),Y(:,:,10),'-
',X(:,:,11),Z(:,:,11),Y(:,:,11),'-',X(:,:,12),Z(:,:,12),Y(:,:,12),'-
',X(:,:,13),Z(:,:,13),Y(:,:,13),'-',X(:,:,14),Z(:,:,14),Y(:,:,14),'-
',X(:,:,15),Z(:,:,15),Y(:,:,15),'-',X(:,:,16),Z(:,:,16),Y(:,:,16),'-
',X(:,:,17),Z(:,:,17),Y(:,:,17),'-',X(:,:,18),Z(:,:,18),Y(:,:,18),'-
',X(:,:,19),Z(:,:,19),Y(:,:,19),'-',X(:,:,20),Z(:,:,20),Y(:,:,20),'-
',X(:,:,21),Z(:,:,21),Y(:,:,21),'-',X(:,:,22),Z(:,:,22),Y(:,:,22),'-
',X(:,:,23),Z(:,:,23),Y(:,:,23),'-',X(:,:,24),Z(:,:,24),Y(:,:,24),'-
',X(:,:,25),Z(:,:,25),Y(:,:,25),'-',X(:,:,26),Z(:,:,26),Y(:,:,26),'-
',X(:,:,27),Z(:,:,27),Y(:,:,27),'-',X(:,:,28),Z(:,:,28),Y(:,:,28),'-
',X(:,:,29),Z(:,:,29),Y(:,:,29),'-',X(:,:,30),Z(:,:,30),Y(:,:,30),'-
',X(:,:,31),Z(:,:,31),Y(:,:,31),'-',X(:,:,32),Z(:,:,32),Y(:,:,32),'-
',X(:,:,33),Z(:,:,33),Y(:,:,33),'-',X(:,:,34),Z(:,:,34),Y(:,:,34),'-
',X(:,:,35),Z(:,:,35),Y(:,:,35),'-',X(:,:,36),Z(:,:,36),Y(:,:,36),'-
',X(:,:,37),Z(:,:,37),Y(:,:,37),'-',X(:,:,38),Z(:,:,38),Y(:,:,38),'-
',X(:,:,39),Z(:,:,39),Y(:,:,39),'-',X(:,:,40),Z(:,:,40),Y(:,:,40),'-
',X(:,:,41),Z(:,:,41),Y(:,:,41),'-',X(:,:,42),Z(:,:,42),Y(:,:,42),'-
',X(:,:,43),Z(:,:,43),Y(:,:,43),'-',X(:,:,44),Z(:,:,44),Y(:,:,44),'-
',X(:,:,45),Z(:,:,45),Y(:,:,45),'-',X(:,:,46),Z(:,:,46),Y(:,:,46),'-
',X(:,:,47),Z(:,:,47),Y(:,:,47),'-',X(:,:,48),Z(:,:,48),Y(:,:,48),'-
',X(:,:,49),Z(:,:,49),Y(:,:,49),'-',X(:,:,50),Z(:,:,50),Y(:,:,50),'-
',X(:,:,51),Z(:,:,51),Y(:,:,51),'-',X(:,:,52),Z(:,:,52),Y(:,:,52),'-
',X(:,:,53),Z(:,:,53),Y(:,:,53),'-',X(:,:,54),Z(:,:,54),Y(:,:,54),'-
',X(:,:,55),Z(:,:,55),Y(:,:,55),'-',X(:,:,56),Z(:,:,56),Y(:,:,56),'-
',X(:,:,57),Z(:,:,57),Y(:,:,57),'-',X(:,:,58),Z(:,:,58),Y(:,:,58),'-
',X(:,:,59),Z(:,:,59),Y(:,:,59),'-',X(:,:,60),Z(:,:,60),Y(:,:,60),'-
',X(:,:,61),Z(:,:,61),Y(:,:,61),'-',X(:,:,62),Z(:,:,62),Y(:,:,62),'-
',X(:,:,63),Z(:,:,63),Y(:,:,63),'-',X(:,:,64),Z(:,:,64),Y(:,:,64),'-
',X(:,:,65),Z(:,:,65),Y(:,:,65),'-',X(:,:,66),Z(:,:,66),Y(:,:,66),'-
',X(:,:,67),Z(:,:,67),Y(:,:,67),'-',X(:,:,68),Z(:,:,68),Y(:,:,68),'-
',X(:,:,69),Z(:,:,69),Y(:,:,69),'-',X(:,:,70),Z(:,:,70),Y(:,:,70),'-
',X(:,:,71),Z(:,:,71),Y(:,:,71),'-',X(:,:,72),Z(:,:,72),Y(:,:,72),'-
```

```matlab
',X(:,:,73),Z(:,:,73),Y(:,:,73),'-',X(:,:,74),Z(:,:,74),Y(:,:,74),'-
',X(:,:,75),Z(:,:,75),Y(:,:,75),'-',X(:,:,76),Z(:,:,76),Y(:,:,76),'-
',X(:,:,77),Z(:,:,77),Y(:,:,77),'-',X(:,:,78),Z(:,:,78),Y(:,:,78),'-
',X(:,:,79),Z(:,:,79),Y(:,:,79),'-',X(:,:,80),Z(:,:,80),Y(:,:,80),'-
',X(:,:,81),Z(:,:,81),Y(:,:,81),'-',X(:,:,82),Z(:,:,82),Y(:,:,82),'-
',X(:,:,83),Z(:,:,83),Y(:,:,83),'-',X(:,:,84),Z(:,:,84),Y(:,:,84),'-
',X(:,:,85),Z(:,:,85),Y(:,:,85),'-',X(:,:,86),Z(:,:,86),Y(:,:,86),'-
',X(:,:,87),Z(:,:,87),Y(:,:,87),'-',X(:,:,88),Z(:,:,88),Y(:,:,88),'-
',X(:,:,89),Z(:,:,89),Y(:,:,89),'-',X(:,:,90),Z(:,:,90),Y(:,:,90),'-
',X(:,:,91),Z(:,:,91),Y(:,:,91),'-',X(:,:,92),Z(:,:,92),Y(:,:,92),'-
',X(:,:,93),Z(:,:,93),Y(:,:,93),'-',X(:,:,94),Z(:,:,94),Y(:,:,94),'-
',X(:,:,95),Z(:,:,95),Y(:,:,95),'-',X(:,:,96),Z(:,:,96),Y(:,:,96),'-
',X(:,:,97),Z(:,:,97),Y(:,:,97),'-',X(:,:,98),Z(:,:,98),Y(:,:,98),'-
',X(:,:,99),Z(:,:,99),Y(:,:,99),'-',X(:,:,100),Z(:,:,100),Y(:,:,100),'-');
    xlabel('Time (sec)');
    zlabel('Radial displacement along sensing direction (m)');
    ylabel('Number of sample');
    grid on; hold on;
end


function [Q_dot] = mass_s2(t,q,n)


Q_dot=(zeros(size(q)));
omega=164536;
m_p = 0.00000000036;       %kg Gyroscope proof mass
omega_x = 164536;     %rad/sec Nominal X-Axis natural frequency
omega_y = 164536;     %rad/sec Nominal Y-Axis natural frequency
q_x = 1000;     % X-Axis quality factor
q_y = 1000;     % Y-Axis quality factor
f = 0.00000001;    %N amplitude of X-Axis drive force
% Capital omega(OMEGA)(Angular rate, rad/sec)
t1=0.0; t2=0.005; % Time for the transient part of the angular speed
y1=2*pi; % Steady state part of the angular speed
if t==t1
    y=0.0;
elseif t<t2
    y=y1/2*sin(3.14159*(t-t1)/(t2-t1)-0.5*3.14159)+y1/2; % Transient part of
the angular speed
else
    y=y1; % Steady state of the angular speed
end
Omega=y;
%------------------------------------------------------------------------
-----------------------------------------
% Noise and Drift
sigma1=0.0245; sigma2=0.001;
a_d=1.0;
std_dev=(n/100)*Omega;
xi=normrnd(Omega,std_dev);
d_d=sigma1*(exp(a_d*t))+sigma2*xi; % equation for noise and drift
OMEGA=Omega+d_d; % Capital OMEGA with noise and drift
%------------------------------------------------------------------------
-----------------------------------------
% Derivative of Capital omega(OMEGA_dot)
if t==t1
    y_dot=0.0;
elseif t<t2
```

```
    y_dot=y1/2*cos(3.14159*(t-t1)/(t2-t1)-0.5*3.14159)*(3.14159/(t2-t1)); %
Transient part of the angular speed
else
    y_dot=0.0; % Steady state of the angular speed
end
OMEGA_dot=y_dot;


Q_dot(1)=q(3);
Q_dot(2)=q(4);
Q_dot(3)=((OMEGA).^2-(omega_x)^2)*q(1)+(OMEGA_dot)*q(2)+(-
(omega_x)/(q_x))*q(3)+(2.*OMEGA)*q(4)+(f/m_p)*sin(omega*t);
Q_dot(4)=-(OMEGA_dot)*q(1)+((OMEGA).^2-(omega_x)^2)*q(2)+(-2.*OMEGA)*q(3)+(-
(omega_x)/(q_x))*q(4);


end
```

A Sample of MATLAB Routine for uncertainty quantification of output time response for 50 samples with mismatch

```
clc; clear all;
for i=1:10
    N1=1.0:1.0:50.0;
    n=N1(i);
    for i1=1:50
        [T,Q]=ode45(@(t,q)
mass_s3(t,q,n),0.0:0.00001:0.2,[0.0;0.0;0.0;0.0]);% ordinary differential
equation solver(initial value problem)(calling function, range, initial value
q1,q2,q1_dot,q2_dot)
        P=findpeaks(Q(:,2));
        for i2=1:length(P)
            A(i2)=P(i2);
        end
        nc=1.0;
        for j=4501:4501
            B(nc)=A(j);
            nc=nc+1;
        end
        a=T;
        X(:,:,i1)=a';
        Y(:,:,i1)=B;
        meanY(i1)=mean(Y(:,:,i1));
        stdY(i1)=std(Y(:,:,i1));
    end
    X1(:,:,i)=X;
    X2(:,:,i)=(X1(:,:,i))';
    Y1(:,:,i)=Y;
    Y2(:,:,i)=(Y1(:,:,i))';
    meanX2(:,:,i)=mean(X2(:,:,i)); % Ensemble mean
    meanY2(:,:,i)=mean(Y2(:,:,i)); % Ensemble mean
    stdY2(:,:,i)=std(Y2(:,:,i)); % Ensemble standard deviation
    ensemble_mean=mean(meanY2(:,:,i)); % Mean of ensemble mean
    mean_stdY2(i)=mean(stdY2(:,:,i)); % Mean of ensemble standard deviation
end

function [Q_dot] = mass_s3(t,q,n)
```

```
Q_dot=(zeros(size(q)));
omega=164536;
m_p = 0.00000000036;         %kg Gyroscope proof mass
[std_dev,nu]=i_nput(n);
omega_x = 164536*(1.0+nu);      %rad/sec Nominal X-Axis natural frequency
omega_y = 164536;       %rad/sec Nominal Y-Axis natural frequency
q_x = 1000;      % X-Axis quality factor
q_y = q_x;       % Y-Axis quality factor
f = 0.00000001;     %N amplitude of X-Axis drive force
% Capital omega(OMEGA)(Angular rate, rad/sec)
t1=0.0; t2=0.005; % Time for the transiant part of the angular speed
y1=2*pi; % Steady state part of the angular speed
if t==t1
    y=0.0;
elseif t<t2
    y=y1/2*sin(3.14159*(t-t1)/(t2-t1)-0.5*3.14159)+y1/2; % Transiant part of
the angular speed
else
    y=y1; % Steady state of the angular speed
end
Omega=y;
%-------------------------------------------------------------------------
------------------------------------------
% Noise and Drift
sigma1=0.0245; sigma2=0.001;
a_d=1.0;
std_dev=(n/100)*Omega;
xi=normrnd(Omega,std_dev);
d_d=sigma1*(exp(a_d*t))+sigma2*xi; % equation for noise and drift
OMEGA=Omega+d_d; % Capital OMEGA with noise and drift
%-------------------------------------------------------------------------
------------------------------------------
% Derivative of Capital omega(OMEGA_dot)
if t==t1
    y_dot=0.0;
elseif t<t2
    y_dot=y1/2*cos(3.14159*(t-t1)/(t2-t1)-0.5*3.14159)*(3.14159/(t2-t1)); %
Transiant part of the angular speed
else
    y_dot=0.0; % Steady state of the angular speed
end
OMEGA_dot=y_dot;

Q_dot(1)=q(3);
Q_dot(2)=q(4);
Q_dot(3)=((OMEGA).^2-(omega_x)^2)*q(1)+(OMEGA_dot)*q(2)+(-
(omega_x)/(q_x))*q(3)+(2.*OMEGA)*q(4)+(f/m_p)*sin(omega*t);
Q_dot(4)=-(OMEGA_dot)*q(1)+((OMEGA).^2-(omega_x)^2)*q(2)+(-2.*OMEGA)*q(3)+(-
(omega_x)/(q_x))*q(4);

end

function [std_dev,nu]=i_nput(n)
std_dev=(n/100)*0.01;
nu=normrnd(0.0,std_dev);
end
```

A Sample of MATLAB Routine for output frequency response for amplitude ratio $|Q2/Q1|$

```
clc; clf; clear all;
omega=164536;
m_p = 0.00000000036;        %kg Gyroscope proof mass
q_x = 1000;      % X-Axis quality factor
q_y = 1000;      % Y-Axis quality factor
f = 0.00000001;
n=[1 2 5 10 20];
for i1=1:5
    for i=1:1
        std_dev=n(i1)*0.00001;
        nu=normrnd(0.0001,std_dev); % frequency mismatch
        omega_x = 164536;      %rad/sec Nominal X-Axis natural frequency
        omega_y = 164536*(1+nu);      %rad/sec Nominal Y-Axis natural
frequency
        Omega=n(i1)*pi;
        H=tf([2.*Omega],[1.0 omega_y/q_y ((omega_y).^2-(Omega).^2)]); %
Transfer function for bode plot
        w=linspace(1.6452E5,1.6459E5,10000);
        [mag,phase,wout] = bode(H,w);
        P = bodeoptions;
        P.MagUnits='abs';
        P.FreqScale='linear';
        P.MagVisible='on';
        bodemag(H,w);
        hold on; grid on;
        xlabel('Frequency');
        ylabel('Magnitude of amplitude ratio');
        mag1(:,:,i)=mag;
        mag2(:,:,i)=mag1(:,:,i)';
        c1(:,:,i)=max(mag2(:,:,i));
        wout1(:,:,i)=wout;
        wout2(:,:,i)=wout1(:,:,i)';
        for j=1:length(mag2)
            if mag2(j)==c1;
                f(j)=wout2(j);
            end
        end
        d1(:,:,i)=max(f);
    end
    c2(:,:,i1)=c1;
    c(:,:,i1)=(c2(:,:,i1))';
    mean_c(:,:,i1)=mean(c(:,:,i1)); % Mean of magnitude of peaks
    std_c(:,:,i1)=std(c(:,:,i1)); % Standard deviation of peak magnitude
    d2(:,:,i1)=d1;
    d(:,:,i1)=(d2(:,:,i1))';
    mean_d(:,:,i1)=mean(d(:,:,i1)); % Mean of corresponding peak frequency
    std_d(:,:,i1)=std(d(:,:,i1)); % Standard deviation of corresponding peak
frequency
end
```

A Sample of MATLAB Routine for uncertainty quantification of output frequency response amplitude ratio $|Q2/Q1|$

```
clc; clf; clear all;
omega=164536;
m_p = 0.00000000036;      %kg Gyroscope proof mass
q_x = 1000;    % X-Axis quality factor
q_y = 1000;    % Y-Axis quality factor
f = 0.00000001;
n=1.0:1.0:10;
for i1=1:10
    for i=1:50
        std_dev=n(i1)*0.00001;
        nu=normrnd(0.0001,std_dev); % frequency mismatch
        omega_x = 164536;      %rad/sec Nominal X-Axis natural frequency
        omega_y = 164536*(1+nu);     %rad/sec Nominal Y-Axis natural
frequency
        Omega=n(i1)*pi;
        H=tf([2.*Omega],[1.0 omega_y/q_y ((omega_y).^2-(Omega).^2)]); %
Transfer function for bode plot
        w=linspace(1.6452E5,1.6459E5,10000);
        [mag,phase,wout] = bode(H,w);
        P = bodeoptions;
        P.MagUnits='abs';
        P.FreqScale='linear';
        P.MagVisible='on';
        bodemag(H,w);
        hold on; grid on;
        xlabel('Frequency');
        ylabel('Magnitude of amplitude ratio');
        mag1(:,:,i)=mag;
        mag2(:,:,i)=mag1(:,:,i)';
        c1(:,:,i)=max(mag2(:,:,i));
        wout1(:,:,i)=wout;
        wout2(:,:,i)=wout1(:,:,i)';
        for j=1:length(mag2)
            if mag2(j)==c1;
                f(j)=wout2(j);
            end
        end
        d1(:,:,i)=max(f);
    end
    c2(:,:,i1)=c1;
    c(:,:,i1)=(c2(:,:,i1))';
    mean_c(:,:,i1)=mean(c(:,:,i1)); % Mean of magnitude of peaks
    std_c(:,:,i1)=std(c(:,:,i1)); % Standard deviation of peak magnitude
    d2(:,:,i1)=d1;
    d(:,:,i1)=(d2(:,:,i1))';
    mean_d(:,:,i1)=mean(d(:,:,i1)); % Mean of corresponding peak frequency
    std_d(:,:,i1)=std(d(:,:,i1)); % Standard deviation of corresponding peak
frequency
end
```

A Sample of MATLAB Routine of output forced frequency response $|Q2/F1|$

```matlab
clc; clf; clear all;
omega=164536;
m_p = 0.00000000036;        %kg Gyroscope proof mass
q_x = 1000;      % X-Axis quality factor
q_y = 1000;      % Y-Axis quality factor
f = 0.00000001;
n=[1 2 5 10 20];
for i1=1:5
    for i=1:1
        std_dev=n(i1)*0.00001;
        nu=normrnd(0.0001,std_dev); % frequency mismatch
        omega_x = 164536;     %rad/sec Nominal X-Axis natural frequency
        omega_y = 164536*(1+nu);     %rad/sec Nominal Y-Axis natural
frequency
        Omega=n(i1)*pi;
        H=tf([2*Omega],[1+nu ((omega_x/q_x)*(1+nu)*(omega_y/q_y))
(((1+nu)*(omega_x).^2-(Omega).^2)+((omega_y).^2-
(Omega).^2)+(omega_x*omega_y)/(q_x*q_y)+4*((Omega).^2)) (((omega_x).^2-
(Omega).^2)*(omega_y/q_y)+((omega_y).^2-(Omega).^2)*(omega_x/q_x))
(((omega_x).^2-(Omega).^2)*((omega_y).^2-(Omega).^2))]);
        w=linspace(1.6452E5,1.6456E5,100000);
        [mag,phase,wout] = bode(H,w);
        P = bodeoptions;
        P.MagUnits='abs';
        P.FreqScale='linear';
        P.MagVisible='on';
        bodemag(H,w);
        hold on; grid on;
        xlabel('Frequency');
        ylabel('Frequency response magnitude');
        mag1(:,:,i)=mag;
        mag2(:,:,i)=mag1(:,:,i)';
        c1(:,:,i)=max(mag2(:,:,i));
        wout1(:,:,i)=wout;
        wout2(:,:,i)=wout1(:,:,i)';
        for j=1:length(mag2)
            if mag2(j)==c1;
                f(j)=wout2(j);
            end
        end
        d1(:,:,i)=max(f);
    end
    c2(:,:,i1)=c1;
    c(:,:,i1)=(c2(:,:,i1))';
    mean_c(:,:,i1)=mean(c(:,:,i1)); % Mean of magnitude of peaks
    std_c(:,:,i1)=std(c(:,:,i1)); % Standard deviation of peak magnitude
    d2(:,:,i1)=d1;
    d(:,:,i1)=(d2(:,:,i1))';
    mean_d(:,:,i1)=mean(d(:,:,i1)); % Mean of corresponding peak frequency
    std_d(:,:,i1)=std(d(:,:,i1)); % Standard deviation of corresponding peak
frequency
end
```

A Sample of MATLAB Routine for uncertainty quantification of output forced frequency response $|Q2/F1|$

```
clc; clf; clear all;
omega=164536;
m_p = 0.00000000036;       %kg Gyroscope proof mass
q_x = 1000;     % X-Axis quality factor
q_y = 1000;     % Y-Axis quality factor
f = 0.00000001;
n=1.0:1.0:10;
for i1=1:10
    for i=1:50
        std_dev=n(i1)*0.00001;
        nu=normrnd(0.0001,std_dev); % frequency mismatch
        omega_x = 164536;       %rad/sec Nominal X-Axis natural frequency
        omega_y = 164536*(1+nu);      %rad/sec Nominal Y-Axis natural
frequency
        Omega=n(i1)*pi;
        H=tf([2*Omega],[1+nu ((omega_x/q_x)*(1+nu)*(omega_y/q_y))
(((1+nu)*(omega_x).^2-(Omega).^2)+((omega_y).^2-
(Omega).^2)+(omega_x*omega_y)/(q_x*q_y)+4*((Omega).^2)) (((omega_x).^2-
(Omega).^2)*(omega_y/q_y)+((omega_y).^2-(Omega).^2)*(omega_x/q_x))
(((omega_x).^2-(Omega).^2)*((omega_y).^2-(Omega).^2))]);
        w=linspace(1.6452E5,1.6456E5,100000);
        [mag,phase,wout] = bode(H,w);
        P = bodeoptions;
        P.MagUnits='abs';
        P.FreqScale='linear';
        P.MagVisible='on';
        bodemag(H,w);
        hold on; grid on;
        xlabel('Frequency');
        ylabel('Frequency response magnitude');
        mag1(:,:,i)=mag;
        mag2(:,:,i)=mag1(:,:,i)';
        c1(:,:,i)=max(mag2(:,:,i));
        wout1(:,:,i)=wout;
        wout2(:,:,i)=wout1(:,:,i)';
        for j=1:length(mag2)
            if mag2(j)==c1;
                f(j)=wout2(j);
            end
        end
        d1(:,:,i)=max(f);
    end
    c2(:,:,i1)=c1;
    c(:,:,i1)=(c2(:,:,i1))';
    mean_c(:,:,i1)=mean(c(:,:,i1)); % Mean of magnitude of peaks
    std_c(:,:,i1)=std(c(:,:,i1)); % Standard deviation of peak magnitude
    d2(:,:,i1)=d1;
    d(:,:,i1)=(d2(:,:,i1))';
    mean_d(:,:,i1)=mean(d(:,:,i1)); % Mean of corresponding peak frequency
    std_d(:,:,i1)=std(d(:,:,i1)); % Standard deviation of corresponding peak
frequency
end
```

Appendix A2: MATLAB Routine for Ring Gyroscope

Driving Direction

```
clc; clf; clear all;
[T,Q]=ode45(@(t,q) Ring_3(t,q),0.0:0.00001:0.01,[0.0;0.0;0.0;0.0]);% ordinary
differential equation solver(initial value problem)(calling function, range,
initial value q1,q2,q1_dot,q2_dot)
plot(T,Q(:,1),'-'); % displacement at driving direction vs time curve
grid on; hold on;
xlabel('time,(sec)');
ylabel('Radial displacement in the driving direction,(m)');


function [Q_dot] = Ring_3(t,q,n)

Q_dot=(zeros(size(q)));
p=8800;
E=210E9;
r=500E-6;
h=12.5E-6;
b=30E-6;
omega01=1.89189E5; % Natural Frequency OMEGA 01
omega02=1.89189E5;% Natural Frequency OMEGA 02
A=3.7500E-010; % Cross sectional area of the ring
I=4.8828E-021; % moment of inertia
n=2.0; % number of mode
a=3.1507E8;
b=1.2601E9;
c=3.1526E8;
k1=3.5792E10;
k2=-0.1606;
f1=4.8483e-15;
gamma=0.8;
[std_dev,nu]=i_nput(n);
zeta=0.01*(1+nu);

% Capital omega(OMEGA)(Angular rate, rad/sec)
t1=0.0; t2=0.005; % Time for the transient part of the angular speed
y1=2*pi; % Steady state part of the angular speed
if t==t1
    y=0.0;
elseif t<t2
    y=y1/2*sin(3.14159*(t-t1)/(t2-t1)-0.5*3.14159)+y1/2; % Transient part of
the angular speed
else
    y=y1; % Steady state of the angular speed
end
OMEGA=y; % Input angular rate (rad/sec)
%------------------------------------------------------------------------
-----------------------------------------
% Derivative of Capital omega(OMEGA_dot)
if t==t1
    y_dot=0.0;
elseif t<t2
```

```
    y_dot=y1/2*cos(3.14159*(t-t1)/(t2-t1)-0.5*3.14159)*(3.14159/(t2-t1)); %
Transiant part of the angular speed
else
    y_dot=0.0; % Steady state of the angular speed
end
OMEGA_dot=y_dot;

Q_dot(1)=q(3);
Q_dot(2)=q(4);
Q_dot(3)=-(k1+k2*(OMEGA)^2)*q(1)+((OMEGA_dot)*gamma)*q(2)-
(2*zeta*omega01)*q(3)+(2*OMEGA*gamma)*q(4)+f1*cos((omega01*t)); % add shift
Q_dot(4)=((-((OMEGA_dot)*gamma)*q(1)-(k1+k2*(OMEGA)^2)*q(2)-
2*(OMEGA)*gamma)*q(3)-(2*zeta*omega02)*q(4))/(1);

end

Sensing Direction
clc; clf; clear all;
[T,Q]=ode45(@(t,q) Ring_3(t,q),0.0:0.00001:0.01,[0.0;0.0;0.0;0.0]);% ordinary
differential equation solver(initial value problem)(calling function, range,
initial value q1,q2,q1_dot,q2_dot)
plot(T,Q(:,2),'-'); % displacement at sensing direction vs time curve
grid on; hold on;
xlabel('time,(sec)');

function [Q_dot] = Ring_3(t,q,n)

Q_dot=(zeros(size(q)));
p=8800;
E=210E9;
r=500E-6;
h=12.5E-6;
b=30E-6;
omega01=1.89189E5; % Natural Frequency OMEGA 01
omega02=1.89189E5;% Natural Frequency OMEGA 02
A=3.7500E-010; % Cross sectional area of the ring
I=4.8828E-021; % moment of inertia
n=2.0; % number of mode
a=3.1507E8;
b=1.2601E9;
c=3.1526E8;
k1=3.5792E10;
k2=-0.1606;
f1=4.8483e-15;
gamma=0.8;
[std_dev,nu]=i_nput(n);
zeta=0.01*(1+nu);

% Capital omega(OMEGA)(Angular rate, rad/sec)
t1=0.0; t2=0.005; % Time for the transient part of the angular speed
y1=2*pi; % Steady state part of the angular speed
if t==t1
    y=0.0;
elseif t<t2
    y=y1/2*sin(3.14159*(t-t1)/(t2-t1)-0.5*3.14159)+y1/2; % Transient part of
the angular speed
else
```

```
    y=y1; % Steady state of the angular speed
end
OMEGA=y; % Input angular rate (rad/sec)
%--------------------------------------------------------------------------
------------------------------------------
% Derivative of Capital omega(OMEGA_dot)
if t==t1
    y_dot=0.0;
elseif t<t2
    y_dot=y1/2*cos(3.14159*(t-t1)/(t2-t1)-0.5*3.14159)*(3.14159/(t2-t1)); %
Transiant part of the angular speed
else
    y_dot=0.0; % Steady state of the angular speed
end
OMEGA_dot=y_dot;

Q_dot(1)=q(3);
Q_dot(2)=q(4);
Q_dot(3)=-(k1+k2*(OMEGA)^2)*q(1)+((OMEGA_dot)*gamma)*q(2)-
(2*zeta*omega01)*q(3)+(2*OMEGA*gamma)*q(4)+f1*cos((omega01*t)); % add shift
Q_dot(4)=((-((OMEGA_dot)*gamma)*q(1)-(k1+k2*(OMEGA)^2)*q(2)-
2*(OMEGA)*gamma)*q(3)-(2*zeta*omega02)*q(4))/(1);

end
```

A Sample of MATLAB Routine for output time response with mass mismatch

```
clc; clf; clear all;
N=[0.0 1.0 3.0];
col_or=['k' 'b' 'r'];
for i=1.0:1.0:3.0
    n=N(i);
    [T,Q]=ode45(@(t,q) Ring_3(t,q,n),0.0:0.00001:0.1,[0.0;0.0;0.0;0.0]);%
ordinary differential equation solver(initial value problem)(calling
function, range, initial value q1,q2,q1_dot,q2_dot)
    plot(T,Q(:,2),col_or(i)); % displacement at sensing direction vs time
curve
    grid on; hold on;
end
xlabel('time,(sec)');
ylabel('Radial displacement in the sensing direction,(m)');


function [Q_dot] = Ring_3(t,q,n)

Q_dot=(zeros(size(q)));
p=8800;
E=210E9;
r=500E-6;
h=12.5E-6;
b=30E-6;
omega01=1.89189E5; % Natural Frequency OMEGA 01
omega02=1.89189E5;% Natural Frequency OMEGA 02
A=3.7500E-010; % Cross sectional area of the ring
I=4.8828E-021; % moment of inertia
```

```matlab
n=2.0; % number of mode
a=3.1507E8;
b=1.2601E9;
c=3.1526E8;
k1=3.5792E10;
k2=-0.1606;
f1=4.8483e-15;
gamma=0.8;
[std_dev,nu]=i_nput(n);
zeta=0.01*(1+nu);

% Capital omega(OMEGA)(Angular rate, rad/sec)
t1=0.0; t2=0.005; % Time for the transient part of the angular speed
y1=2*pi; % Steady state part of the angular speed
if t==t1
    y=0.0;
elseif t<t2
    y=y1/2*sin(3.14159*(t-t1)/(t2-t1)-0.5*3.14159)+y1/2; % Transient part of
the angular speed
else
    y=y1; % Steady state of the angular speed
end
OMEGA=y; % Input angular rate (rad/sec)
%---------------------------------------------------------------------------
-------------------------------------------
% Derivative of Capital omega(OMEGA_dot)
if t==t1
    y_dot=0.0;
elseif t<t2
    y_dot=y1/2*cos(3.14159*(t-t1)/(t2-t1)-0.5*3.14159)*(3.14159/(t2-t1)); %
Transiant part of the angular speed
else
    y_dot=0.0; % Steady state of the angular speed
end
OMEGA_dot=y_dot;

Q_dot(1)=q(3);
Q_dot(2)=q(4);
Q_dot(3)=-(k1+k2*(OMEGA)^2)*q(1)+((OMEGA_dot)*gamma)*q(2)-
(2*zeta*omega01)*q(3)+(2*OMEGA*gamma)*q(4)+f1*cos((omega01*t)); % add shift
Q_dot(4)=((-((OMEGA_dot)*gamma)*q(1)-(k1+k2*(OMEGA)^2)*q(2)-
2*(OMEGA)*gamma)*q(3)-(2*zeta*omega02)*q(4))/(1);

end
```

A Sample of MATLAB Routine for output time response without and with randomness (Radial displacement in the driving and sensing direction). In order to achieve the responses without drift, drift term sigma1*(exp(a_d*t)) is considered to be zero.

```
clc; clear all;
for i=1:1
    N1=1.0:1.0:5.0;
    n=N1(i);
    for i1=1:5
        options = odeset('RelTol',1e-10,'AbsTol',1e-10);
        [T,Q]=ode45(@(t,q)
Ring_1(t,q,n),0.0:0.000001:0.25,[0.0;0.0;0.0;0.0],options);% ordinary
differential equation solver(initial value problem)(calling function, range,
initial value q1,q2,q1_dot,q2_dot)
        plot(T,Q(:,2),'m'); % displacement at sensing direction vs time curve
        grid on; hold on;
        P=findpeaks(Q(:,2));
        for i2=1:length(P)
            A(i2)=P(i2);
        end
        nc=1.0;
        for j=6201:6205
            B(nc)=A(j);
            nc=nc+1;
        end
        a=T;
        X(:,:,i1)=a';
        Y(:,:,i1)=B;
        meanY(i1)=mean(Y(:,:,i1));
        stdY(i1)=std(Y(:,:,i1));
    end
    X1(:,:,i)=X;
    X2(:,:,i)=(X1(:,:,i))';
    Y1(:,:,i)=Y;
    Y2(:,:,i)=(Y1(:,:,i))';
    meanX2(:,:,i)=mean(X2(:,:,i)); % Ensemble mean
    meanY2(:,:,i)=mean(Y2(:,:,i)); % Ensemble mean
    stdY2(:,:,i)=std(Y2(:,:,i)); % Ensemble standard deviation
    ensemble_mean=mean(meanY2); % Mean of ensemble mean
    mean_stdY2(i)=mean(stdY2(:,:,i)); % Mean of ensemble standard deviation
end


function [Q_dot] = Ring_1(t,q,n)

Q_dot=(zeros(size(q)));
p=8800;
E=210E9;
r=500E-6;
h=12.5E-6;
b=30E-6;
omega01=1.89189E5;% Natural Frequency OMEGA 01
omega02=omega01;% Natural Frequency OMEGA 02
A=3.7500E-010; % Cross sectional area of the ring
I=4.8828E-021; % moment of inertia
n=2.0; % number of mode
```

```
a=3.1507E8;
b=1.2601E9;
c=3.1526E8;
k1=3.5792E10;
k2=-0.1606;
f1=4.8483e-15;
gamma=0.8;
zeta=0.01;
% Capital omega(OMEGA)(Angular rate, rad/sec)
t1=0.0; t2=0.005; % Time for the transiant part of the angular speed
y1=2*pi; % Steady state part of the angular speed
if t<t1
    y=0.0;
elseif t<t2
    y=y1/2*sin(3.14159*(t-t1)/(t2-t1)-0.5*3.14159)+y1/2; % Transiant part of
the angular speed
else
    y=y1; % Steady state of the angular speed
end
Omega=y;
%-------------------------------------------------------------------------
-----------------------------------------
% Noise and Drift
sigma1=0.0245; sigma2=0.0001;
a_d=1.0;
std_dev=(n/100)*Omega;
xi=normrnd(Omega,std_dev);
d_d=sigma1*(exp(a_d*t))+sigma2*xi; % equation for noise and drift
OMEGA=Omega+d_d; % Capital OMEGA with noise and drift
%-------------------------------------------------------------------------
-----------------------------------------
% Derivative of Capital omega(OMEGA_dot)
if t<t1
    y_dot=0.0;
elseif t<t2
    y_dot=y1/2*cos(3.14159*(t-t1)/(t2-t1)-0.5*3.14159)*(3.14159/(t2-t1)); %
Transiant part of the angular speed
else
    y_dot=0.0; % Steady state of the angular speed
end
OMEGA_dot=y_dot;

Q_dot(1)=q(3);
Q_dot(2)=q(4);
Q_dot(3)=-(k1+k2*(OMEGA)^2)*q(1)+((OMEGA_dot)*gamma)*q(2)-
(2*zeta*omega01)*q(3)+(2*OMEGA*gamma)*q(4)+f1*cos((omega01*t)); % add shift
Q_dot(4)=((-((OMEGA_dot)*gamma)*q(1)-(k1+k2*(OMEGA)^2)*q(2)-
2*(OMEGA)*gamma)*q(3)-(2*zeta*omega02)*q(4))/(1);

end
```

A Sample of MATLAB Routine for output time response for 100 samples (3D plot)

```
clc; clear all;
for i=1:1
    N1=1.0:1.0:50.0;
    n=N1(i);
    for i1=1:100
        [T,Q]=ode45(@(t,q)
Ring_1(t,q,n),0.0:0.00001:0.25,[0.0;0.0;0.0;0.0]);% ordinary differential
equation solver(initial value problem)(calling function, range, initial value
q1,q2,q1_dot,q2_dot)
        a=T;
        B=Q(:,2);
        X(:,:,i1)=a';
        Y(:,:,i1)=B;
        d=1:100;
        c(i1)=d(i1)-1;
        e=(ones(size(a)))*c(i1);
        Z(:,:,i1)=e';
    end
    plot3(X(:,:,1),Z(:,:,1),Y(:,:,1),'-',X(:,:,2),Z(:,:,2),Y(:,:,2),'-
',X(:,:,3),Z(:,:,3),Y(:,:,3),'-',X(:,:,4),Z(:,:,4),Y(:,:,4),'-
',X(:,:,5),Z(:,:,5),Y(:,:,5),'-',X(:,:,6),Z(:,:,6),Y(:,:,6),'-
',X(:,:,7),Z(:,:,7),Y(:,:,7),'-',X(:,:,8),Z(:,:,8),Y(:,:,8),'-
',X(:,:,9),Z(:,:,9),Y(:,:,9),'-',X(:,:,10),Z(:,:,10),Y(:,:,10),'-
',X(:,:,11),Z(:,:,11),Y(:,:,11),'-',X(:,:,12),Z(:,:,12),Y(:,:,12),'-
',X(:,:,13),Z(:,:,13),Y(:,:,13),'-',X(:,:,14),Z(:,:,14),Y(:,:,14),'-
',X(:,:,15),Z(:,:,15),Y(:,:,15),'-',X(:,:,16),Z(:,:,16),Y(:,:,16),'-
',X(:,:,17),Z(:,:,17),Y(:,:,17),'-',X(:,:,18),Z(:,:,18),Y(:,:,18),'-
',X(:,:,19),Z(:,:,19),Y(:,:,19),'-',X(:,:,20),Z(:,:,20),Y(:,:,20),'-
',X(:,:,21),Z(:,:,21),Y(:,:,21),'-',X(:,:,22),Z(:,:,22),Y(:,:,22),'-
',X(:,:,23),Z(:,:,23),Y(:,:,23),'-',X(:,:,24),Z(:,:,24),Y(:,:,24),'-
',X(:,:,25),Z(:,:,25),Y(:,:,25),'-',X(:,:,26),Z(:,:,26),Y(:,:,26),'-
',X(:,:,27),Z(:,:,27),Y(:,:,27),'-',X(:,:,28),Z(:,:,28),Y(:,:,28),'-
',X(:,:,29),Z(:,:,29),Y(:,:,29),'-',X(:,:,30),Z(:,:,30),Y(:,:,30),'-
',X(:,:,31),Z(:,:,31),Y(:,:,31),'-',X(:,:,32),Z(:,:,32),Y(:,:,32),'-
',X(:,:,33),Z(:,:,33),Y(:,:,33),'-',X(:,:,34),Z(:,:,34),Y(:,:,34),'-
',X(:,:,35),Z(:,:,35),Y(:,:,35),'-',X(:,:,36),Z(:,:,36),Y(:,:,36),'-
',X(:,:,37),Z(:,:,37),Y(:,:,37),'-',X(:,:,38),Z(:,:,38),Y(:,:,38),'-
',X(:,:,39),Z(:,:,39),Y(:,:,39),'-',X(:,:,40),Z(:,:,40),Y(:,:,40),'-
',X(:,:,41),Z(:,:,41),Y(:,:,41),'-',X(:,:,42),Z(:,:,42),Y(:,:,42),'-
',X(:,:,43),Z(:,:,43),Y(:,:,43),'-',X(:,:,44),Z(:,:,44),Y(:,:,44),'-
',X(:,:,45),Z(:,:,45),Y(:,:,45),'-',X(:,:,46),Z(:,:,46),Y(:,:,46),'-
',X(:,:,47),Z(:,:,47),Y(:,:,47),'-',X(:,:,48),Z(:,:,48),Y(:,:,48),'-
',X(:,:,49),Z(:,:,49),Y(:,:,49),'-',X(:,:,50),Z(:,:,50),Y(:,:,50),'-
',X(:,:,51),Z(:,:,51),Y(:,:,51),'-',X(:,:,52),Z(:,:,52),Y(:,:,52),'-
',X(:,:,53),Z(:,:,53),Y(:,:,53),'-',X(:,:,54),Z(:,:,54),Y(:,:,54),'-
',X(:,:,55),Z(:,:,55),Y(:,:,55),'-',X(:,:,56),Z(:,:,56),Y(:,:,56),'-
',X(:,:,57),Z(:,:,57),Y(:,:,57),'-',X(:,:,58),Z(:,:,58),Y(:,:,58),'-
',X(:,:,59),Z(:,:,59),Y(:,:,59),'-',X(:,:,60),Z(:,:,60),Y(:,:,60),'-
',X(:,:,61),Z(:,:,61),Y(:,:,61),'-',X(:,:,62),Z(:,:,62),Y(:,:,62),'-
',X(:,:,63),Z(:,:,63),Y(:,:,63),'-',X(:,:,64),Z(:,:,64),Y(:,:,64),'-
',X(:,:,65),Z(:,:,65),Y(:,:,65),'-',X(:,:,66),Z(:,:,66),Y(:,:,66),'-
',X(:,:,67),Z(:,:,67),Y(:,:,67),'-',X(:,:,68),Z(:,:,68),Y(:,:,68),'-
',X(:,:,69),Z(:,:,69),Y(:,:,69),'-',X(:,:,70),Z(:,:,70),Y(:,:,70),'-
',X(:,:,71),Z(:,:,71),Y(:,:,71),'-',X(:,:,72),Z(:,:,72),Y(:,:,72),'-
```

```
',X(:,:,73),Z(:,:,73),Y(:,:,73),'-',X(:,:,74),Z(:,:,74),Y(:,:,74),'-
',X(:,:,75),Z(:,:,75),Y(:,:,75),'-',X(:,:,76),Z(:,:,76),Y(:,:,76),'-
',X(:,:,77),Z(:,:,77),Y(:,:,77),'-',X(:,:,78),Z(:,:,78),Y(:,:,78),'-
',X(:,:,79),Z(:,:,79),Y(:,:,79),'-',X(:,:,80),Z(:,:,80),Y(:,:,80),'-
',X(:,:,81),Z(:,:,81),Y(:,:,81),'-',X(:,:,82),Z(:,:,82),Y(:,:,82),'-
',X(:,:,83),Z(:,:,83),Y(:,:,83),'-',X(:,:,84),Z(:,:,84),Y(:,:,84),'-
',X(:,:,85),Z(:,:,85),Y(:,:,85),'-',X(:,:,86),Z(:,:,86),Y(:,:,86),'-
',X(:,:,87),Z(:,:,87),Y(:,:,87),'-',X(:,:,88),Z(:,:,88),Y(:,:,88),'-
',X(:,:,89),Z(:,:,89),Y(:,:,89),'-',X(:,:,90),Z(:,:,90),Y(:,:,90),'-
',X(:,:,91),Z(:,:,91),Y(:,:,91),'-',X(:,:,92),Z(:,:,92),Y(:,:,92),'-
',X(:,:,93),Z(:,:,93),Y(:,:,93),'-',X(:,:,94),Z(:,:,94),Y(:,:,94),'-
',X(:,:,95),Z(:,:,95),Y(:,:,95),'-',X(:,:,96),Z(:,:,96),Y(:,:,96),'-
',X(:,:,97),Z(:,:,97),Y(:,:,97),'-',X(:,:,98),Z(:,:,98),Y(:,:,98),'-
',X(:,:,99),Z(:,:,99),Y(:,:,99),'-',X(:,:,100),Z(:,:,100),Y(:,:,100),'-');
    xlabel('Time (sec)');
    zlabel('Radial displacement along sensing direction (m)');
    ylabel('Number of sample');
    grid on; hold on;
end

function [Q_dot] = Ring_1(t,q,n)

Q_dot=(zeros(size(q)));
p=8800;
E=210E9;
r=500E-6;
h=12.5E-6;
b=30E-6;
omega01=1.89189E5;% Natural Frequency OMEGA 01
omega02=omega01;% Natural Frequency OMEGA 02
A=3.7500E-010; % Cross sectional area of the ring
I=4.8828E-021; % moment of inertia
n=2.0; % number of mode
a=3.1507E8;
b=1.2601E9;
c=3.1526E8;
k1=3.5792E10;
k2=-0.1606;
f1=4.8483e-15;
gamma=0.8;
zeta=0.01;
% Capital omega(OMEGA)(Angular rate, rad/sec)
t1=0.0; t2=0.005; % Time for the transiant part of the angular speed
y1=2*pi; % Steady state part of the angular speed
if t<t1
    y=0.0;
elseif t<t2
    y=y1/2*sin(3.14159*(t-t1)/(t2-t1)-0.5*3.14159)+y1/2; % Transiant part of
the angular speed
else
    y=y1; % Steady state of the angular speed
end
Omega=y;
%-----------------------------------------------------------------------
------------------------------------------
% Noise and Drift
sigma1=0.0245; sigma2=0.0001;
```

```matlab
a_d=1.0;
std_dev=(n/100)*Omega;
xi=normrnd(Omega,std_dev);
d_d=sigma1*(exp(a_d*t))+sigma2*xi; % equation for noise and drift
OMEGA=Omega+d_d; % Capital OMEGA with noise and drift
%--------------------------------------------------------------------
-------------------------------------------
% Derivative of Capital omega(OMEGA_dot)
if t<t1
    y_dot=0.0;
elseif t<t2
    y_dot=y1/2*cos(3.14159*(t-t1)/(t2-t1)-0.5*3.14159)*(3.14159/(t2-t1)); %
Transiant part of the angular speed
else
    y_dot=0.0; % Steady state of the angular speed
end
OMEGA_dot=y_dot;

Q_dot(1)=q(3);
Q_dot(2)=q(4);
Q_dot(3)=-(k1+k2*(OMEGA)^2)*q(1)+((OMEGA_dot)*gamma)*q(2)-
(2*zeta*omega01)*q(3)+(2*OMEGA*gamma)*q(4)+f1*cos((omega01*t)); % add shift
Q_dot(4)=((-((OMEGA_dot)*gamma)*q(1)-(k1+k2*(OMEGA)^2)*q(2)-
2*(OMEGA)*gamma)*q(3)-(2*zeta*omega02)*q(4))/(1);

end
```

A Sample of MATLAB Routine for uncertainty quantification of output time response for 70 samples with mismatch

```matlab
clc; clear all;
for i=1:10
    N1=1.0:1.0:70.0;
    n=N1(i);
    for i1=1:70
        options = odeset('RelTol',1e-10,'AbsTol',1e-10);
        [T,Q]=ode45(@(t,q)
Ring_2(t,q,n),0.0:0.000001:0.25,[0.0;0.0;0.0;0.0],options);% ordinary
differential equation solver(initial value problem)(calling function, range,
initial value q1,q2,q1_dot,q2_dot)
        plot(T,Q(:,2),'m'); % displacement at sensing direction vs time curve
        grid on; hold on;
        P=findpeaks(Q(:,2));
        for i2=1:length(P)
            A(i2)=P(i2);
        end
        nc=1.0;
        for j=6205:6205
            B(nc)=A(j);
            nc=nc+1;
        end
        a=T;
        X(:,:,i1)=a';
        Y(:,:,i1)=B;
        meanY(i1)=mean(Y(:,:,i1));
```

```matlab
        stdY(i1)=std(Y(:,:,i1));
    end
    X1(:,:,i)=X;
    X2(:,:,i)=(X1(:,:,i))';
    Y1(:,:,i)=Y;
    Y2(:,:,i)=(Y1(:,:,i))';
    meanX2(:,:,i)=mean(X2(:,:,i)); % Ensemble mean
    meanY2(:,:,i)=mean(Y2(:,:,i)); % Ensemble mean
    stdY2(:,:,i)=std(Y2(:,:,i)); % Ensemble standard deviation
    ensemble_mean=mean(meanY2); % Mean of ensemble mean
    mean_stdY2(i)=mean(stdY2(:,:,i)); % Mean of ensemble standard deviation
end

function [Q_dot] = Ring_3(t,q,n)

Q_dot=(zeros(size(q)));
p=8800;
E=210E9;
r=500E-6;
h=12.5E-6;
b=30E-6;
[std_dev,nu]=i_nput(n);
omega01=1.89189E5;% Natural Frequency OMEGA 01
omega02=1.89189E5;% Natural Frequency OMEGA 02
A=3.7500E-010; % Cross sectional area of the ring
I=4.8828E-021; % moment of inertia
n=2.0; % number of mode
a=3.1507E8;
b=1.2601E9;
c=3.1526E8;
k1=3.5792E10;
k2=-0.1606;
f1=4.8483e-15;
gamma=0.8;
zeta=0.01*(1+nu);
% Capital omega(OMEGA)(Angular rate, rad/sec)
t1=0.0; t2=0.005; % Time for the transiant part of the angular speed
y1=2*pi; % Steady state part of the angular speed
if t<t1
    y=0.0;
elseif t<t2
    y=y1/2*sin(3.14159*(t-t1)/(t2-t1)-0.5*3.14159)+y1/2; % Transiant part of
the angular speed
else
    y=y1; % Steady state of the angular speed
end
Omega=y;
%-------------------------------------------------------------------------
----------------------------------------
% Noise and Drift
sigma1=0.0245; sigma2=0.0001;
a_d=1.0;
std_dev=(n/100)*Omega;
xi=normrnd(Omega,std_dev);
d_d=sigma1*(exp(a_d*t))+sigma2*xi; % equation for noise and drift
OMEGA=Omega+d_d; % Capital OMEGA with noise and drift
```

```
%-------------------------------------------------------------------------
------------------------------------------
% Derivative of Capital omega(OMEGA_dot)
if t<t1
    y_dot=0.0;
elseif t<t2
    y_dot=y1/2*cos(3.14159*(t-t1)/(t2-t1)-0.5*3.14159)*(3.14159/(t2-t1)); %
Transiant part of the angular speed
else
    y_dot=0.0; % Steady state of the angular speed
end
OMEGA_dot=y_dot;

Q_dot(1)=q(3);
Q_dot(2)=q(4);
Q_dot(3)=-(k1+k2*(OMEGA)^2)*q(1)+((OMEGA_dot)*gamma)*q(2)-
(2*zeta*omega01)*q(3)+(2*OMEGA*gamma)*q(4)+f1*cos((omega01*t)); % add shift
Q_dot(4)=((-((OMEGA_dot)*gamma)*q(1)-(k1+k2*(OMEGA)^2)*q(2)-
2*(OMEGA)*gamma)*q(3)-(2*zeta*omega02)*q(4))/(1);

end
```

A Sample of MATLAB Routine for output frequency response for amplitude ratio $|Q2/Q1|$

```
clc; clf; clear all;
p=8800;
E=210E9;
r=500E-6;
h=12.5E-6;
b1=30E-6;
omega01=1.89189E5;% Natural Frequency OMEGA 01
omega02=omega01;% Natural Frequency OMEGA 02
A=b1*h; % Cross sectional area of the ring
I=(b1*(h^3))/12; % moment of inertia
n=2.0; % number of mode
fr=1E-15;
a=((n^2)*(E*I)/(r^4))+((E*A)/(r^2));
b=(n^2)*(((E*I)/(r^4))+((E*A)/(r^2)));
c=((n^4)*((E*I)/(r^4)))+(E*A)/r^2;
k1=((b*c)-((n^2)*(a^2)))/(p*A*(a+b));
k2=((n^2)*(b+c-4*a))/(a+b)-((2+n^2)*(b*c-(n^2)*a))/((a+b)^2);
f1=(2*fr*b)/(p*A*(a+b));
gamma=(b+(n^2)*a)/(n*(a+b));
zeta=0.01;
n=[1 2 5 10 20];
for i1=1:5
    for i=1:1
        std_dev=n(i1)*0.00001;
        nu=normrnd(0.0001,std_dev);
        Omega=n(i1)*pi;
        H=tf([2*gamma*Omega],[1.0+nu 2*zeta*omega02 k1+k2*Omega.^2]);
        w=linspace(1.891E5,1.8925E5,100000);
        [mag,phase,wout] = bode(H,w);
        P = bodeoptions;
```

```
        P.MagUnits='abs';
        P.FreqScale='linear';
        P.MagVisible='on';
        bodemag(H,w);
        hold on; grid on;
        xlabel('Frequency');
        ylabel('Magnitude of amplitude ratio (Q2/Q1)');
        mag1(:,:,i)=mag;
        mag2(:,:,i)=mag1(:,:,i)';
        c1(:,:,i)=max(mag2(:,:,i));
        wout1(:,:,i)=wout;
        wout2(:,:,i)=wout1(:,:,i)';
        for j=1:length(mag2)
            if mag2(j)==c1;
                f(j)=wout2(j);
            end
        end
        d1(:,:,i)=max(f);
    end
    c2(:,:,i1)=c1;
    c3(:,:,i1)=(c2(:,:,i1))';
    mean_c3(:,:,i1)=mean(c3(:,:,i1)); % Mean of magnitude of peaks
    std_c3(:,:,i1)=std(c3(:,:,i1)); % Standard deviation of peak magnitude
    d2(:,:,i1)=d1;
    d(:,:,i1)=(d2(:,:,i1))';
    mean_d(:,:,i1)=mean(d(:,:,i1)); % Mean of corresponding peak frequency
    std_d(:,:,i1)=std(d(:,:,i1)); % Standard deviation of corresponding peak
frequency

end
```

A Sample of MATLAB Routine for uncertainty quantification of output frequency response amplitude ratio $|Q2/Q1|$

```
clc; clf; clear all;
p=8800;
E=210E9;
r=500E-6;
h=12.5E-6;
b1=30E-6;
omega01=1.89189E5;% Natural Frequency OMEGA 01
omega02=omega01;% Natural Frequency OMEGA 02
A=b1*h; % Cross sectional area of the ring
I=(b1*(h^3))/12; % moment of inertia
n=2.0; % number of mode
fr=1E-15;
a=((n^2)*(E*I)/(r^4))+((E*A)/(r^2));
b=(n^2)*(((E*I)/(r^4))+((E*A)/(r^2)));
c=((n^4)*((E*I)/(r^4)))+(E*A)/r^2;
k1=((b*c)-((n^2)*(a^2)))/(p*A*(a+b));
k2=((n^2)*(b+c-4*a))/(a+b)-((2+n^2)*(b*c-(n^2)*a))/((a+b)^2);
f1=(2*fr*b)/(p*A*(a+b));
gamma=(b+(n^2)*a)/(n*(a+b));
zeta=0.01;
n=1:1:30;
```

```
for i1=1:5
    for i=1:1
        std_dev=n(i1)*0.00001;
        nu=normrnd(0.0001,std_dev);
        Omega=n(i1)*pi;
        H=tf([2*gamma*Omega],[1.0+nu 2*zeta*omega02 k1+k2*Omega.^2]);
        w=linspace(1.891E5,1.8925E5,100000);
        [mag,phase,wout] = bode(H,w);
        P = bodeoptions;
        P.MagUnits='abs';
        P.FreqScale='linear';
        P.MagVisible='on';
        bodemag(H,w);
        hold on; grid on;
        xlabel('Frequency');
        ylabel('Magnitude of amplitude ratio (Q2/Q1)');
        mag1(:,:,i)=mag;
        mag2(:,:,i)=mag1(:,:,i)';
        c1(:,:,i)=max(mag2(:,:,i));
        wout1(:,:,i)=wout;
        wout2(:,:,i)=wout1(:,:,i)';
        for j=1:length(mag2)
            if mag2(j)==c1;
                f(j)=wout2(j);
            end
        end
        d1(:,:,i)=max(f);
    end
    c2(:,:,i1)=c1;
    c3(:,:,i1)=(c2(:,:,i1))';
    mean_c3(:,:,i1)=mean(c3(:,:,i1)); % Mean of magnitude of peaks
    std_c3(:,:,i1)=std(c3(:,:,i1)); % Standard deviation of peak magnitude
    d2(:,:,i1)=d1;
    d(:,:,i1)=(d2(:,:,i1))';
    mean_d(:,:,i1)=mean(d(:,:,i1)); % Mean of corresponding peak frequency
    std_d(:,:,i1)=std(d(:,:,i1)); % Standard deviation of corresponding peak
frequency

end
```

A Sample of MATLAB Routine of output forced frequency response $|Q2/F1|$

```
clc; clf; clear all;
p=8800;
E=210E9;
r=500E-6;
h=12.5E-6;
b1=30E-6;
omega01=1.89189E5;% Natural Frequency OMEGA 01
omega02=omega01;% Natural Frequency OMEGA 02
A=b1*h; % Cross sectional area of the ring
I=(b1*(h^3))/12; % moment of inertia
n=2.0; % number of mode
fr=1E-15;
a=((n^2)*(E*I)/(r^4))+((E*A)/(r^2));
```

```matlab
b=(n^2)*(((E*I)/(r^4))+((E*A)/(r^2)));
c=((n^4)*((E*I)/(r^4)))+(E*A)/r^2;
k1=((b*c)-((n^2)*(a^2)))/(p*A*(a+b));
k2=((n^2)*(b+c-4*a))/(a+b)-((2+n^2)*(b*c-(n^2)*a))/((a+b)^2);
f1=(2*fr*b)/(p*A*(a+b));
gamma=(b+(n^2)*a)/(n*(a+b));
zeta=0.01;
n=[1 2 5 10 20];
for i1=1:5
    for i=1:1
        std_dev=n(i1)*0.00001;
        nu=normrnd(0.0001,std_dev);
        Omega=2*pi;
        w=linspace(1.85E5,1.95E5,10000);
        H=tf([2*Omega*gamma],[1.0+nu (2*zeta*omega02+(1+nu)*2*zeta*omega01)
(1+nu)*((k1+k2*Omega.^2)+4*zeta^2*omega01*omega02+4*gamma^2*Omega.^2+(k1+k2*O
mega.^2)) (2*zeta*omega01+2*zeta*omega02)*(k1+k2*Omega.^2)
(k1+k2*Omega.^2).^2]);
        [mag,phase,wout] = bode(H,w);
        P = bodeoptions;
        P.MagUnits='abs';
        P.FreqScale='linear';
        P.MagVisible='on';
        bodemag(H,w);
        hold on; grid on;
        xlabel('Frequency');
        ylabel('Magnitude of frequency response (Q2/F1)');
        mag1(:,:,i)=mag;
        mag2(:,:,i)=mag1(:,:,i)';
        c1(:,:,i)=max(mag2(:,:,i));
        wout1(:,:,i)=wout;
        wout2(:,:,i)=wout1(:,:,i)';
        for j=1:length(mag2)
            if mag2(j)==c1;
                f(j)=wout2(j);
            end
        end
        d1(:,:,i)=max(f);
    end
    c2(:,:,i1)=c1;
    c3(:,:,i1)=(c2(:,:,i1))';
    mean_c3(:,:,i1)=mean(c3(:,:,i1)); % Mean of magnitude of peaks
    std_c3(:,:,i1)=std(c3(:,:,i1)); % Standard deviation of peak magnitude
    d2(:,:,i1)=d1;
    d(:,:,i1)=(d2(:,:,i1))';
    mean_d(:,:,i1)=mean(d(:,:,i1)); % Mean of corresponding peak frequency
    std_d(:,:,i1)=std(d(:,:,i1)); % Standard deviation of corresponding peak
frequency

end
```

A Sample of MATLAB Routine for uncertainty quantification of output forced frequency response $|Q2/F1|$

```
clc; clf; clear all;
p=8800;
E=210E9;
r=500E-6;
h=12.5E-6;
b1=30E-6;
omega01=1.89189E5;% Natural Frequency OMEGA 01
omega02=omega01;% Natural Frequency OMEGA 02
A=b1*h; % Cross sectional area of the ring
I=(b1*(h^3))/12; % moment of inertia
n=2.0; % number of mode
fr=1E-15;
a=((n^2)*(E*I)/(r^4))+((E*A)/(r^2));
b=(n^2)*(((E*I)/(r^4))+((E*A)/(r^2)));
c=((n^4)*((E*I)/(r^4)))+(E*A)/r^2;
k1=((b*c)-((n^2)*(a^2)))/(p*A*(a+b));
k2=((n^2)*(b+c-4*a))/(a+b)-((2+n^2)*(b*c-(n^2)*a))/((a+b)^2);
f1=(2*fr*b)/(p*A*(a+b));
gamma=(b+(n^2)*a)/(n*(a+b));
zeta=0.01;
n=1:1:10;
for i1=1:10
    for i=1:70
        std_dev=n(i1)*0.00001;
        nu=normrnd(0.0001,std_dev);
        Omega=2*pi;
        w=linspace(1.85E5,1.95E5,10000);
        H=tf([2*Omega*gamma],[1.0+nu (2*zeta*omega02+(1+nu)*2*zeta*omega01)
(1+nu)*((k1+k2*Omega.^2)+4*zeta^2*omega01*omega02+4*gamma^2*Omega.^2+(k1+k2*O
mega.^2)) (2*zeta*omega01+2*zeta*omega02)*(k1+k2*Omega.^2)
(k1+k2*Omega.^2).^2]);
        [mag,phase,wout] = bode(H,w);
        P = bodeoptions;
        P.MagUnits='abs';
        P.FreqScale='linear';
        P.MagVisible='on';
        bodemag(H,w);
        hold on; grid on;
        xlabel('Frequency');
        ylabel('Magnitude of frequency response (Q2/F1)');
        mag1(:,:,i)=mag;
        mag2(:,:,i)=mag1(:,:,i)';
        c1(:,:,i)=max(mag2(:,:,i));
        wout1(:,:,i)=wout;
        wout2(:,:,i)=wout1(:,:,i)';
        for j=1:length(mag2)
            if mag2(j)==c1;
                f(j)=wout2(j);
            end
        end
        d1(:,:,i)=max(f);
    end
    c2(:,:,i1)=c1;
```

```
    c3(:,:,i1)=(c2(:,:,i1))';
    mean_c3(:,:,i1)=mean(c3(:,:,i1)); % Mean of magnitude of peaks
    std_c3(:,:,i1)=std(c3(:,:,i1)); % Standard deviation of peak magnitude
    d2(:,:,i1)=d1;
    d(:,:,i1)=(d2(:,:,i1))';
    mean_d(:,:,i1)=mean(d(:,:,i1)); % Mean of corresponding peak frequency
    std_d(:,:,i1)=std(d(:,:,i1)); % Standard deviation of corresponding peak
frequency

end
```

Curriculum Vitae

Name: Nujhat Abedin

Post-secondary Education and Degrees: The University of Western Ontario (UWO)
London, Ontario, Canada
2012-2014 M.E.Sc. Mechanical and Materials Engineering

Bangladesh University of Engineering and Technology (BUET)
Dhaka, Bangladesh
2006-2010 B.Sc. Mechanical Engineering

Honours and Awards: Western Graduate Research Scholarship (WGRS)
The University of Western Ontario
2012-2014

Related Work Experiences: Teaching Assistant
The University of Western Ontario
London, Ontario, Canada
2012-2014

Engineer
Hi-Tech Bangla Inc.
Dhaka, Bangladesh
2011-2012

Publications:

- Abedin N. and Asokanthan S. F. Uncertainty Quantification for a Class of MEMS Based Ring Gyroscopes, *Probabilistic Engineering Mechanics* (to be submitted).

- Abedin N. and Asokanthan S. F. Uncertainty Quantification for a Class of MEMS Based Vibratory Gyroscopes, *Journal of Sound and Vibration* (to be submitted).